Biofilm formation by the manganese-oxidizing bacterium *Leptothrix discophora* strain SS-1 and corrosion of stainless steel

Dissertation

zur Erlangung des akademischen Grades eines
Doktors der Naturwissenschaften
- Dr. rer. Nat. -

vorgelegt von

Christian Thyssen

geboren in Meerbusch

Fakultät für Chemie
der Universität Duisburg-Essen

2018

Die vorliegende Arbeit wurde im Zeitraum von April 2011 bis September 2017 im Arbeitskreis von Prof. Dr. W. Sand Fakultät für Chemie, Biofilm Center, Aquatische Biotechnologie der Universität Duisburg-Essen durchgeführt.

Tag der Disputation: 13.07.2018

Gutachter:	Prof. Dr. W. Sand
	PD. Dr. W. Fürbeth
Vorsitzender:	Prof. Dr. M. Epple

...to my family and in memory of my grandparents...

"Life would be tragic if it weren't funny"

(Stephen Hawking)

Acknowledgements

I am deeply grateful to Prof. Dr. Wolfgang Sand for giving me the opportunity to do research in the fascinating field of microbially influenced corrosion, for the opportunity to work in his group, for his supervision, the possibility to extend my scientific background and to present my results in various conferences around the world.

I would like to express my sincere gratitude to PD. Dr. Wolfram Fürbeth for his great support during this work, the possibility to join scientific discussions during numerous sessions of the expert group "Mikrobielle Materialzerstörung und Materialschutz" and for proof-reading of this thesis.

A sincere thanks go to Dr. Tilman Gehrke for sharing his knowledge during scientific discussions, his help with the gas chromatographic analysis and proof-reading of this thesis.

I would like to express my sincere gratitude to Prof. Dr. Rainer Meckenstock for giving me the opportunity to finish the practical work of my PhD in his group and for his warm welcome.

I would also like to thank David for working all these years with me in our joint project, his support and for helping me with corrosion measurements.

I also gratefully acknowledge the financial support from the German Federal Ministry for Economic Affairs and Energy within the Program for Funding Industrial Joint Research (IGF) (IGF 16953 N and IGF 18352 N/2).

I am grateful to all former and current colleagues at the Biofilm Centre for mutual support and for providing a pleasant working atmosphere. Special thanks go to Agathe, Astrid, Jens, Sadjad, Qian, Felix, Arne, Ruiyong, Claudia, Sören, Mario and Petra for all the big and little things throughout the years. Special thanks go to Friederike, Jens, Igor, Natascha and Jan for squashing, tons of cake, coffee and their friendship.

My warmest thanks to Beate, Nanni, Bianca, Jürgen, David, Andrzej and Mark for having a great time together, for all the help, fun, drinks, travelling and for not only being colleagues, but being friends. I am deeply indebted for your support throughout all these years.

I further wish to thank my friends back home, who had to suffer from my lack of time, especially during the more demanding periods of this work, for their understanding, invaluable friendship and support. I especially like to express my gratitude to Fabian, Melli, Jens, Lydia, Christian and Oliver.

I will be forever grateful to my parents Ingrid and Ralf as well as to my beloved sisters Kathrin and Julia who were always there for me. Without you, this thesis would not have been possible.

Finally, my very special thanks go to Meike, for her love, patience and never ending support during the most demanding time of this thesis.

Content

List of Tables

List of Figures

Abbreviations

AFM	atomic force microscopy
AAS	atomic absorption spectroscopy
ATP	adenosine triphosphate
n.d.	not detectable
BP	band pass
BSA	bovine serum albumin
CCM	czech culture collection of microorganisms
CER	cation exchange resin
CLSM	confocal laser scanning microscopy
CPD	contact potential difference
DAPI	4',6-diamidino-2-phenylindole
di. water	deionized water
DNA	deoxyribonucleic acid
EFM	epifluorescence microscope
E_{pit}	pitting potential
EPS	extracellular polymeric substances
FITC	fluorescein isothiocyanate
FLBA	fluorescence lectin-binding analysis
G6PDH	glucose-6-phosphate dehydrogenase
IEP	isoelectric point
LB	loosely bound
LP	long pass
MCO	multicopper oxidase
MIC	microbiologically influenced corrosion
MICI	microbiologically influenced corrosion inhibition
MOMO	manganese oxidizing microorganism
MSVP-2	minimal salts vitamin pyruvate medium 2
OCP	open circuit potential
PBS	phosphate-buffered saline
rpm	revolutions per minute
SiC	silicon carbide
SKP	scanning Kelvin probe
SKPFM	scanning Kelvin probe force microscopy
SS	stainless steel
TB	tightly bound
TCC	total cell count
TRITC	tetramethylrhodamine

SI units not listed.

Abbreviations of lectins are separately listed in Table 6.

Abstract

Nowadays it is generally accepted that microorganisms play a pivotal role in corrosion, by influencing and/or accelerating the electrochemical corrosion processes. Microbiologically influenced corrosion (MIC) is associated with biofilm formation leading to (in)direct changes of the materials surface characteristics. The biofilm is consisting of a heterogeneous matrix of extracellular polymeric substances (EPS), which is comprised mainly (in addition to water) of polysaccharides, proteins, lipids, and nucleic acids. The metabolic activity of biofilm cells and the EPS itself strongly influence the interfacial processes associated with the electrochemical processes. In this study the importance of biofilm formation and manganese oxidation for the corrosion of stainless steel was elucidate by using *Leptothrix discophora* SS-1 as model organism.

The growth of *L. discophora* SS-1 cells was tested with two different growth media with and without addition of manganese ions. It was shown that the addition of manganese ions resulted in an increased lag phase as well as an increase in generation time (from approximately 2 h to 3 h). Concomitant with the oxidation of manganese(II) ions to manganese(IV) oxides the total ATP and protein content of stationary cultures decreased up to 40 % and 55 %, respectively. This indicates a negative effect of manganese ions on the physiology of *L. discophora* SS-1.

The analysis of the (EPS) under four different growth conditions showed that *L. discophora* SS-1 adapts its EPS to the environmental conditions and that the EPS possess all features to facilitate biofilm formation on SS. The amount of uronic acids was increased in EPS extracted from cells grown in the presence of manganese ions. This indicates that the carboxyl groups of uronic acids might be involved in retaining manganese ions in the EPS for subsequent oxidation. Analysis of (un)saturated fatty acids identified C18:1 as a unique unsaturated fatty acid only present in EPS of cells grown in the presence of manganese ions. Additionally, the fatty acids C8:0 and C16:0 were downregulated while C12:0 was upregulated in EPS of cells grown in presence of manganese ions. The main fatty acid under all conditions was C16:1, which is in agreement with literature reports for the *Leptothrix* group. Fluorescent lectin binding analysis (FLBA) and EPS analysis proved to be a useful combination to identify carbohydrate monomers (in case of FLBA by the ability of lectins to bind to certain glycoconjugate residues) and to identify genuine features of the biofilm. Sorbitol, mannose and rhamnose represent the major carbohydrate constituents in EPS of *L. discophora* SS-1. The lectins ConA, GS-II, PWM and LPA were specific for EPS of *L. discophora* SS-1 under all conditions. A particular striking staining feature was observed for

the lectins MPA, PWM, DBA and UEA-I. These lectins stained repeatedly a filament-like structure connecting the separated individual cells.

Analysis of contact potential difference (CPD) mapping (measurement of the surface potential) and corrosion measurements strongly indicates an effect of biofilm formation concomitant with manganese oxidation for the electrochemical degradation of stainless steel. Single cells and microcolonies were successfully labeled by fluorescence staining and in combination with Leucoberbelin blue allowed an identification of cells, microcolonies and manganese oxides on the surface. CPD mapping identified manganese oxides as cathodic areas with a negative CPD (-220 mV) and anodic areas (regularly but not always associated with identified cells) with a positive CPD (+200 mV) towards the steel surface. The potential difference of up to 420 mV between cathodic and anodic areas correlates with the 400 mV anodic shift (ennoblement) observed in open circuit potential (OCP) measurements with biofilms of *L. discophora* SS-1 cells precipitating manganese oxides on a stainless steel surface. The OCP shifted from initially 242 mV_{she} (uninfluenced by biofilms or manganese oxides) to 635 mV_{she}, which is well beyond the determined pitting potential (416 mV_{she} to 511 mV_{she}) of the stainless steel under the given conditions. Thus, the ennoblement of the stainless steel caused by bacteria and manganese oxides could directly be shown by this technique.

1 Introduction

1.1 Manganese in the environment

Manganese is the fifth most abundant element in the lithosphere and the second most abundant transition metal next to iron. It accounts for 0.1 mass percent of the Earth´s crust (Graedel 1978; Tebo et al. 2004). Manganese is almost ubiquitous in the environment and occurs in different chemical speciations. It can exist in the oxidation states 0, +II, +III, +IV, +VI, and +VII (Ehrlich and Newman 2009), of which the most commons are +II, +III and +IV (Tebo et al. 2007). Mn(II) is, in general, soluble and occurs as a cation (e.g. Mn^{2+}, $MnOH^{+}$, $MnCl^{+}$) in aqueous solution. Nevertheless, it can be oxidized to form insoluble phosphates or carbonates as well as insoluble manganese (VI) oxides that can contain minor amounts of Mn(II) (Tebo et al. 2007). Even though Mn(II) is only favored under oxygen free conditions at low pH (in contrast to Mn(III or IV) that are stable in the presence of oxygen and at high pH), Mn(II) can still occur up to millimolar ranges in natural waters at neutral pH in presence of oxygen. This is possible even in the presence of oxygen because of the relatively high activation energy for the transformation into higher oxidation states. The net reaction of Mn(II) oxidation is (Ehrlich et al. 2015; Tebo et al. 2005):

$$\boldsymbol{Mn^{2+} + 0.5O_2 + H_2O \rightarrow MnO_2 + 2H^{+}} \qquad \textbf{Eq 1}$$

However, there are also Mn(III)-oxides formed during Mn(II) oxidation such as MnOOH. Mn(III) is thermodynamically unstable in the environment and, hence, can only persist in complexes. In aqueous media Mn(III) disproportionates to Mn(II) and Mn(IV) (Butterfield et al. 2013; Ehrlich et al. 2015; Learman et al. 2011; Su et al. 2013):

$$\boldsymbol{2Mn^{3+} + 2H_2O \Leftrightarrow Mn^{2+} + MnO_2 + 4H^{+}} \qquad \textbf{Eq 2}$$

The environmental manganese cycle is summed up in Figure 1.

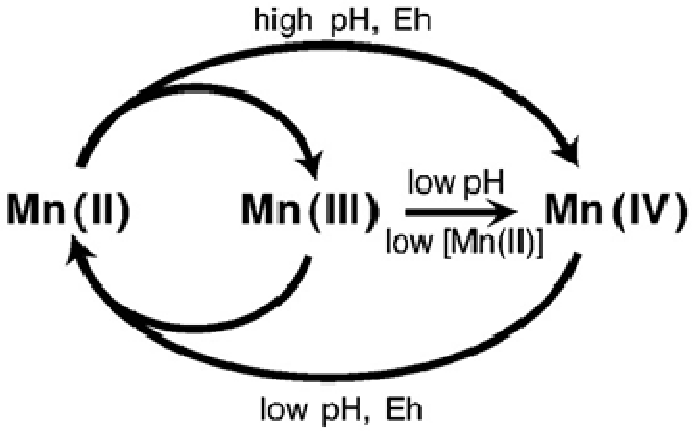

Figure 1: The redox cycle of naturally occurring manganese. Mn(II) is oxidized to Mn(III) and Mn(IV). Mn(III) is thermodynamically unstable and disproportionates to Mn(II) and Mn(IV). The reduction of Mn(IV) to Mn(II) closes the cycle (Tebo et al. 2004).

The biogeochemical cycling of manganese is mediated both by biotic and abiotic oxidation and reduction processes. The hereby formed insoluble manganese oxides are - next to oxygen - among the strongest naturally occurring oxidants (Tebo et al. 2005) and influence mobility, bioavailability and toxicity of trace elements and other metal(loid)s such as arsenic via diverse redox and sorption reactions (Lafferty et al. 2010; Zhu et al. 2009). However, they are less abundant than other minerals like iron or aluminum oxides. In nature, both, tunneled (such as todorokite) and layered structures (e.g. birnessite or birnessite-like manganese oxides) have been identified, whereby the latter ones occur more frequently (Post 1999). Vernadite, a random-stacked birnessite-like manganese oxide is the predominant form of manganese oxides in water bodies and surface coatings of other minerals (Chukhrov et al. 1979; Hochella et al. 2005; Zhu et al. 2012). These oxides are poorly crystalline with a high stacking disorder and are enriched with cation defects in the crystallographic structure leading to a higher surface area compared to their well-crystalline counterparts. Due to sorption processes of other cations, poorly crystalline manganese oxides play a major role in geochemical reactions and are mainly catalyzed by manganese oxidizing microorganisms (Bargar et al. 2009; Wehrli et al. 1995; Zhu et al. 2012). A popular example of the importance of birnessite-like manganese oxides are (fero)manganese concretions (nodules) on deep-see floors (Horn et al. 1972; Margolis and Burns 1976). Here, microbial oxidation processes are thought to be a major player in the formation these nodules (Ehrlich 1972; Wu et al. 2013). Even though, based on 16S rRNA the fraction of Mn(II)-oxidizing bacteria is in some parts low (Yli-Hemminki et al. 2014), the nodules seem to universally select for a microbiome that include genera with a high number of Mn(II)-oxidizing representatives (Ehrlich et al. 2015; Templeton et al. 2005; Wu et al. 2013; Yli-Hemminki et al. 2014). Therefore, biological

oxidation processes exert a powerful influence on the natural manganese cycle in aquatic and terrestrial environments.

Manganese is not only important for the biogeochemical cycling of metal(loid)s or oxidation processes. It also serves as a cofactor in a variety of enzymes with a broad spectrum of functions and as an essential nutrient for most organisms (Geszvain et al. 2012; Tebo et al. 2004). Manganese superoxide dismutase serves as a key antioxidant for organisms respiring oxygen (Law et al. 1998; McCord and Fridovich 1988) and manganese is the cofactor. It is also a cofactor in Photosystem II catalyzing (as part of the oxygen-evolving complex) the oxidation of water and transporting electrons to the special chlorophyll dimer P680 (Raymond and Blankenship 2008). Moreover, manganese is crucial for the pyruvatecarboxylase, which catalyses a step in the gluconeogenesis, i.e. the carboxylation of pyruvate (Jitrapakdee et al. 2006; Scrutton et al. 1972).

However, biologically produced manganese oxides have negative impacts on manmade materials such as stainless steel. They might induce, speed up or in general influence corrosion, which then may cause constructions to fail (Linhardt 2004). This topic will be discussed in detail in chapter 1.6.2.

1.2 Microorganisms in manganese cycling

Manganese oxidizing microorganisms (MOMO) are ubiquitous in the environment and consist of phylogenetically diverse taxa. Among them are Firmicutes, Actinobacteria, Alpha-, Beta- and Gamma-proteobacteria as well as fungi (Akob et al. 2014; Santelli et al. 2010; Tebo et al. 2004; Tebo et al. 2005; Yang et al. 2013). The cycling of manganese is (besides abiotic redox processes) strongly affected by biotic transformation (Nealson et al. 1988; Tebo et al. 2004). The most important ones are mobilization of insoluble forms of manganese and immobilization due to precipitation. Since abiotic Mn(II) oxidation is thermodynamically unfavorable (due to its slow kinetic) (Ulrich and Kretzschmar 2007), biological Mn(II) oxidation dominates in the environment with kinetics increased by up to five orders of magnitude (Geszvain et al. 2012; Tebo 1991). As a consequence, MOMO´s carry out the majority of environmental Mn(II) oxidation (Tebo et al. 2004). They are widespread and found in soils, sediments, rivers, lakes (Bräuer et al. 2011; Geszvain et al. 2012; Ghiorse 1984) as well as ocean water (Moffett 1997) and ocean floors (Ehrlich 2000; Templeton et al. 2005). As diverse as the MOMO are, so diverse, are the possible reasons of biological manganese oxidation. One of the more controversial discussed theories is the energy conservation by manganese oxidation. It has been discussed that the organisms have the capability to grow (aerobically or anaerobically) autotrophically using manganese as only energy source (Beijerinck 1913), mixotrophically using manganese as additional energy source (Ali and Stokes 1971; Lieske 1919) or heterotrophically without energy gain by manganese oxidation

(Adams and Ghiorse 1986; Ehrlich and Newman 2009; Hajj and Makemson 1976; Zhang et al. 2002). The gram-negative marine bacterium strain SSW_{22} oxidizes Mn(II) by an oxidoreductase located at the outer membrane and was thought to couple Mn(II) oxidation to ATP production. The gained electrons were postulated to be transferred to the electron transport system. The passage of electrons from Mn(II) to oxygen as the terminal electron acceptor might be linked to proton pumps generating the proton gradient necessary to drive the ATP-synthase (Ehrlich and Newman 2009; Ehrlich and Salerno 1990). The ability to generate energy for the genus *Leptothrix* was for a long time under debate, however, recent results suggest that they do not couple Mn(II) oxidation to ATP synthesis. Ali and Stokes (Ali and Stokes 1971) reported that *L. discophora* grows autotrophically and mixotrophically with Mn(II) as the energy source but this could not be confirmed in later studies by Hajj and Makemson (Hajj and Makemson 1976). For *L. discophora* SS-1 Adams and Ghiorse (Adams and Ghiorse 1987) already showed that Mn(II) oxidation is not coupled to ATP synthesis. Nowadays, there is little evidence for a link between ATP synthesis and Mn(II) oxidation in MOMOs, instead bacteria might use this reaction coincidentally (Ehrlich et al. 2015; Learman and Hansel 2014). The mechanisms, however, used by MOMO to oxidize manganese are rather diverse. The oxidation involves direct enzymatic oxidation as well as indirect oxidation of manganese via metabolic end-products (Brouwers et al. 2000; Geszvain et al. 2012; Tebo et al. 2004; Tebo et al. 2005). There is also evidence that Mn(III) intermediates are formed during the oxidation of Mn(II) to Mn(IV) (Butterfield et al. 2013; Learman et al. 2011; Su et al. 2013).

Despite the possible involvement of laccases and peroxidases in bacterial manganese oxidation (Ehrlich et al. 2015), numerous manganese oxidizing bacteria share the involvement of multicopper oxidases (MCO) in Mn(II) oxidation (Brouwers et al. 2000; Corstjens et al. 1997; Francis and Tebo 2001; Tebo et al. 2007; Van Waasbergen et al. 1996). MCO´s are a broad family of enzymes potent to oxidize diverse (in)organic substances. They are also discussed to be involved in the oxidation of Mn(II) by *Bacillus* (*B.*) SG-1. While the vegetative cells do not oxidize Mn(II), it has been reported that dormant spores oxidize Mn(II) via a protein complex at the outer exosporium (Francis and Tebo 1999; Rosson and Nealson 1982). While this might be disputable, several genes have been identified to be involved in manganese oxidation by *B.* SG-1 including mnxG that encodes for a multicopper oxidase (Tebo et al. 1997; Van Waasbergen et al. 1996). While MCO´s were also identified in *Leptothrix* species (Brouwers et al. 2000; Corstjens et al. 1997), this issue is up to date unresolved. *L. discophora* SS-1 releases an Mn(II)-oxidizing protein linked to a polysaccharide moiety with a molecular weight of 100,000 - 110,000 kDa into the liquid culture (Adams and Ghiorse 1987; Adams and Ghiorse 1986). This was not directly linked to

MCO´s, however, the *mofA* gene in *L. discophora* SS-1 was identified encoding for an Mn(II)-oxidizing protein linked to a MCO (Corstjens et al. 1997). While the MofA protein was thought to be involved in the Mn(II) oxidation, the levels do not correspond to manganese oxidation (El Gheriany et al. 2009; El Gheriany et al. 2011). Additionally, mofA knock out mutants still posses the ability to oxidize Mn(II) (Bocioaga 2013), indicating that the MCO related MofA is dispensable for *L. discophora* SS-1. It has been discussed that the gene mnxG2 encoding for a putative MCO, similar to the one found in *Bacillus sp* SG-1 (Van Waasbergen et al. 1996) or genes encoding for an unidentified putative protein, a putative cytochrome c or a putative copper metallochaperone might be key for Mn(II) oxidation in *L. discophora* SS-1 (Bocioaga 2013). The direct oxidation of Mn(II) via MCO´s or other enzymes for bacteria using oxygen as terminal electron acceptor can be summarized as:

$$Mn^{2+} + 0,5O_2 + H_2O \rightarrow MnO_2 + 2H^+ \qquad \textbf{Eq 3}$$

While in direct Mn(II) oxidation, an enzyme(complex) directly oxidizes Mn(II), in indirect biological Mn(II) oxidation the enzymes only promote this reaction through production of metabolic end-products, which cause a chemical oxidation. Among these end products are hydroxycarboxylic acids like gluconate, malate, citrate or lactate (Söhngen 1914; Van Veen 1973), polysaccharides (Ghiorse and Hirsch 1979; Van Veen et al. 1978) or extracellular superoxide (O_2^-) (Learman et al. 2011; Tang et al. 2013). The chemical oxidation of Mn(II) might be a direct one to Mn(IV) or via the intermediate Mn(III) (Butterfield et al. 2013; Learman et al. 2011; Su et al. 2013). The Mn(III) intermediate might either be reduced to Mn(II) again by e.g. H_2O_2 (Learman et al. 2013) or disproportionates to Mn(II) and Mn(IV) (Butterfield et al. 2013).

However, besides energy conservation, there are other evolutionary benefits possibly explaining the metabolic performance of organisms not linking the manganese oxidation to ATP synthesis. Manganese oxide coatings insulate microorganisms from environmental hazards such as UV radiation, heavy metal toxicity or predation. Further on, manganese oxides may be used as an antioxidant protecting the cells from reactive oxygen species (ROS). ROS can be, for example, superoxide- or hydroxyl-radicals, hydrogen peroxide or singlet oxygen and are produced concomitantly with respiration as a by-product. The bacteria are able to protect themselves against ROS by Mn(II) oxidation also in the absence of a ROS scavenging superoxide dismutase (Tebo et al. 2005). Moreover, manganese oxides have the oxidizing power to degrade humic substances into smaller compounds thereby making them available as a nutrient (Tebo et al. 2005). Some of the theories about the reason for the

bacterial Mn(II) oxidation presumes an evolutionary remainder; other suggestions include a clear evolutionary benefit like energy conservation or increased stress tolerance (Tebo et al. 2005; Ulrich and Kretzschmar 2007).

1.2.1 *Leptothrix discophora* SS-1

Representatives of the genera *Leptothrix* and *Sphaerotilus* are known to scientists for centuries and the type species of the genus *Leptothrix*, *L. ochracea*, was firstly described in 1797 by Roth (Roth 1797) under the name "Conferva ochracea" (Spring 2006). The species *L. discophora* was discovered by Schwers in 1912 (Schwers 1912), who named it *Megalothrix discophora*. The *Sphaerotilus-Leptothrix* group was subjected to several reclassifications and all strains were merged under the genus *Sphaerotilus* (Pringsheim 1949), a change highly disputed between the 1950´s and 70´s (Mulder and Van Veen 1963; Petitprez and Leclerc 1969). Finally, Pringsheim's nomenclature was proven wrong (Mulder 1964) in favor of a classification like *Sphaerotilus* and *Leptothrix* as distinct genera (Mulder and Deinema 1981; Van Veen et al. 1978). Strain *L. discophora* SS-1 was isolated in 1981 from a surface film of a swamp in Ithaca, New York, and described by Adams and Ghiorse (Adams and Ghiorse 1985; Adams and Ghiorse 1986). *Leptothrix discophora* SS-1 is a Gram-negative, rod-shaped *β*-proteobacterium (Tebo et al. 2005; Ulrich and Kretzschmar 2007) with an average width of 0.6 µm and a length of 2 - 7 µm. It is an obligate aerobic, polarly flagellated, formerly sheath-forming (it lost this ability during laboratory culturing shortly after its isolation), heterotrophic freshwater bacterium that uses the Entner-Doudoroff-pathway for carbohydrate catabolism (Adams and Ghiorse 1986; Zhang et al. 2002). The optimum pH for Mn(II)- oxidation is 7.5 with a temperature optimum at 30°C (Zhang et al. 2002).

1.3 Biofilms

Biofilms are the most common form of microbial life. Approximately more than 99 % of all microorganism on earth live in biofilms or similar aggregates (Costerton et al. 1987; Flemming 2002). They are the first signs of life on earth and can be dated back up to 3.5 billion years ago (Schopf et al. 1983). Biofilms are microenvironments consisting of cell assemblages embedded into a matrix, commonly but not solely found on surfaces or interfaces (Flemming and Wingender 2010; Sutherland 2001). Biofilms are the natural habitat of microorganisms (MO). Besides MO, the main constituents are extracellular polymeric substances (EPS), inorganic ions and water (Flemming et al. 2007; Thierry and Sand 2011). A biofilm is a strongly hydrated system and consists of up to 99 % water (Wingender et al.

1999). In living, fully hydrated biofilms MO account for approximately 15 % of the total volume with the EPS accounting for up to 85 % of it (Donlan and Costerton 2002). Expressed as a proportion of dry weight, this percentage is even lower, with MO accounting for approximately less than 10 % and the EPS matrix for more than 90 % of the biofilm's mass (Flemming and Wingender 2010) clearly indicating the importance of EPS for the biofilm itself. Biofilms are a very diverse ecosystem and give room for several ecological niches (O'Toole et al. 2000). For example, in aerobic zones the consumption of oxygen by bacterial metabolism is faster than the rate of rediffusion from the environment, therefore anaerobic zones are created (Wingender et al. 1999). Apart from the formation of different aerated zones, the close proximity of cells and the diffusion limitation in a biofilm give several advantages to the biofilm lifestyle compared to the planktonic one (Wingender et al. 1999). The benefits range from prevention of desiccation to protection from biocides, antibiotics, metallic cations, or ultraviolet radiation as well as from protozoan grazers (Flemming and Wingender 2010; Wingender et al. 1999; Wolfaardt et al. 1999). The proximity of MO in biofilms allows cells to form synergetic micro consortia to feed each other, to communicate and/or to undergo horizontal gene transfer. The cell to cell communication (quorum sensing) is based on the production of auto-inducing molecules such as oligopeptides and N-acyl homoserine lactones (AHL), which accumulate in the matrix. They induce the expression of certain genes or physiological changes in neighboring cells allowing the bacteria to respond to environmental changes (Bellenberg et al. 2014; Lorenz and Wackernagel 1994; McLean et al. 1997; Swift et al. 1996). The matrix also retains dissolved and particulate nutrients (which are pre-digested by extracellular enzymes to serve as an energy source) as well as lysed cells, which also may serve as a nutrient source (Flemming et al. 1996; Fuqua and Greenberg 2002; Späth et al. 1998). However, as beneficial as biofilms are for microorganisms, they may cause severe problems in industry and hygiene relevant systems (Cloete et al. 1998; Control and Prevention 2001; Davies 2003; Donlan and Costerton 2002). The term "biofouling" refers to an "undesirable accumulation of a biotic deposition on a surface" (Characklis 1990) and originates from heat exchanger technology (Epstein 1981). Biofouling might be caused by macroscopic organisms like mussels ("macrofouling") or microorganisms ("microbial biofouling") (Flemming 2011a). Apart from biofouling, bacteria are able to initiate, facilitate or accelerate corrosion of metallic or non-metallic materials. This process is commonly called "microbially influenced corrosion" or MIC (Beech and Gaylarde 1999; Sand and Gehrke 2003) and is discussed in detail in section 1.6.2. The formation of a biofilm is a multi-stage process initiated once bacteria "sense" a surface (O'Toole et al. 2000). The very first step, however, is not directly associated with MO. It is the formation of a conditioning film formed by the adhesion of macromolecules like humic substances, polysaccharides, lipids or proteins, immediately after a surface comes into contact with water

(Baier 1975; Flemming 2002). During the next step, bacteria attach reversibly to the surface. They may start EPS production and, hence, become irreversibly attached. The bacteria then start to replicate and grow. The secretion of EPS is enhanced, and a fully mature biofilm is formed. In the final step, parts of the mature biofilm detach through erosion and/or sloughing off and may form a new biofilm. The different steps are summed up and illustrated in Figure 2 (Bryers and Ratner 2004).

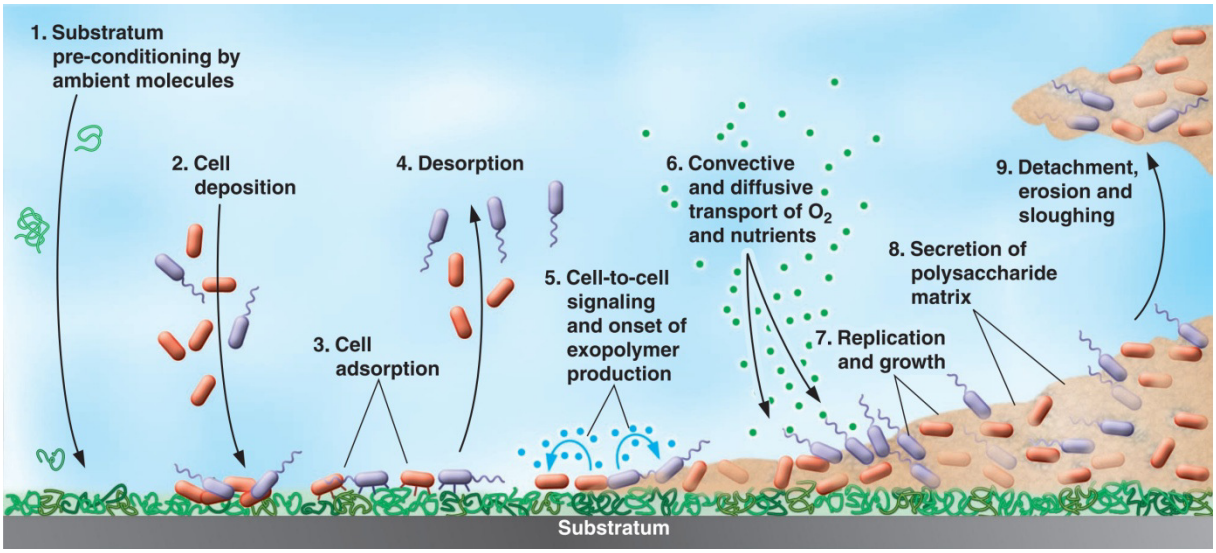

Figure 2: Different phases of biofilm formation on surfaces (Bryers and Ratner 2004). Cells adhere to a preconditioned substratum, start EPS synthesis initiated by cell-to-cell communication and grow to a heterogeneous biofilm where partial detachment may occur.

1.4 Extracellular Polymeric Substances

EPS represent the chemical building blocks of a biofilm and are mainly responsible for its stability, structure, adherence, protectiveness and many other crucial functions (Wingender et al. 1999). EPS consist of various substances, mainly polysaccharides, proteins, glycoproteins, glycolipids, phospholipids, extracellular DNA (e-DNA) as well as humic acids (Frølund et al. 1996; Sutherland 2001; Wingender et al. 1999). The EPS matrix is linked by weak physicochemical interactions like electrostatic- or ionic-attractive forces, van-der-Waals interactions, multivalent cations and hydrogen bonds as well as hydrophilic and hydrophobic interactions as summarized in Figure 3 (Flemming and Wingender 2010).

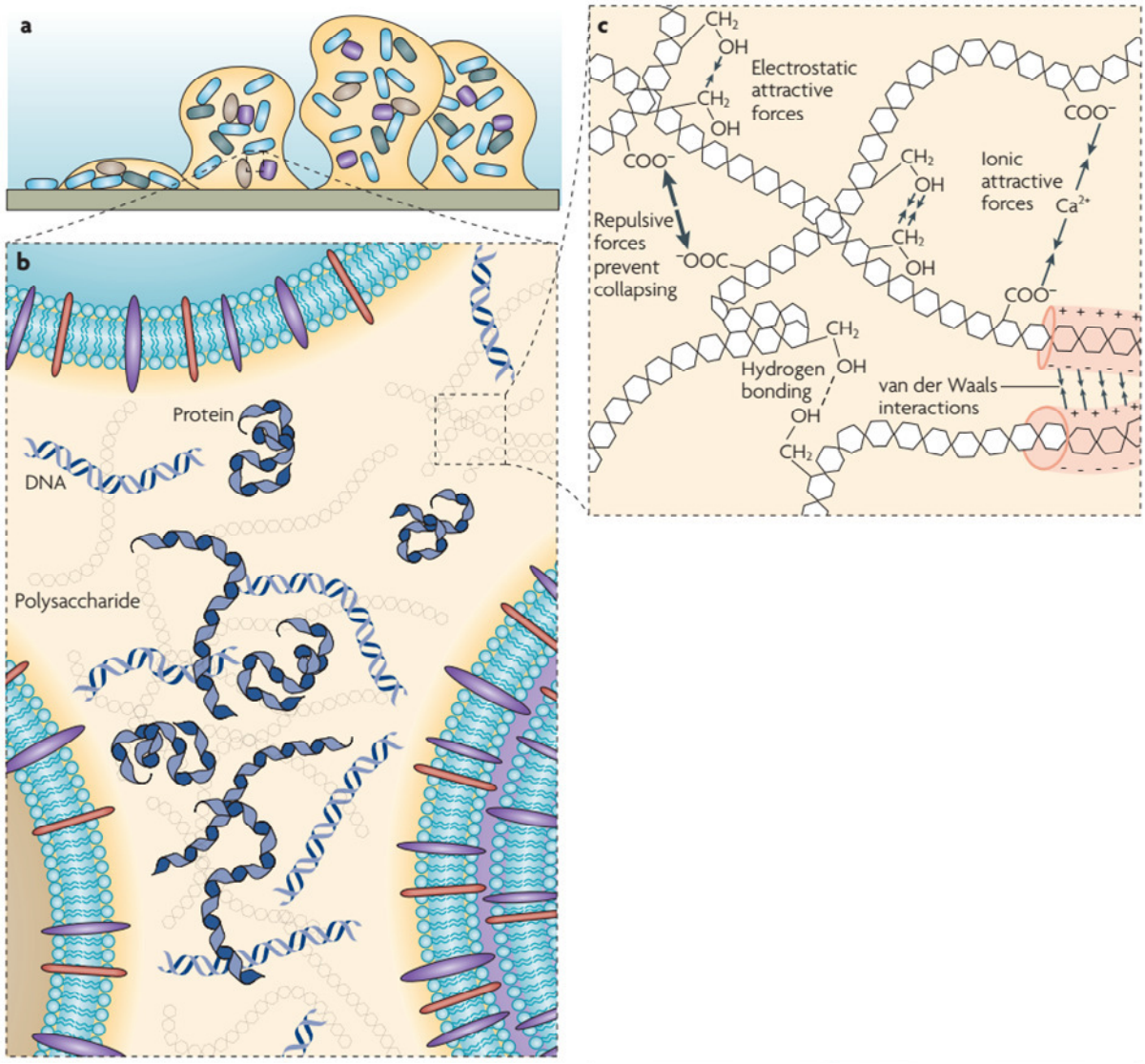

Figure 3: The EPS matrix at different scales. a: A model of a mushroom-like biofilm-structure attached to a surface. b: Distribution of major EPS constituents between the cells. c: Dominating interactions between the matrix constituents dominating EPS stability. Modified after (Flemming and Wingender 2010).

The most abundant compounds found in EPS are polysaccharides, proteins and lipids. The former are either homopolysaccharides composed of only one monosaccharide type (D-glucose, L-fructose) or heteropolysaccharides formed of repeating units of monosaccharides such as D-glucose, D-galactose or D-glucuronic acid (Czaczyk and Myszka 2007). Most of them are of polyanionic nature due to the presence of uronic acids or ketal-linked pyruvate and, therefore, water-soluble. Others are neutral, hydrophobic (Sutherland 2001), or polycationic (Flemming and Wingender 2010). As an example, functional groups with cationic properties like ß-(1,6)-linked poly-N-acetylglucosamine strongly contribute to biofilm formation of *Staphylococcus* ssp. (Mack et al. 1996) and might

mediate adhesion to net negatively charged surfaces. Polysaccharides contribute to the development and the three-dimensional structure of the biofilm and the overall stability by increasing the adhesive and cohesive properties (Lewandowski and Beyenal 2013). Uronic acids are essentially sugar acids, where the terminal carbon´s hydroxyl group has been oxidized to carboxylic acid. They have strong anionic properties and also contribute to the stability of the biofilm by interactions with cations such as Ca^{2+}. Glucose-based glucuronic acid, mannose-based mannuronic acid and galactose-based galacturonic acid are very common and may compose up to 8 % (w/w) of the EPS (Al-Halbouni et al. 2009; Sutherland 2001). Proteins represent the second large fraction of the EPS. Extracellular enzymes function as the external "digestive system" of the bacterial cells and are involved in the degradation of biopolymers into low-molecular weight products thereby increasing the availability of nutrients (Flemming and Wingender 2010). However, proteins also strongly increase biofilm stability by electrostatic cross-linkages with multivalent cations (e.g. Ca^{2+}-bridges) due to large negatively charged reactive sites (Higgins and Novak 1997; Laspidou and Rittmann 2002). The presence of eDNA in the EPS was firstly attributed to cell lysis only (Flemming et al. 2007; Nishikawa and Kuriyama 1968; Whitchurch et al. 2002). During the 1980´s, however, it was shown that DNA might deliberately be excreted in the biofilm for transformation purposes (Muto and Goto 1986). More recently, it was shown that eDNA is a key component for biofilm formation in *Pseudomonas aeruginosa* and that DNAse dissolves structural elements of young (60h-old) biofilms but do not alter cell growth (Whitchurch et al. 2002). Nowadays it is generally accepted that eDNA are deliberately produced and contribute to biofilm stability and rigidity due to interactions with polysaccharides and proteins (Das et al. 2013). Lipids are often disregarded but can also constitute a significant part of the EPS. For example, in *Acidithiobacillus ferrooxidans* lipids were identified to be crucial for the adhesion to sulfur surfaces (Gehrke et al. 1998; Sand and Gehrke 2006). Lipids have surface active properties and provide sorption sites for hydrophobic and amphiphilic organic compounds (Conrad et al. 2003). Together with polysaccharides they form lipopolysaccharides and thereby contribute to the structural stability of the EPS (Al-Halbouni et al. 2009).

1.5 Biofilm analysis

In general, biofilm analysis and EPS characterization are challenging. Due to the chemical complexity of microbial biofilms and heterogeneity of the EPS composition it is necessary to study biofilms with intrinsic methods (such as DNA staining and labeling of the biofilm structure with lectins) and to chemically analyze and characterize the EPS components.

1.5.1 Biofilm study

Microscopy is a widely used non-invasive technique to study preserved fully hydrated microbial biofilms *in situ* without disrupting their genuine structure (Karunakaran et al. 2011). Epifluorescence microscopy (EFM) is basically comparable to conventional light microscopy but shows significant advantages. Using fluorescing nucleic acid stains like 4',6-diamidino-2-phenylindole (DAPI) or Syto® 9, it is possible to certainly distinguish between bacteria and particles (Karunakaran et al. 2011). While EFM is restricted to thin biofilms (since this technique maps fluorescence from above and below the focal plane, which in the case of thick biofilms would result in blurry pictures), confocal laser scanning microscopy (CLSM) represents a more advanced method to study the 3-dimensional biofilm structure. CLSM collects fluorescence data only directly from the focal plane. This technique uses lasers of a specific wavelength allowing for a more precise excitation of the DNA stain resulting in reduced background fluorescence and false positive emittance of co-excited DNA stains (Karunakaran et al. 2011; Lawrence et al. 2007; Pawley 2006). However, independent of the detection technique, DNA stains are restricted to identify the bacteria , but not to characterize the biofilm matrix (EPS) . To overcome this restriction, fluorescence lectin-binding analyses (FLBA) via CLSM imaging were applied as the method of choice (Neu et al. 2010; Neu et al. 2001) to investigate (i) glycoconjugate distribution, (ii) to identify exopolymers, and (iii) to gain information of the 3-dimensional structure of the biofilm (Neu et al. 2001; Savidge and Pothulakis 2004). Lectins are plant-, animal- or bacteria-derived proteins (glycoproteins) with two or more carbohydrate-residue specific binding sides (Neu and Lawrence 1999). Fluorescently labeled lectins allow the visualization of extracellular polysaccharides and their distribution within a biofilm (Flemming and Wingender 2010). Combining DNA with lectin staining allows the investigation of a biofilm regarding the spatial structure, the distribution of the microorganisms and the extracellular polymeric polysaccharides to get a detailed insight into the "house of biofilm cells" (Flemming et al. 2007; Neu et al. 2001).

1.5.2 Characterization of extracellular polymeric substances

Characterization of EPS components is a crucial step to understand biofilm properties and to elucidate the function of its components. The first step in EPS characterization is the separation of the EPS matrix from the cells. Due to the complexity and variety of biofilms and EPS constituents, there is no universal method (Wingender et al. 1999). However, for EPS extraction different approaches exists that aim to destabilize the EPS matrix to overcome the binding forces. Common methods include the treatment with chemicals like NaOH, formaldehyde, EDTA, or crown ether or physical methods like centrifugation, sonication, filtration or heating. Additionally, combinations of both chemical and physical methods exist

such as the use of a cation exchange resin (CER) and shear force (by stirring) (Comte et al. 2006; Neu and Lawrence 1999; Nielsen and Jahn 1999). The latter combination targets to destabilize the EPS by scavenging multivalent cations like Ca^{2+} or Mg^{2+} bridging negatively-charged biopolymers and then separating the EPS from the cells by shear forces (D'Abzac et al. 2010; Frølund et al. 1996). A careful chosen technique allows for the isolation of both water-soluble and water-insoluble compounds and additionally provides the separation between loosely-bound EPS (separated by centrifugation) and tightly-bound EPS (separated by aforementioned extraction technique). Even though no universal method exists, there are principals that need to be fulfilled for a suitable extraction method. The procedure should (i) cause minimal cell lysis to prevent contamination of the EPS with intracellular compounds, (ii) extract the maximum amount of the analyte, and (iii) not alter the biopolymers (Nielsen and Jahn 1999). Additionally, the extraction method should not interfere with subsequent analysis techniques. The use of the CER method in combination with centrifugation and shear force is considered as the method of choice (Wingender et al. 1999). It extracts proteins, carbohydrates, eDNA and also lipids and does not interfere with the subsequent analysis like other bivalent cation extracting agents (e.g. EDTA) (Frølund et al. 1996; Nielsen and Jahn 1999). Furthermore, extraction of EPS with the CER method showed the highest extraction efficiency among physical methods while having the lowest risk of cell lysis (D'Abzac et al. 2010). Nevertheless, this needs to be confirmed for each setup with cell lysis markers, such as the membrane bound enzyme glucose-6-phosphate dehydrogenase (G6PDH).

Some of the most common techniques to quantify EPS are spectrophotometrical methods based on colorimetric or fluorometric assays. By these assays a specific EPS component reacts with a certain reagent to form a product or complex that absorbs light or emits fluorescence upon excitation. The methods used in this study are summarized in Table 1.

Table 1: Photometric and fluorometric methods for the quantification of EPS components

EPS component	Main reagent(s)	Reference
Carbohydrates	H_2SO_4/ Phenol	(DuBois et al. 1956)
Proteins	Coomassie Brilliant Blue G-250	(Bradford 1976)
DNA	PicoGreen	(Ahn et al. 1996)
Uronic acids	m-Hydroxydiphenyl	(Blumenkrantz and Asboe-Hansen 1973)
Lipids	H_2SO_4/ phospho-vanillin	(Cheng et al. 2011)
Humic acids	$CuSO_4$/ Folin-Ciocalteu reagent	(Frølund et al. 1996)

More advanced methods to further analyze EPS components and gain additional insights into the composition and function of the EPS include chromatographic methods such as gas-

liquid chromatography coupled with a flame ionization detector (GLC-FID) or a mass spectrometer (GLC-MS) as well as spectroscopic methods like Fourier Transform Infrared Spectroscopy, FTIR (Beech and Tapper 1999; Schmitt and Flemming 1998).

1.6 Concepts and analysis of corrosion

Corrosion of metals can be defined generally as the degradation of a refined metal to a thermodynamically more stable (e.g. oxidized) form by the chemical action of certain external agents (Speller 1926). According to the "Deutsches Istitut für Normung" the definition is "corrosion: the reaction of a metallic material with its environment, which effects a measurable change in the material and can lead to impairment of the function of a metal component or of an entire system. In most cases, this reaction is of electrochemical nature; in some instances it can however also be of chemical or metal physical nature" (DIN_EN_ISO_8044 2015). Electrochemical corrosion is driven by cathodic and anodic reactions. At the cathode, a certain chemical species such as oxygen is reduced by the uptake of electrons originating from anodic sites, on which metallic cations (oxidation) are released (Beech and Gaylarde 1999).

1.6.1 (Electro)chemical Corrosion

As mentioned before, the redox-reactions that occur during electrochemical corrosion can be divided into anodic and cathodic partial reactions. An example of oxygenic iron corrosion in a humid environment is shown below (Ahmad 2006):

$$Fe \rightarrow Fe^{2+} + 2e^{-}$$ **anodic oxidation** **Eq 4**

$$H_2O + 0.5\,O_2 + 2e^{-} \rightarrow 2\,OH^{-}$$ **cathodic reduction** **Eq 5**

The net reaction is:

$$Fe + H_2O + 0.5\,O_2 \rightarrow Fe(OH)_2$$ **Eq 6**

The anode and cathode are conducted through the iron specimen. This allows for the electrons to pass from the anode to the cathode, while the surrounding electrolyte is essential to close the electrical cycle by passing the ions. This leads to the formation of a corrosion cell (Ahmad 2006; Mortimer and Müller 2015).

In the presence of additional oxygen, ferrous hydroxide is converted to ferric hydroxide (Iverson 1987).

$$2\,Fe(OH)_2 + 0.5\,O_2 \rightarrow 2\,FeO(OH) + H_2O$$ **Eq 7**

The principals of the electrochemical corrosion process are exemplified (Figure 4) by a galvanic cell. The cathode and the anode are in electrical contact allowing the electrons to pass. The electrical circuit is closed by an ion flow in the surrounding electrolyte. This galvanic cell consists of the two half cells zinc/ zinc sulfate and copper/ copper sulfate (Ahmad 2006). The half and net reactions are shown below:

$$Zn \rightarrow Zn^{2+} + 2e^{-}$$ **anodic oxidation** **Eq 8**

$$Cu^{2+} + 2e^{-} \rightarrow Cu$$ **cathodic reduction** **Eq 9**

At the anode, the metallic zinc is oxidized and zinc ions go into solution. The resulting electrons are passed to the cathode. At the cathode, aqueous copper ions are reduced to metallic copper.

The net reaction is:

$$Zn + Cu^{2+} \rightarrow Zn^{2+} + Cu$$ **Eq 10**

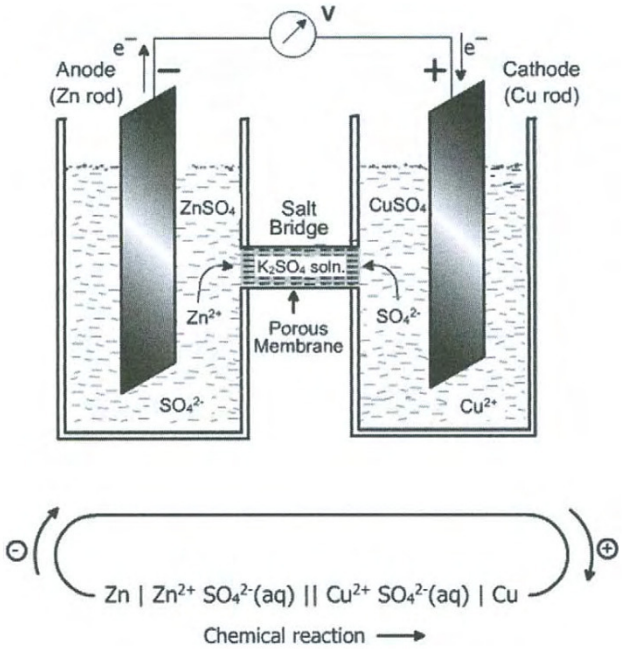

Figure 4: Galvanic cell consisting of two half cells. Anode and cathode are electrically connected and the cells are then connected by a salt bridge. The first half cell consists of zinc/ zinc sulfate and the second one, copper/copper sulfate (Ahmad 2006).

However, even in the absence of oxygen, iron can be corroded by e.g. an acid (protons). The acid corrosion is a chemically driven process not separating the metallic surface into distinct anodes and cathodes since they are evenly distributed over the surface. The redox-reactions leading to the dissolution of the iron are shown below (Ahmad 2006):

$$Fe \rightarrow Fe^{2+} + 2e^{-}$$ **oxidation** **Eq 11**

$$2\,H^{+} + 2e^{-} \rightarrow H_2$$ **reduction** **Eq 12**

The net reaction is:

$$Fe + 2\,H^{+} \rightarrow Fe^{2+} + H_2$$ **Eq 13**

1.6.2 Microbially Influenced Corrosion

The capability of microorganisms to initiate, facilitate or accelerate corrosion reactions of metallic or non-metallic materials is called microbially influenced corrosion (MIC) or biocorrosion (Sand and Gehrke 2003; Thierry and Sand 2011; Videla and Characklis 1992). The economic loss due to corrosion in industrialized countries is approximated to 3 % of the gross domestic product summing up to 2.2 trillion USD worldwide (Hays and General 2010). Biocorrosion causes problems especially in heat exchangers, pipes, ships, tanks, industrial facilities, buildings and (hydroelectric) power plants (Flemming 2011a; Licina and Cubicciotti 1989; Linhardt 2004; Sand and Gehrke 2003; Thierry and Sand 2011). It accounts for up to 20 % of all damage cases in such environments (Brözel and Cloete 1989), even though the exact number may vary (Flemming 1996).

Several MO are known to cause biocorrosion. Among them are sulfur-oxidizers, sulfate-reducers, iron-oxidizers, manganese-oxidizers and in general bacteria or fungi secreting (in)organic acids (Beech and Gaylarde 1999). MO may influence the corrosion (rate) in various ways, i.e. through degradation of corrosion inhibitors, destruction of protective layers, stimulation of electrochemical reactions and formation of differential aeration or concentration cells (Beech and Gaylarde 1999; Sand and Gehrke 2003; Thierry and Sand 2011). Biocorrosion is caused by biofilms in aerobic as well as in anaerobic environments (Lee et al. 1995).

Under anaerobic conditions, it is generally accepted that sulfate reducing prokaryotes (SRP; formerly known as sulfate reducing bacteria, SRB) are mainly responsible for biocorrosion (Beech and Sunner 2007; Hamilton 1985; Lee et al. 1995) although methane-producing,

hydrogen-producing and iron-reducing bacteria and/or archaea may also contribute (Ford and Mitchell 1990). Under sterile anaerobic conditions at neutral pH, iron based construction materials are expected to last for centuries, since corrosion rates are normally negligible (Enning et al. 2012). Despite the economic impact of biocorrosion in anaerobic environments and the role of SRP, the mechanism is still not fully understood (Beech and Sunner 2007). The cathodic-depolarisation-theory, proposed by von Wolzogen-Kühr and van der Vlugt in 1934 (Von Wolzogen-Kühr and Van der Vlugt 1934) assumed that the iron itself act as the only source of reducing equivalents for the sulfate reduction. Due to the high affinity of SRP to (molecular and absorbed) hydrogen as a growth substrate it was considered that a hydrogenase system degrades the layer of the cathodically generated hydrogen resulting in accelerated corrosion of the metal surface (Enning et al. 2012; von Wolzogen-Kühr 1961; Von Wolzogen-Kühr and Van der Vlugt 1934). However, this mechanism is nowadays highly disputed because the acceleration of corrosion does not correlate to hydrogenase activity (Costello 1974; Dinh et al. 2004; Enning et al. 2012; Venzlaff et al. 2013). Several other compounds might play a significant role in the corrosion acceleration, for example iron sulfide (King and Wakerley 1973) or hydrogen sulfide (Booth et al. 1968). Alternative mechanisms have been proposed to explain the acceleration of corrosion by SRP. Among them are the stimulation by chemical reactions with metabolites such as H_2S (resulting in the formation of large cathodic FeS layers), elemental sulfur or corrosive iron phosphates (Iverson and Olson 1983; King et al. 1973; Venzlaff et al. 2013). Recently, Dinh and co-workers (Dinh et al. 2004) developed a theory called electrical MIC, a modification of the cathodic-depolarization-theory (Von Wolzogen-Kühr and Van der Vlugt 1934). It is indicated that SRP can take up electrons directly from metallic iron. The direct uptake circumvents the slow, previously rate determining step of molecular hydrogen formation and thereby explains the corrosion rates much more reliable than any of the previous theories (Dinh et al. 2004; Enning et al. 2012; Heyer 2013; Venzlaff et al. 2013).

Under aerobic conditions, three groups of microorganisms are of special interest for biocorrosion: sulfur-oxidizing bacteria and archaea, iron-oxidizing bacteria and manganese-oxidizing microorganisms (Kuklinski and Sand 2014; Sand 1997; Thierry and Sand 2011). One of the most frequently found effects on corrosion in aerobic environments is based on the formation of differential aeration (or concentration) cells as a result of biological activity. Inhomogeneous biofilms cover, for example, metal surfaces leading to oxygen-enriched zones, who become cathodes, and anoxic or oxygen-depleted anodic zones beneath the biofilm (Beech and Gaylarde 1999; Ford and Mitchell 1990). This effect is amplified by the formation of “tubercles”, in which the anodic iron oxidation can take place, while the cathodic oxygen reduction occurs around the tubercle basis (Beech and Gaylarde 1999; Lee et al.

1995). In terms of the production of corrosive metabolites, a prominent example is the sulfuric acid-producing genus *Acidithiobacillus* (Coetser and Cloete 2005). Members of this genus can withstand extreme pH conditions even below 1 and produce large amounts of sulfuric acid by oxidizing elemental sulfur, thiosulfate, trithionate, tetrathionate or other reduced sulfur compounds. Consequently, this leads to pitting, crevice corrosion, or stress corrosion cracking (Sand and Gehrke 2003).

The present study pays particular attention to the corrosion of stainless (alloyed) steel (SS) under aerobic conditions related to MOMOs. MOMOs are ubiquitous in the natural environment and may form biofilms on diverse types of construction materials (Carpén et al. 2003; Dickinson et al. 1997; Lewandowski et al. 2002; Linhardt 1997; Linhardt 2004). Within their biofilms they deposit amorphous, non-stoichiometric manganese(III/IV)-oxides and -hydroxides (Linhardt 2010). For reasons of simplicity these oxides are further on summarized as Mn(IV) oxides or manganese oxides (MnO_2). In MIC by MOMOs, the bacteria themselves do not directly "attack" the metal but they influence or initiate the corrosion process by precipitating the aforementioned manganese oxides on the steel surface. If the manganese oxides are in electrical contact to the metal, a process called ennoblement is initiated. Ennoblement is a term frequently used to describe the phenomenon of a shift in the free corrosion potential of SS from typical values reached under abiotic conditions into the anodic direction exceeding the critical pitting potential (point of pit formation) (Dickinson et al. 1996; Linhardt 2004). The free corrosion potential or open circuit potential (OCP) is determined by the cathodic oxygen reduction balancing the small current of passive SS. Since these reaction kinetics are rather slow, the calculated redox potential of 804 mV_{she} is never observed for SS in fresh water. The typical OCP of SS under environmental conditions varies between 144 and 344 mV_{she} (1987; Scotto et al. 1985). However, if MnO_2 is precipitated on a SS surface, the OCP is determined by the Mn(II)/Mn(IV)-redox system. At neutral pH (c(Mn(II)) = 0.1 mg L^{-1}) the calculated OCP of SS in this system is 571 mV_{she}. This value corresponds well with the OCP determined for SS in neutral media with manganese oxides being in electrical contact to the steel surface (Dickinson et al. 1996; Dickinson et al. 1997; Linhardt 2004; Thyssen et al. 2015). In consequence, the anodic shift initiated by microbiological activity leads to a significantly increased susceptibility to chloride induced pitting and crevice corrosion (Linhardt 2006; Olesen et al. 2001). In this process, manganese oxides are reduced to Mn(II) ions, which represent the final product of the cathodic reaction. The reduction is a two step mechanism (Linhardt 2004; Shi et al. 2002a), with the first step being the reduction of Mn(IV) to intermediate Mn(III):

$$MnO_2 + H^+ + e^- \rightarrow MnOOH$$ **Eq 14**

This step is followed by disproportion of Mn to the oxidation states (II) and (IV):

$$2MnOOH + 2H^+ \rightarrow MnO_2 + Mn^{2+} + 2H_2O$$ **Eq 15**

The net overall reaction is:

$$MnO_2 + 4H^+ + 2e^- \rightarrow Mn^{2+} + 2H_2O$$ **Eq 16**

The electrons consumed in the cathodic reaction are released by the anodic iron dissolution. The extent of the iron dissolution is directly correlated with the (increasing) anodic potential shift (Kielemoes et al. 2002).

$$Fe^0 \rightarrow Fe^{2+} + 2e^-$$ **Eq 17**

The whole mechanism relies on the cycling of manganese on the metal surface. The manganese oxides act as recycable cathodic reactants and the MOMOs continuously replenish this reservoir (Lewandowski et al. 2002; Shi et al. 2002a). However, MOMOs not only grow on stainless steel but might also grow and precipitate manganese oxides on carbon or other grades of steel and therefore speed up the corrosion. However, literature indicates that the effect of MOMO on e.g. carbon steel is negligible, since the formed corrosion products (e.g. iron(III) oxides or iron(III) oxide-hydroxide) have an insulating effect and therefore interrupt the electrical contact between the manganese oxides (MnO_2) to the steel (Linhardt 2010; Olesen et al. 2000). Figure 5 illustrates the mechanism of MIC by MOMOs on stainless steel presented by Paul Linhardt (Linhardt 2004). Other authors concluded a very similar scenario of this mechanism (Dickinson and Lewandowski 1996; Olesen et al. 2001).

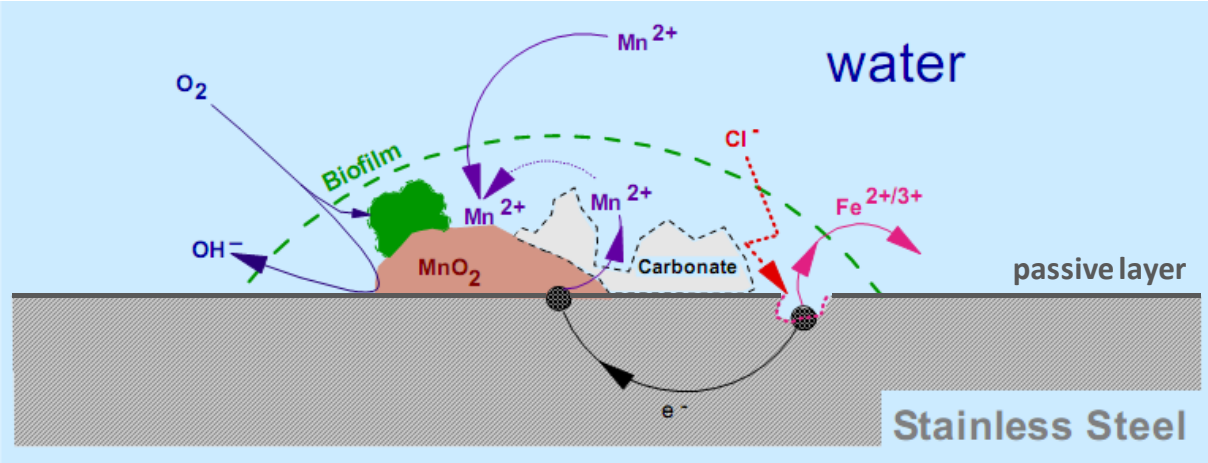

Figure 5: Schematic representation of the mechanism of MIC by MOMO's. Biofilm formation on SS with concomitant oxidation of Mn(II) and precipitation of manganese oxides on the surface. MnO_2 is reduced by the cathodic reaction to Mn(II) ions, which are then re-oxidized by MOMOs. MnO_2 is a strong oxidant and catalyzes the oxygen reduction on the metal surface acting as an electron sink. This leads to an anodic shift initiating the chloride induced pitting and anodic metal dissolution. Modified after (Linhardt 2004).

1.6.3 Surface and corrosion analysis

The influence of bacteria on corrosion is often hard to predict (Sand and Gehrke 2003) and assessments of the bulk water phase usually do not allow a valid risk assessment (Eul et al. 1996). The mere presence of bacteria or manganese in the bulk water does not necessarily lead to a higher susceptibility of the working material to corrosion (Linhardt 2010). To understand MIC, it is necessary to investigate the interface between the substratum and the biofilm to improve our understanding of attachment and biofilm formation as well as to determine the effect of the concomitant manganese oxide deposition on the surface potential of the steel itself.

A promising technique to understand the interaction of bacteria with a surface and the effect of manganese oxides on SS in particular is the use of an atomic force microscope (AFM) equipped with a scanning Kelvin probe module coupled to an epifluorescence microscope. The AFM belongs to the group of scanning probe microscopes, and is based on an indirect non-optical microscopic technique scanning the sample surface with a cantilever and creating a three dimensional topographic image (Binnig et al. 1986). The cantilever with a tip radius of < 10 nm bends and deflects while scanning the surface. The deflection of the cantilever is directly proportional to local attractive or repulsive forces and is detected using a laser beam. The laser beam is reflected from the back of the cantilever onto a photodetector. The movement of the laser on this detector is then used to compute an image (Meyer and Amer 1988). In ultrahigh vacuum the resolution of the AFM is only limited by the thickness of the cantilever tip and even atomic resolution can be achieved (Binnig et al. 1987). However, even in ambient air or liquid the AFM reaches sub-nanometer resolution (Weisenhorn et al.

1990). For the visualization of a surface there are essentially two scanning methods: The contact mode at all times keeps a physical contact of the tip with the sample surface resulting in a high dependency to the spring constant of the cantilever (Binnig et al. 1986). If the lateral force is too high, soft biological samples might be damaged; if the lateral force is too low this leads to a high sensitivity to vibrations (noise) from the environment. These shortcomings can be overcome by the frequency-modulated AFM mode also known as the intermittent contact mode. The intermittent contact mode strongly reduces the lateral forces on the sample, while increasing the lateral resolution at the same time. To achieve this, the cantilever oscillates at a fixed amplitude over the sample surface and interactions with the surface result in variations of the cantilever frequency. This frequency-change is then used as a feedback signal to visualize the surface (Giessibl 2005). The AFM has been used in a variety of studies elucidating the interfacial processes between microbes (biofilms or single cells) and metallic substrates such as bioleaching (Gehrke et al. 1998; Harneit et al. 2006; Noël et al. 2010) and biocorrosion (Beech 1996; Telegdi et al. 1998; Xu et al. 2002). However, the high versatility and the non-specific tip-sample-interactions strongly limit the capability of the AFM to discriminate between particles and bacteria (Mangold et al. 2008). The combination with an EFM can overcome this limitation by providing the specificity to distinguish between abiotic particles and microbial cells by the use of fluorescently labeled DNA-stains while keeping the sub nanometer resolution of the AFM (Mangold et al. 2008). To study corrosion processes additional information besides the identification of the bacteria or the surface topography are necessary such as the potential or potential shift of a specimen. In classical corrosion studies on SS, the pitting potential is tested in a 3-electrode setup to determine the corrosion resistance of SS. This setup usually consists of a working electrode (the metal to be tested), a counter electrode (passing the electrons) and a reference electrode (calibrated to determine the actual potential). This is the basic setup in Voltammetry. In linear potential sweep voltammetry, the potential is increased and the current at the working electrode is recorded. While increasing the potential, the passive layer of the SS hinders the electron flow until the passive layer breaks down and pit formation occurs. At this point a sudden rise in the current at the working electrode is measured concomitant with anodic iron dissolution (active corrosion). This value determines the corrosion resistance but does not allow prediction of the stability of SS in a certain environment. Therefore, the OCP needs to be determined. The OCP is monitored without adding an external potential or current. The circuit is supposed to be open. If the OCP is significantly below the pitting potential the SS will be passive under this specific environmental condition. If the OCP is around or above the pitting potential, it is highly likely that the SS will actively corrode under these conditions (Silverman 2011). As a consequence, only in combination with the pitting potential OCP allows a valid risk assessment. However,

both techniques cannot assess localized corrosion phenomena or identify anodic and cathodic regions on the surface accompanied by metabolic products like manganese oxides. To elucidate the influence of microorganisms on the surface characteristics of SS, scanning Kelvin probe force microscopy (SKPFM) is the method of choice (Little et al. 2011). The SKPFM is based on the classical vibrating-plate Kelvin method but with an superior resolution (≤ 1 µm) and the advantage to record topography at the same time (Nonnenmacher et al. 1991; Rohwerder and Turcu 2007). SKPFM imaging involves a two-step scan of each line (trace and re-trace). First, the topography is determined in intermittent contact mode (trace). As an illustration see the schematic representation of the JPK™ SKPFM setup used in this study (Figure 6). In the subsequent second scan (re-trace), after the conductive cantilever was fixed at a defined height above the sample surface, the contact potential difference (CPD) between the tip and the sample can be determined. During this scan a defined voltage is applied to the cantilever consisting of an alternating- and direct current. The physical oscillation generated by the piezo during intermittent contact mode is turned off. The difference in electrical charge between the tip and the sample results in a capacitive force, which is defined by the tip voltage, the tip capacitance and the surface potential. Without applying an external force, the cantilever starts to oscillate driven by the harmonic force established between the tip and the surface. For each point, the direct current component applied to the tip is changed, until the force between the tip and the surface is zero. In consequence, the tip stops oscillating. The change in the direct current equals the surface potential (Kratochvílová et al. 2009; Rohwerder and Turcu 2007).

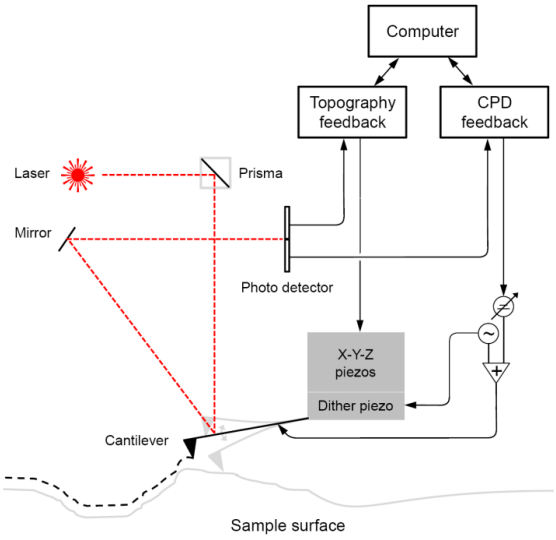

Figure 6: Schematic representation of the JPK™ SKPFM setup. The laser is focused by a prism onto the cantilever and the beam reflection is directed by a mirror to the photo detector. The laser position is converted into an electrical signal and feed into the computer by the topographic feedback which controls the X-Y-Z piezos. The Z-movement of the piezo is recorded to construct the topographic profile. The second CPD feedback is used to map the surface potential. The CPD feedback controls the direct current and records the voltage necessary to stop cantilever oscillation.

2 Aims of the study

Corrosion processes of e.g. stainless steel (with regard to this study) possess a severe economic impact for industry and a technological challenge for researchers. Microbiologically influenced corrosion (MIC) has been underestimated in science and industry for a long time. Nowadays it is generally accepted that microorganisms play a pivotal role in influencing and accelerating the corrosion processes. MIC is associated with biofilm formation leading to (in)direct changes of the materials surface characteristics. Although the role of biofilm formation in MIC is acknowledged and scientific fundamentals have been advanced over the past decades, there are still open questions. The following aims were subsequently addressed in this study to elucidate the importance of biofilm formation and manganese oxidation on the corrosion of stainless steel exemplified with *Leptothrix discophora* SS-1 as a model organism:

- Influence of two different growth media and the supplementation of manganese ions on the growth of *L. discophora* SS-1

- Influence of different growth conditions on the (bio)chemical composition of the EPS of cells of *L. discophora* SS-1

- Visualization of biofilm formation of cells of *L. discophora* SS-1 by DNA stains combined with fluorescent lectin binding analysis

- Characterization of the localized effects of cells of *L. discophora* SS-1 and manganese oxides on the surface potential of stainless steel with particular regard to its electrochemical corrosion.

3 Materials and methods

3.1 Chemicals

If not otherwise stated all chemicals listed in Table 2 were of analytical grade.

Table 2: List of chemicals

Substance	Formula	Manufacturer
4-(2-Hydroxyethyl)-1-piperazine-1-Ethanesulfonic acid (HEPES)	$C_8H_{18}N_2O_4S$	Applichem
4′,6-Diamidine-2-phenylindole (DAPI)	$C_{16}H_{15}N_5$	Sigma
4-Amino benzoic acid	$C_7H_7NO_2$	Merck
Acetic acid anhydride	$C_4H_6O_3$	Sigma
Acetone (technical grade, >99 %)	C_3H_6O	AppliChem
Ammonium acetate	$C_2H_7NO_2$	Sigma
Ammonium chloride	NH_4Cl	Roth
Ammonium sulfate	$(NH_4)_2SO_4$	
Biotin	$C_{10}H_{16}N_2O_3S$	Roth
Bovine Serum Albumin (BSA)		Merck
Bradford Protein Assay Kit		BioRad
β -Nicotinamide dinucleotide phosphate (β-NADP)		Sigma
β -Hydroxydiphenyl	$C_{12}H_{10}O$	Sigma
Calcium chloride dihydrate	$CaCl_2$ x $2H_2O$	Roth
Deionized water		
D-Glucuronic acid sodium salt monohydrate	$C_6H_9NaO_7$ x H_2O	Sigma
Dichloromethane	CH_2Cl_2	Merck
Dipotassium hydrogen phosphate	K_2HPO_4	Merck
Dimethyl sulphoxide (DMSO)	C_2H_6OS	Merck
Disodium carbonate	Na_2CO_3	Sigma
Disodium hydrogen phosphate	Na_2HPO_4	Merck
Disodium sulphate, anhydrous	Na_2SO_4	Roth
DOWEX Marathon™ C sodium form	$C_{10}H_{12}\cdot C_{10}H_{10}\cdot C_8H_8\cdot Na$	Sigma
Ethanol (≥ 96 %)	C_2H_6O	
Ferric ammonium citrate	$C_6H_8FeNO_7$	Sigma
Folin-Ciocalteus phenol reagent		Merck
Glucose	$C_6H_{12}O_6$	Sigma
Glucose-6-phosphate (G6P)	$C_6H_{13}O_9P$	Sigma
Glucose-6-phosphate dehydrogenase (G6PDH) from *Leuconostoc mesenteroides*		Sigma

Table 2 continued

Glutardialdehyde (25 %)	$C_5H_8O_2$	Merck
Humic acid		Sigma
Iron(II) sulphate heptahydrate	$FeSO_4$ x 7 H_2O	Roth
Iron(II) chloride tetrahydrate	$FeCl_2$ x 4 H_2O	Riedel de Haën
Iron(III) chloride hexahydrate	$FeCl_3$ x 6 H_2O	Roth
L-Ascorbic acid	$C_6H_8O_6$	Sigma
Manganese(II) nitrate	$Mn(NO_3)_2$	Merck
Magnesium chloride	$MgCl_2$	Sigma
Magnesium sulfate heptahydrate	$MgSO_4$ x 7 H_2O	RTY Ltd.
Manganese sulfate monohydrate	$MnSO_4$ x H_2O	Fluka
Methanol	CH_3OH	Roth
Methanolic HCl	HCl in CH_3OH	Merck
Native olive oil		
n-Hexane	C_6H_{14}	Roth
n-methylimidazole	$C_4H_6N_2$	Sigma
Peptone		Merck
Phenol	C_6H_6O	Merck
Phosphoric acid (15 %)	H_3PO_4	Roth
PicoGreen© reagent		Invitrogen
Potassium chloride	KCl	Roth
Potassium dihydrogen phosphate	KH_2PO_4	Merck
Potassium hydrogen phthalate	$C_{12}H_{25}KO_4S$	Sigma
Potassium hydroxide	KOH	Sigma
Sodium borohydride	$NaBH_4$	Sigma
Sodium carbonate	Na_2CO_3	Sigma
Sodium chloride	NaCl	Sigma
Sodium dihydrogen phosphate	NaH_2PO_4	Merck
Sodium hydrogen carbonate	$NaHCO_3$	Sigma
Sodium hydrogen phthalate	$C_8H_5KO_4$	Sigma
Sodium hydroxide	NaOH	Sigma
Sodium pyruvate	$C_3H_3NaO_3$	Merck
Sodium tartrate, anhydrous	$C_4H_4O_6Na_2$	Sigma
Sodium tetraborate decahydrate	$Na_2B_4O_7$ x 10H2O	Sigma
Sulphuric acid	H_2SO_4	Roth
Syto9™		Molecular Probes
Trifluoroacetic acid	$C_2HF_3O_2$	Sigma
TRIS hydrochloride	$C_4H_{11}NO_3 \cdot HCl$	Roth
Trisodium phosphate dodecahydrate	Na_3PO_4 x $12H_2O$	Merck
Ultrapure water	Type 1	Merck

Table 2 continued

Vanillin	$C_8H_8O_3$	Sigma
Vitamin B_{12}	$C_{72}H_{100}CoN_{18}O_{17}P$	Sigma
Yeast extract		Roth

Table 3 lists the fatty acid methyl ester kits used for the quantification of lipids by gas chromatography.

Table 3: List of fatty acid methyl ester kits for lipid analysis by gas chromatography

Substance	Product no.	Manufacturer
Fatty Acid Methyl Esters, Saturated Straight Chain	ME7-1KT	Supelco
Fatty Acid Methyl Esters, Saturated Straight Chain	ME19-1KT	Supelco
Fatty Acid Methyl Esters, Unsaturated Kit	ME14-1KT	Supelco

3.2 Cultivation media

Minimal Salts Vitamin Pyruvate Medium 2 (MSVP-2)

The MSVP-2 medium (Table 4) was used for cultivation of *L. discophora* (El Gheriany et al. 2009). For electrochemical measurements a total amount of 0.35 % (w/v) NaCl was adjusted to deliver sufficient amounts of chlorine ions to induce pit formation at given experimental setups (see chapter 3.10.1). For particular experiments, MSVP-2 was supplemented with 0.02 % (w/v) yeast extract. If not otherwise stated the MSVP-2 medium was used without addition of supplements. The HEPES buffer was prepared first with 200 mL di. water, afterwards, all other components were added and filled up with di. water to 1000 mL. The pH (MIKK 3.069, WTW) was adjusted at 7.0 with NaOH before autoclaving (FVA3/a1, Fedegari) at 121°C and 1.5 bar for 20 min. After autoclavation, 10 mL of a filter sterilized (0.22 µm, Millex®-GS, Roth) sodium pyruvate solution (100 g L^{-1}) and 20 µL of a filter sterilized (0.22 µm, Millex®-GS, Roth) vitamin solution containing biotin (120 mg L^{-1}) and vitamin B12 (250 mg L^{-1}) were added. MSVP-2 agar plates were prepared the same way with the addition of 0.2 mM Mn(II) (MnSO4), 18 g ml^{-1} Agar-Agar and 0.2 g ml^{-1} yeast extract.

Table 4: Composition of MSVP-2 medium

Substance	Formula	Weight
Calcium chloride dihydrate	$CaCl_2$ x $2H_2O$	58.8 mg
Magnesium sulfate heptahydrate	$MgSO_4$ x $7H_2O$	59.15 mg
Ammonium sulfate	$(NH_4)_2SO_4$	240.49 mg
Potassium dihydrogen phosphate	KH_2PO_4	19.44 mg
Iron(II) sulfate heptahydrate	$FeSO_4$ x $7H_2O$	2.78 mg
HEPES	$C_8H_{18}N_2O_4S$	2383.1 mg
Disodium hydrogen phosphate	Na_2HPO_4	32.9 mg
Di. water	H_2O	Ad to 1000 mL

B12 *L. discophora* culture medium

B12 medium was prepared according to Table 5 and used to grow precultures of *L. discophora* as inoculum.

Table 5: Composition of B12 medium

Substance	Formula	Weight
Yeast extract		1 g
Peptone		1.5 g
Magnesium sulfate heptahydrate	$MgSO_4$ x $7H_2O$	0.2 g
Calcium chloride dihydrate	$CaCl_2$ x $2H_2O$	0.05 g
Ferric ammonium citrate	$C_6H_8FeNO_7$	0.05 g
Iron(III) chloride hexahydrate	$FeCL_3$ x $6H_2O$	0.05 g
Di. water	H_2O	Ad to 1000 mL

All components were mixed in 200 mL di. water and filled up to 1000 mL. The pH was adjusted to 7.1 with NaOH before autoclaving at 121°C and 1.5 bar for 20 minutes.

3.3 Growth conditions of *L. discophora*

L. discophora SS-1 was selected as a model organism to simulate MIC by MOMO and obtained from the Czech Culture Collection of Microorganisms (CCM). Stock cultures were kept on MSVP-2 agar plates (see chapter 3.2). To ensure purity, 13-streak agar plates were prepared from single colonies once a month throughout the study. Prior to each experiment, a single colony was used as an inoculum for liquid cultures in B12 medium. Cultures were grown in 100 mL long neck culture flasks on a rotary shaker (Multitron, Infors HT) at 110 rpm at 28 °C for 2 d. Harvesting of the cells was done in 50 mL centrifuge tube (Corning) by centrifugation (Biofuge 28RS, Heraeus) at 10,000 g for 10 min at room temperature. The

supernatant was discarded to remove remaining components from the B12 medium. Subsequently, the cell pellet was resuspended in MSVP-2 medium and used as an inoculum for the following experiments. Total cell count was determined (see chapter 3.6). Initial cell numbers are described in the respective chapters.

3.4 Preparation of stainless steel coupons

In this study austenitic stainless steel (SS) with the material number 1.4301 and the quality class X5CrNi18-10 was used. Analyses of the typical chemical composition yielded in 0.07 % C, 1 % Si, 2 % Mn, 18 % Cr and 9 % Ni. The metal was provided by the DECHEMA Research Institute (Frankfurt/Main, Germany) as sheets (coupons) of the dimension 20 x 15 x 1 mm or 200 x 25 x 1 mm . The little coupons were used for biofilm studies while the larger ones were used in EPS extraction experiments.

The coupon surface was pretreated by using different grades of polishing, depending on the type of experiment. For all experiments except SKPFM the final polishing grade was P180, for SKPFM experiments involving biofilm formation the final polishing grade was P1200. For SKPFM experiments involving coupons sputtered with gold, mirror polishing with a final grade of 1 µm diamond polish was used.

All coupons were manually wet-ground on a rotating polishing machine (LaboPol-1, Struers) using abrasive silicon carbide (SiC) P180 paper, rinsed with di. water, cleaned with ethanol (70 %) and degreased in an ultrasonic bath (Digitech D-510H, Bandelin Sonorex) for 15 minutes after submerging in acetone. Finally, coupons were dried with a hair dryer to remove remaining acetone and stored in a desiccator. To achieve P1200 grade, coupons were successively wet-ground with P500, P800 and P1200 SiC paper (Struers). Mirror polish was achieved after successive polishing to P1200, cleaning and degreasing the coupons, polishing with an oil based 6 µm polycrystalline diamond suspension (ATM) using medium-haired artificial silk polishing cloth (MD-Floc, Struers) with intermittent cleaning and degreasing and a final polishing step with 1 µm diamond suspension (ATM) using short-haired artificial silk polishing cloth (MD-Nap, Struers). Finally, coupons were cleaned and stored as described above.

Ready prepared coupons were heat sterilized using a drying oven (ST5050, Heraeus) at 120 °C for 8 h in aluminum foil covered glass vessels, each placed in a glass container filled with dry silica gel (Orange 2-5 mm, Roth) to absorb humidity.

3.5 Leucoberbelin blue assay

To determine manganese oxidation in biofilms, a drop of an aqueous solution of leucoberbelin (4 % w/v) was mixed directly with the biofilm material. In the presence of Mn(III) or Mn(IV) ions leucoberbelin is oxidized to a blue colored complex (Krumbein and Altmann 1973) indicating manganese oxidation activity.

3.6 Determination of total cell count

Total cell count (TCC) of the planktonic cells was determined using a "Thoma" type haemocytometer (Thoma counting chamber, Assistent) with 400-fold magnification under phase contrast (Leica DMLS, Leica). Cells were counted in 5 individual counting fields and averaged (depth = 0.100 mm, volume = 0.0025 m^2).

3.7 Analysis of generation time

3.7.1 Determination of generation time

The experiment was performed in 500 ml screw cap glass bottles in duplicates stirred on a magnetic stirrer (RCT REO, Ikamag) at 300 rpm. Growth was monitored in B12 medium and in MSVP-2 medium with and without 0.2 mM Mn(II) at 28 °C. MSVP-2 medium was supplemented with 0.02 % yeast extract. To cover full sampling period of 24 h, time delayed batch cultures were set up to omit sampling during night time hours. These cultures were inoculated from the same inoculum but started with a delay of 12 h. Results of delayed cultures were combined to gain coherent growth curves. Samples were taken and bacterial enumeration was carried out by total cell count analysis (TCC). The Determination of the specific doubling time was calculated by $\mathbf{t = ln^2\ k^{-1}}$, with k being the specific growth rate. It corresponds to the slope of the logarithmic plot of cell number vs. time. Similar experiments were performed with the addition of 0.2 mM Mn(II) to the growth media. The bacterial formation of MnO_2 was monitored by analyzing the decrease of the manganese supplement in the medium via atomic absorption spectroscopy (AAS). Inoculum was prepared as described in chapter 3.3, initial cell numbers were determined directly after inoculation and given in chapter 4.1.1 and 4.1.2.

3.7.2 Atomic Absorption Spectroscopy

The bacterial formation of MnO_2 was monitored by analyzing the decrease of the manganese supplement in the medium with the help of an atomic absorption spectroscope (1100B, Perkin-Elmer) powered by an acetylene/air flame (modified after (Nelson et al. 1999). An aliquot of the culture was centrifuged (18/14, VWR) at 10,000 g for 15 min. The supernatant was diluted 1:1 with 0.005 M H_2SO_4 and taken for measurement of (soluble) manganese ions.

A $Mn(NO_3)_2$ solution was used as a standard. A 5-point calibration was performed ranging from 0 - 5 mg L^{-1} Mn.

3.7.3 Determination of ATP and protein content

The effect of Mn(II) on the total ATP content of cell cultures of *L. discophora* was tested. The inoculum was prepared as described in chapter 3.3, the initial cell number was 10^6 cells mL^{-1}. Cells were grown in 100 mL long neck culture flasks filled with 50 mL MSVP-2 medium at 28 °C for 24 h. To analyze the total ATP content, stationary phase cultures were homogenized (to guarantee a homogenous dispersion of cells in the liquid) after 24 h of growth using a homogenizer (Ultra Turrax T25, IKA) equipped with a dispersion tool (S 25 N - 18 G, IKA) for 20 sec. at 18,000 rpm. Samples were measured in duplicates. Quantification was done using the luciferase-based Promega BacTiter-Glo™ microbial cell viability assay. The assay was carried out according to the manufacturer's instructions using a luminometer (Glomax 20/20, Promega). An ATP stock solution from Promega was used as a standard. A 4-point calibration was performed ranging from 10-1000 nM. To compare ATP with the total protein content, protein measurements (see chapter 3.11.2) of the same aliquots with additional bead beading (HT 24, OPS Diagnostics) for 2 x 30 s at 6,800 rpm were performed.

3.8 Biofilm formation

3.8.1 Biofilms on floating filters and stainless steel coupons

Biofilms on floating filters

The floating filter cultivation method (de Bruyn et al. 1990) was used for microscopic investigations of *L. discophora* SS-1 biofilms and fluorescence lectin binding analysis (FLBA). A total of 10^8 cells of a liquid culture (prepared as described in chapter 3.3) were filtered onto a sterile polycarbonate membrane (0.2 µm Isopore, Millipore). The filter device consisted of a membrane filter holder connected to a vacuum pump (ME 2, Vaccubrand). The whole filter holder was sterilized with ethanol (70 %). After inoculation, the filters were washed with 2 mL of sterile di. water and transferred to 100 mL wide neck culture flasks filled with either B12- or MSVP-2-medium. The filters were incubated floating on top of the medium for 2 d at 28°C without shaking. For particular experiments, 0.2 mM Mn(II) were added and the presence of manganese oxides on the filter surface associated biofilms was verified with the leucoberbelin blue assay (3.5). If not otherwise stated, the media were prepared without the addition of Mn(II).

Biofilms on stainless steel coupons

Stainless steel coupons were used as model surface for MOMO attachment, which might cause MIC on this particular working material. SS coupons were prepared as described in chapter 3.4 and used for microscopic investigations of *L. discophora* SS-1 biofilms and FLBA. SS coupons were glued (Repair Extreme, Pattex) in pairs on 76x26 mm microscope slides, three of these slides were placed facing up at the bottom of a cylindrical 1.5 L glass vessel. The glass vessel was aerated with pressurized air, filled with 1 L MSVP-2 medium and inoculated with 10^6 cells mL^{-1} (prepared as described in chapter 3.3). The system was incubated at 28°C for maximal 10 d. For particular experiments, 0.2 mM Mn(II) were added and the presence of manganese oxides in biofilms on the SS coupon was verified with the leucoberbelin blue assay (3.5). The media were prepared without the addition of Mn(II), unless otherwise stated.

Biofilms grown on stainless steel coupons in a flow chamber

For contact potential difference mapping a flow chamber was used to simulate environmental conditions. SS coupons were prepared as described in chapter 3.4, one SS coupon was glued to a 76x26 mm microscope slide and 4 of these microscope slides were placed into a flow chamber. The flow chamber was a modified Hellendahl staining box (63 x 58 x 98, Roth) with two hose connectors, one positioned at the bottom (liquid inflow) and the other at the top (liquid outflow). This particular setup enabled the liquid vertically passing the coupons and leaving the chamber at the top, which resulted in homogenous flow condition. A homogenous distribution was tested and verified beforehand by the use of a colored liquid pumped through the chamber. The chamber had a total volume of 90 mL. It was connected to a pump (IPC 8, Ismatek), the average medium exchange rate was 270 mL h^{-1}. The chamber was supplied with fresh MSVP-2 medium and the waste was collected. The medium was not circulated and therefore only fresh medium passed the coupons. After initial inoculation of MSVP-2 medium with 10^8 cells mL^{-1} (prepared as described in chapter 3.3), the medium was pumped through the chamber for 24 h and cells could attach and grow on the coupons. After 24 h the medium was replaced with cell free MSVP-2 medium, the chamber was flushed with this medium to remove residual planktonic cells. Further on, only fresh medium was supplied, preventing further growth and attachment from the liquid phase to the coupons. Therefore, the biofilm was formed presumably by cells attached on the coupons after initial inoculation. The experiment was conducted for 7 days at 28 °C and the medium was supplemented with 0.2 mM Mn(II). The presence of manganese oxides in the biofilm on the SS coupon was verified with the leucoberbelin blue assay (3.5).

3.8.2 Visualization of biofilm formation and fluorescence lectin binding analysis

Single cells and biofilms on floating filters and SS coupons were stained using the red fluorescent nucleic acid stains Syto61 or Syto83 (Molecular Probes). Visualization of the EPS matrix was done using FITC labeled lectins. The lectins used in this study are listed in Table 6. In FLBA, nucleic acid stains were used as a counter stain to visualize cells. Syto61 (0.5 mM) was used on floating filters and Syto83 (0.5 mM) on SS coupons. Filters and coupons were rinsed with 0.5 mL of di. water before application of the fluorescent dyes. The respective nucleic acid dyes were applied with a residence time of 15 min. The lectins were applied with a concentration of 50 µg/mL and diluted in the appropriate buffer and centrifuged for 5 min at 13,000 rpm (18/14, VWR). The supernatant was used to reduce nonspecific background and protein aggregates formed during storage. After incubation for 60 min in the dark, coupons were rinsed with the appropriate buffer and air-dried for 5 min. One drop of an antifadent mounting solution (Citifluor TM AF2, Science Services) was added to improve signal preservation. Visualization of single cells and biofilms was done using either an epifluorescence- or a confocal laser scanning microscopy as described in chapter 3.9.1 or 3.9.2, respectively. Both techniques were used to overcome certain methodical limitations, the type of microscope is stated in each experiment.

Table 6: Comprehensive list of all lectins (EY Laboratories) used in this study including: name, abbreviation, origin, specified carbohydrate specificity and the buffer composition used to dissolve the respective lectins

Name Abbreviation	Origin	Carbohydrate Specificity	Buffer
Concanavalin A **ConA**	Jackbean (Canavalia ensiformis)	Mannose, Glucose	0.05 M Tris, 0.15 M NaCl, 0.004 M $CaCl_2$ (pH 7.0-7.2)
Griffonia simplicifolia lectin I **GS-I**	Shrub (Griffonia simplicifolia)	Melibiose, Galactose	0.01 M Phosphate, 0.15 M NaCl, 0.5mM $CaCl_2$, (pH 7.2-7.4)
Griffonia simplicifolia lectin I **GS-II**	Shrub (Griffonia simplicifolia)	N-acetylglucosamine (GlcNAc)	
Wheat germ agglutinin **WGA**	Wheat germ (Triticum vulgare)	GlcNAc	0.01 M Phosphate, 0.15 M NaCl (pH 7.2-7.4)
Cauhinia purpurea agglutinin **BPA**	Camel´s foot tree (Bauhinia purpurea)	N-acetylgalactosamine (GalNAc)	
Soybean agglutinin **SBA**	Soybean (Glycine max)	GalNAc, Galactose	
Ulex Europaeus agglutinin **UEA-I**	Gorse (Ulex europaeus)	Fucose	
Dolichos biflorus agglutinin **DBA**	Horse gram (Dolichos biflorus)	GalNAc	
Phytolacca americana lectin **PWM**	Pokeweed (Phytolacca americana)	GlcNAc, N-Acetyllactosamine	
Phaseolus vulgaris Erythroagglutinin **PHAE-I**	Red kidnex bean (Phaseolus vulgaris)	GalNAc, GlcNAc	
Peanut agglutinin **PNA**	Peanut (Arachis hypogaea)	Galactose	0.02 M Sodium Bicarbonate (pH 9.0-9.5)
Maclura pomifera agglutinin **MPA**	Osage orange (Maclura pomifera)	GalNAc, Galactose	
Limulus polyphemus agglutinin **LPA**	Horseshoe crab (Limulus polyphemus)	Sialic acid	0.05 M Tris, 0.15 M NaCl, 0.01 M $CaCl_2$ (pH 8.0)

3.9 Microscopic imaging techniques

3.9.1 Epifluorescence Microscope

The epifluorescence microscope model Axio Imager A1m (Zeiss) was used, equipped with a camera model Axio Cam MRm, a mercury lamp model HBO100 and a set of a Epiplan Neofluar lenses ranging from 20-100x magnification (Zeiss). The microscope was further equipped with three filter sets for DAPI (exciter G 365 nm, beam splitter FT 395 nm, emission BP 445-450 nm), FITC (exciter BP 450-490 nm, beam splitter FT 510 nm, emission BP 515-565 nm) and TRITC (exciter BP 525-550 nm, beam splitter FT 570 nm, emission BP 605-670 nm). The software was AxioVision 4.8 (Zeiss) and processing of images was done using ZEN 2 (Zeiss).

3.9.2 Confocal Laser Scanning Microscopy

The confocal laser scanning microscope (CLSM) model Axiovert 100M (Zeiss) was used, equipped with a camera model AxioCam MRn, an air lens model N-Achroplan 20x/0,45Pol, LD-Achroplan 40x/0,6cor and oil lens model Plan-Neofluar 100x/1,3 Oil. For excitation, different lasers were used: an argon laser with an excitation wavelength of 488 nm and two helium-neon lasers with an excitation wavelength of 543 nm and 633 nm, respectively. Pictures were taken with either a 20x/0.45 air, 40x/0.6 air or 100x/1.3 oil lens. Red TRITC dyes (e.g. Syto61 and 83) were excited at a wavelength of 543 nm and emission was monitored with a long pass (LP) 560 filter. Green FITC dyes (e.g. Syto9 and lectins) were excited at 488 nm and emission was monitored with a band pass (BP) 505-530 filter. Reflectance imaging to visualize the surface structure of SS coupons was performed with the 633 nm laser without any filter set. The software used was LSM 510 4.2 (Zeiss) and processing of images was done using ZEN 2 (Zeiss).

3.10 Corrosion analysis

3.10.1 Open circuit- and pitting potential determination

Electrochemical parameters like open circuit- (OCP) and pitting potential (E_{pit}) enhance our knowledge about the corrosion resistance and behavior of steel in certain environments. Therefore, experiments were carried out elucidating the effect of *L. discophora* SS-1 biofilm formation on the OCP and E_{pit} with and without active manganese oxide deposition on the steel surface. A sterile setup served as control.

The following classical 3 electrode-setup has been used for electrochemical measurements: reference electrode = $Hg/HgSO_4$; counter electrode = platinum 2 cm^2; working electrode = stainless steel cylinder (1.4301) 3.45 cm^2. The reference electrode was connected to a

Haber Luggin capillary filled with 0.2 M K_2SO_4. The capillary was positioned near the surface of the working electrode. The potential of the reference electrode was tested regularly (659 mV vs. standard hydrogen electrode SHE). All potentials given in this study refer to SHE. All electrodes were connected to a custom-made glass cover, placed on top of a flat flange glass reaction vessel DN 60. The vessels were filled with 200 mL MSVP-2 medium with or without 0.2 mM Mn(II) and either inoculated with 10^8 cells mL^{-1} or kept sterile (control). The medium was supplied with a total of 0.35 % (w/v) NaCl to deliver sufficient chloride ions to initiate pit formation. OCP was monitored for up to 6 days at 28 °C. Subsequently, linear polarization curves were started at OCP or up to 300 mV cathodic from OCP to determine E_{pit}. Linear polarization was done in anodic sweep direction with a scan rate of 0.2 mV sec^{-1}. Measurement was stopped at current-density i = 2 mA cm^{-2}. After the measurements, the presence of manganese oxides on the SS cylinders was verified with the leucoberbelin blue assay (3.5). The setup was connected to a potentiostat (Voltalab PST 050, Radiometer) and data were post processed using the manufacturer software (VoltaMaster 4, v 7.8, Radiometer) and the data analysis software Origin (Pro 2018, OriginLab). The OCP and E_{pit} values were determined manually from the dataset using the data analysis software Origin (Pro 2018, OriginLab).

3.10.2 Contact potential difference mapping

To analyze the effect of biofilm formation of *L. discophora* SS-1 and subsequent manganese deposition on the surface of stainless steel directly at the bacteria-substrate-interface, combined epifluorescence- and scanning Kelvin probe force microscopy (EFM & SKPFM) was used.

To visualize bacteria, surface topography and the surface potential a JPK instruments BioMAT Workstation coupled to an epifluorescence microscope (for EFM details see chapter 3.9.1) was used. The SKPFM was a JPK instruments NanoWizard II atomic force microscope equipped with a Kelvin force module, software was the SPM Control 3.3 (JPK). Images were processed using the JPK SPM Image processing software v 5.0. Surface topography was visualized in intermittent contact mode with a line rate of 0.3 Hz (tip velocities up to 50 µm s^{-1} in dependence of the x- and y-distance) and a target vibration amplitude of 5 V using conductive cantilever (e-tap 300, Mikromasch). The surface potential was determined as a contact potential difference (CPD) between the AFM tip and the cells or rather the substrate. CPD was monitored in hover mode with a 50 nm air gap at 5 V target vibration amplitude. This setup and the parameter given here was proven to deliver best results throughout this study and are adapted from a comprehensive study by (Kuklinski 2017). A shuttle stage was used to combine both instruments, EFM and SKPFM. The shuttle

stage allows an examination of the same spot with both techniques at the expense of a spatial deviation of less than 5 µm (Mangold et al. 2008).

SS coupons and the inoculum were prepared as described in chapter 3.4 and 3.3, respectively. Biofilms were grown in a flow chamber according to chapter 3.8.1 for up to 7 d. After formation of a bacterial layer the stainless steel (SS) coupons were rinsed with 0.5 mL sterile ultrapure water to remove planktonic cells and medium. Afterwards, the coupons were either covered with an aqueous solution of 0.1% (w/v) DAPI (4′,6-Diamidin-2-phenylindol, Sigma-Aldrich) containing 2 % (w/v) formaldehyde for 15 min to visualize single cells or with 6 µM SYTO9® solution (Molecular Probes) for 10 min to visualize mature biofilms including manganese deposits. Finally, coupons were rinsed twice and air dried. To visualize initial attachment, coupons were taken from the flow chamber after 1 h. The presence of manganese oxides in the biofilm attached on the SS coupon surface was verified with the leucoberbelin blue assay (3.5). Cell free manganese oxides were deposited on the SS surface to analyze and calibrate the effect of manganese oxides on the steel itself. Therefore, biologically oxidized manganese were spun for 15 sec at 1,500 g (18/14, VWR), the supernatant was discarded and the pellet was resuspended in di. water. The procedure was repeated three times to achieve cell free manganese oxides. The solution was dripped onto SS coupons and subsequently air dried. Manganese oxides were electrodeposited by cathodic electrosynthesis using a potentiostat (ER466, eDAQ) in a solution containing 0.1 M Mn(II) ions at pH 6.5 by applying a deposition voltage of 0.75 mV using two SS coupons as electrodes. The CPD between the single cell (Figure 50) and the surface was calculated by the difference of the average baseline value of the surface and the maximum of the peak along the position of the cell. The baseline and peak maximum were determined using the "PeakAnalyzer" tool of OriginPro 2018, calculation of the baseline was based on the 2nd derivative of the adjacent-average smoothing using 8 anchor-points, a window of 2 and a threshold of 0.2. This way, anchor-points were set only left and right of the cell, leading to a baseline of the surface omitting the CPD peak of the cell. Peak maximum was identified using the "peak maximum" method. An exemplary graphical illustration is given in Figure 7. The CPD of the cell free manganese oxides and the surface (Figure 51) was calculated in a similar way.

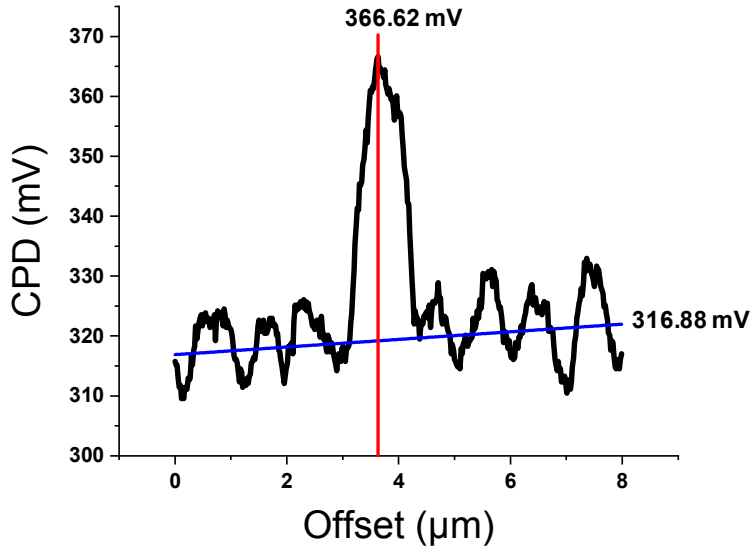

Figure 7: Graphical illustration of the CPD calculation: The blue line is the average of the surface baseline CPD signal (316.88 mV) and the red line indicates the maximum peak CPD signal (366.62 mV). The maximal CPD difference between the cell and the surface is calculated by subtracting the baseline from the peak maximum and is therefore 49.94 mV or approximately 50 mV.

The CPD between the surface and the electrochemically deposited manganese oxides (Figure 52) was calculated by the difference in the average CDP in the first 20 nm offset and in the last 10 nm offset. The first 20 nm were selected because they are strongly influenced by the manganese oxides and well before the boundary between the manganese surface and the SS surface. The steep increase in the CPD around 32 nm offset indicates the boundary line. The last 10 nm (70 - 80 nm offset) were selected because the shift to more positive CPD stopped and the CPD of the steel surface became constant, indicating a steel surface which is not influenced by manganese oxides. The CPD in Figure 54 (arrow 1-3) were calculated by single point measurements.

3.11 Analysis of extracellular polymeric substances

3.11.1 Conditions of growth and extraction procedure

Inoculum was prepared as described in chapter 3.3, the initial cell number was 2 x 10^7 cells mL^{-1}. In general, cultivation was performed at 28°C in 5 L screw cap glass vessels, each aerated with compressed air and mixed by stirring (300 rpm), until early stationary phase (determined by TCC) was reached (typically after 72 h). In total 4 different growth conditions and their influence on the composition of EPS from cells of *L. discophora* SS-1 were tested. First condition: *L. discophora* was grown in MSVP-2 medium without any supplementation, this condition is defined as "-SS -Mn" (without addition of Mn(II) or a steel surface). Second

condition: *L. discophora* was grown in MSVP-2 medium with addition of 0.2 mM Mn(II), this condition is defined as "-SS +Mn" (with addition of Mn(II) but without a steel surface). Third condition: *L. discophora* was grown in MSVP-2 medium without addition of 0.2 mM Mn(II) but in presence of 2000 cm^2 of a SS surface presented as 20 SS coupons standing upright in the culture flask, this condition is defined as "+SS -Mn" (without addition of Mn(II) but with a steel surface). Fourth condition: *L. discophora* was grown in MSVP-2 medium with addition of 0.2 mM Mn(II) and in presence of 2000 cm^2 of a SS surface presented as 20 SS coupons standing upright in the culture flask, this condition is defined as "+SS +Mn" (with addition of Mn(II) and with a steel surface). SS coupons were prepared as described in chapter 3.4. Total cell count was determined as described in chapter 3.6.

The whole culture (4.8 L) was collected via centrifugation (Sorvall RC6+, Thermo Scientific) at 13,000 g for 15 min at 4°C in 500 mL centrifugation bottles (3141, Nalgene). The supernatant was collected and filtered through polycarbonate membrane filters (0.22 µm, Millex®-GS, Roth) to eliminate residual cells. This cell free supernatant is considered as loosely bound EPS (LB-EPS), since it contains only EPS components being detached just by centrifugation or which were already secreted into the medium during growth. The resulting cell pellets after centrifugation were resuspended in PBS solution (Table 7) and washed by centrifugation at 10,000 g for 5 min at 4°C. The supernatant was discarded and the cell pellet was weight (wet weight). After weighing, PBS solution was added (typically 40 mL) to a final concentration of 25 mg cell pellet mL^{-1}. EPS extraction was performed by the addition of a cation-exchange resin (CER) to the PBS in the ration 1:2 w/v (CER:PBS). Prior to use, the CER was washed and activated for 1 h while stirring in PBS solution with a ratio of 1:3 (w/v). The buffer was removed by filtration. The suspensions of PBS, CER and cells were stirred (RTC REO, Ikamag) in 100 mL screw cap flasks for 3 h with 300 rpm at 4 °C in darkness. After 3 h, the suspension was decanted and centrifuged at 10,000 g (Biofuge 28RS, Heraeus) for 10 min at 4 °C. The supernatant was collected as well as filtered (0.22 µm, Millex®-GS, Roth) and the pellet was resuspended in an appropriate amount of PBS solution. The procedure was repeated twice, resulting in 3 cell free supernatants representing the tightly bound EPS (TB-EPS 1 - 3). A PBS solution with CER but without cells served as control and was treated as described above (PBS-Control).

Table 7: Composition of PBS extraction buffer (Frølund et al. 1996). The pH was adjusted to 7.0 using NaOH before autoclaving at 121°C and 1.5 bar for 20 min.

Substance	Formula	Weight
Trisodium phosphate dodecahydrate	Na_3PO_4 x $12H_2O$	0.328 g
Sodiumdihydrogen phosphate	NaH_2PO_4	0.552 g
Sodium chloride	NaCl	0.526 g
Potassium chloride	KCl	0.074 g
di. Water	H_2O	1000 mL

Dialysis of the supernatants and control were performed in dialysis membrane tubes (ZelluTrans, cut off 3.5 kDa, Roth) in ultrapure water at 4 °C with a sample/water volume ratio of 1:100 with stirring at ~200 rpm. The dialysis membranes were washed in di. water for 30 min, sterilized in ethanol (70 %) for 30 min and transferred and washed with sterile di. water prior to use. The water was changed repeatedly until there was no increase in conductivity (conductivity meter, WTW) of the dialysate within 2 h. After dialysis, samples and control were stored at 8°C. Determination of protein, carbohydrates, uronic acids, eDNA, manganese ions and total organic carbon (TOC) was done within 24 h after end of dialysis. Determination of dry weight was done by differential weighing of freeze dried (Lyophilisator, Alpha 2-4, Christ) samples and control (20 mL). Freeze dried samples and control were stored dry at room temperature until further use (extraction and determination of lipids).

3.11.2 Quantification of extracellular polymeric substances

All samples (LB- and TB-EPS as well as PBS-Control) were evaluated for the total amount of proteins, carbohydrates, uronic acids, eDNA, Glucose-6-phosphate dehydrogenase activity and lipids by photometric- and fluorometric methods. All measurements were done in triplicates in microtiter plates (Brand plates®, BRAND) using a microplate reader (Infinite Pro M200, Tecan Instruments). For each determination a calibration was performed in the respective microtiter plate. Centrifugation was done with a VWR 18/14 centrifuge and mixing with a Lab-Line Instruments titer plate shaker. Mixing and centrifugation was done in 2 mL reaction tubes (SafeSeal micro tube, PP, Sarstedt). All values for TB-EPS are given as a sum of the three extracts TB E1, E2, and E3. Control was treated accordingly. The signal of the control was subtracted from the respective result of the TB-EPS. This was done to balance non specific signals. For LB-EPS, ultrapure water was used as control and the signal of ultrapure water was subtracted from LB-EPS signal during sample processing. Manganese in the EPS was measured with AAS (3.7.2). Total organic carbon (TOC) was measured with a total organic carbon analyzer.

Carbohydrates

Carbohydrates were determined with a modified DuBois method (DuBois et al. 1956) using glucose as standard. 0.2 mL sample was mixed with 0.2 mL phenol solution (5 %). After mixing, 1 mL concentrated sulfuric acid was added and mixed. After 10 min of cooling to room temperature, the absorbance at 485 nm (carbohydrate) and at 570 nm (non-specific) of a 200 µL aliquot was measured. To obtain the carbohydrate values the OD_{570} was subtracted from the OD_{485}. Glucose was used as standard. A 6-point calibration was performed ranging from 0 - 100 µg mL^{-1}.

Proteins

Protein quantification was performed with the Bio-Rad Protein Assay kit which is based on the Bradford method (Bradford 1976) in microtiter plates. Therefore 40 µL of kit reagent solution were added to 160 µL sample or standard directly into the microtiter plate well and mixed. Incubation time was 15 min at room temperature on a titer plate shaker (mixing). Bovine serum albumin (BSA) was used as a standard. A 6-point calibration was performed ranging from 0 - 100 µg mL^{-1}.

Uronic acids

A modified microtiter plate assay (Blumenkrantz and Asboe-Hansen 1973) for the determination of uronic acids was used. Glucuronic acid was used as standard. To 200 µL sample or standard 1.25 mL of 0.0125 M $Na_2B_4O_7$ in concentrated H_2SO_4 (80 %) were added on crushed ice. The mixture was heated in a water bath (1003, GFL, Burgwedel) at 100 °C for 5 min with subsequent quick cooling in a water-ice bath. 200 µL were transferred into a microtiter plate and the background absorbance was measured at 520 nm. Then 5 µL 0.15 % (w/v) β-hydroxydiphenyl in 0.5 % NaOH solution were added and mixed. Incubation time was 5 min at room temperature on a titer plate shaker (mixing). After 15 min, absorbance was measured at 540 nm and the background absorption was subtracted from the second measurement. Glucuronic acid (D-Glucuronic acid) was used as a standard. A 7-point calibration was performed ranging from 0 - 100 µg mL^{-1}.

Glucose-6-phosphate dehydrogenase

Glucose-6-phosphate dehydrogenase (G6PDH) activity was measured using modified Ng & Dawes method (Ng and Dawes 1973) in microtiter plates. G6PDH was used as positive control (1 µg mL^{-1}). A substrate solution containing 0.1 mL TRIS/HCl-buffer (120 mM, pH 8.6), 0.075 mL glucose-6-phosphate (20 mM), 0.05 mL β-NADP (10 mM), 0.018 mL $MgCl_2$ (250 mM) and 0.047 mL ultrapure water was mixed with 10 µL of sample in a total volume of 300 µL per well. The absorbance at 340 nm of the mixture was measured at 37°C every min,

over a period of 2 h. The assay included ultrapure water as blank and a cell-free extract of *L. discophora* cells that was mixed with G6P and without G6P (negative control). The cell-free extract was obtained by sonification (Ultrasonic processor, UP 200 S, Dr. Hielscher) for 15 min of a resuspended cell pellet (PBS solution) after the third EPS extraction.

eDNA

The Quant-iT™PicoGreen®dsDNA Reagent and Kit was used to determine the DNA concentration of the samples by photometric measurement of fluorescence emission at room temperature. According to the high-range standard curve protocol, a DNA standard (2 µg mL^{-1}), a TRIS-HCl (10 mM)-EDTA (1 mM)-buffer and the PicoGreen® reagent (200 x dilution) were prepared. Volumes were adapted for microtiter plates. 100 µL sample and 100 µL reagent were mixed and incubated for 5 min before excitation of the samples at 480 nm and measurement of the fluorescence emission intensity at 520 nm. Bacteriophage lambda DNA was used as standard. A 5-point calibration curve was performed from 0 - 1 µg mL^{-1}.

Humic acids

Humic acids were determined using a modified Lowry assay (Frølund et al. 1996). 175 µL reagent (5.60 g L^{-1} NaOH, 26.49 g L^{-1} Na_2CO_3 and 2.41 g L^{-1} $C_4H_4O_6Na_2$ in di. water) were added to 125 µL sample or control. After 20 min incubation on a titer plate shaker at room temperature, 25 µL phenol reagent (2.5 mL Folin-Ciocalteus phenol reagent in 3 mL di. water) were added and samples were shaken again for 30 min. The absorbance was measured at 625 nm. BSA was used as standard. A 5-point calibration curve was performed from 0 - 150 µg mL^{-1}.

Total manganese (soluble Mn-ions)

The manganese content of the EPS was determined using AAS, for details see chapter 3.7.2. Only EPS extracts of cells grown with the addition of manganese and with or without the presence of a stainless steel surface were measured (+Mn -SS and +Mn +SS). The extracts (TB-EPS) were measured before and after filtration (0.22 µm, Millex®-GS, Roth) to exclude the effect of manganese binding to the filter. However, due to extraction procedure and centrifugation, no visible manganese oxide particles were present even before filtration. LB-EPS from the same conditions needed to be filtered to get rid of visible manganese oxide particles which would have perturbed the following measurement of manganese in EPS. All samples were measured after dialysis to get rid of soluble unbound manganese ions from the medium. Additionally, aliquots of the culture medium with cells and manganese oxides (+Mn ±SS) were measured to determine the recovery rate of total manganese. To determine total manganese, the manganese oxides needed to be dissolved in 0.05 M H_2SO_2 in order for

AAS to be detected as Mn(II) ions. 0.2 mM Mn(II) in the medium would lead to a maximum of 10.9 mg L^{-1} Mn in the culture medium.

Total organic carbon

Total organic carbon was measured using the catalytic combustion/NDIR method using a total organic carbon analyzer (TOC-V CPH, Shimadzu) and the TOC-Control software v 2.0 (Shimadzu). TB-EPS and LB-EPS as well as PBS-Control samples were diluted 1:10 in ultrapure water which was also used as blank. The TOC was determined indirectly by measuring total carbon (TC) and total inorganic carbon (TIC), the difference is TOC (TOC = TC - TIC). Potassium hydrogen phthalate ($C_6H_4(COOK)(COOH)$) was used to calibrate TC and a mixture of sodium carbonate (Na_2CO_3) and sodium hydrogen carbonate ($NaHCO_3$) was used to calibrate TIC. For TC and TIC a 5-point calibration curve ranging from 1 - 20 mg L^{-1} was performed.

Lipid extraction and analysis

For lipid analysis the lyophilized (Lyophilisator, Alpha 2-4, Christ) EPS extracts (TB-EPS E1 - E3) were merged. Transfer was done by rinsing with a total of 500 µL ultrapure water. For lipid extraction 500 µL of chloroform/methanol (2:1 v/v) solution was added. The suspension was mixed for 20 s and afterwards treated in an ultrasonic bath (Digitech D-510H, Bandelin Sonorex) for 5 min followed by centrifugation at 10,000 g for 5 min to allow phase separation This was repeated once with additional 500 µL solvent solution. The organic phase was collected. Analysis in micro titer plates was performed according to Cheng et al. (Cheng et al. 2011). Thus, 100 µL of sample or standard were transferred into microtiter plate wells. The plate was placed in an incubator (ST5050, Heraeus) at 85 °C until the organic solvent was fully evaporated. Subsequently, 100 µL of concentrated H_2SO_4 were added (mixed) and the plate was incubated for 45 min at 85 °C. The absorption at 540 nm was measured after cooling on ice to gain the background absorbance signal. Afterwards, 50 µL of 0.2 mg mL^{-1} vanillin in 17 % H_3PO_4 solution were added and absorption at 540 nm was measured again after 10 min incubation on the titer plate shaker at room temperature. The background absorbance was subtracted. Native olive oil was used as a standard and a 8 point calibration was performed from 0 - 340 µg mL^{-1}.

3.11.3 Identification of monomers in the extracellular polymeric substances

TB- and LB-EPS as well as a PBS-Control were analyzed for their lipid and sugar monomers. Gas chromatographic separation (Gas Chromatograph, Fractovap 4160, Carlo Erba) and identification was done as described (Gehrke et al. 2001), the software was Clarity Lite 5.0 (DataApex). Analysis was done from combined lyophilisates (TB-EPS E1 - E3) and from

lyophilisates of LB-EPS and PBS-Control. To gain sufficient amount for analysis, the EPS of 2 EPS extraction per growth condition were combined. For the different growth conditions see chapter 3.11.1. PBS-Control was treated identically to the EPS extracts to identify unspecific signals from the extraction procedure.

Fatty acids

To analyze lipid monomers by gas chromatography, the lipids need to be converted into fatty acid methyl esters (FAME) by methylation. 15 mg of the lyophilized EPS extracts were methylated with 200 µL methanolic HCl (3 M) at 90 °C for 2 h in a water bath (1003, GFL, Burgwedel). A total of 1 µmol undecanoic acid (C11:0) was added to each sample as internal standard beforehand. After cooling to room temperature, 500 µL ultra pure water was added to the FAME and mixed, followed by extraction of FAME by the addition of 500 µL n-Hexane. After mixing and phase separation (centrifugation at 1,000 g for 5 min, 18/14, VWR) the organic phase was collected. Extraction with n-Hexane was repeated twice and the collected organic phase was combined. The combined organic phase was washed acid-free by the addition of 500 µL ultrapure water. After phase separation (centrifugation at 1,000 g for 5 min), the water phase was discarded, this washing step was repeated twice. Finally, the organic phase (containing the FAME) was dried with $CaCl_2$ and concentrated to approx. 100 µL using a nitrogen (quality 5.0) stream.

Chromatographic separation was done using a FFAP CB stationary phase column with a total length of 25 m and 2 mL min^{-1} helium as mobile phase. Injection volume was 1 µL (split 1:25), injector temperature was 200 °C. To enhance peak separation a linear temperature gradient starting from 115 °C (kept constant for 2 min after injection) with an increase of 4 °C min^{-1} until 240 °C was used. A flame ionization detector (FID) using a hydrogen (30 mL min^{-1}) and artificial air (300 mL min^{-1}) flame was used as detector. FID temperature was 275 °C. A 5-point calibration was performed ranging from 0.4 - 20 µM. A 20 µM multi-standard with undecanoic acid as internal standard to calculate peak area correction was used for calibration. The multi-standard was prepared from individual standards ranging from C6:0 to C28:0 (Table 8). Annotation of the individual peaks was done based on their estimated retention index (Julin et al. 1983).

Table 8: Composition of the multi-standard with the individual fatty acids and their corresponding retention time and retention index. The retention index is estimated from retention time and number of carbon atoms (Julin et al. 1983).

Compound	Abbreviation	Ret. time (min)	Ret. index
Caproic acid	C6:0	1.6	600
Caprylic acid	C8:0	2.5	800
Nonanoic acid	C9:0	3.4	900
Capric acid	C10:0	4.8	1000
Undecanoic acid (internal standard)	C11:0	6.6	1100
Lauric acid	C12:0	8.9	1200
Myristic acid	C14:0	14.3	1400
Myristoleic acid	C14:1	15.4	1440
Palmitic acid	C16:0	19.8	1600
Palmitoleic Acid	C16:1	20.7	1633
Stearic acid	C18:0	25.2	1800
Elaidic acid	C18:1	25.8	1824
Linoleic acid	C18:2	27.1	1876
Nonadecanoic acid	C19:0	27.7	1900
Linolenic acid	C18:3	28.6	1936
Arachidic acid	C20:0	30.2	2000
Eicosenaoic acid	C20:1	30.7	2021
Heneicosanoic acid	C21:0	32.6	2100
Behenic acid	C22:0	35.0	2200
Erucic acid	C22:1	35.6	2221
Tricosanoic acid	C23:0	37.9	2300
Lignoceric acid	C24:0	41.3	2400

Neutral carbohydrate monomers

To analyze neutral carbohydrate monomers by gas chromatography, the carbohydrates needed to be hydrolyzed and derivatized into alditol acetates. 15 mg of the lyophilized EPS extracts were hydrolyzed with 150 µL trifluoroacetic acid (4 M) at 100 °C for 4 h in a water bath. After cooling to room temperature, the acid was evaporated on a rotary evaporator (IKA) and 200 µL ultrapure water were added to wash the sample (further evaporation of residual acid) and evaporated to dryness. This was repeated five times and the hydrolyzed sample was resuspended finally in 100 µL ultrapure water. A total of 5 µmol erythritol was added to each sample as internal standard beforehand. After addition of 100 µL NH_3 (1 N) and 100 µL $NaBH_4$ (200 mg mL^{-1} in dimethylsulfoxid, DMSO), the samples were incubated (reduction of the analyte) at 40 °C in a water bath (1003, GFL, Burgwedel) for 90 min. Afterwards, 100 µL acetic acid (18 M) was added drop wise to remove excess borohydride. For acetylation, 100

µL N-methylimidazole and 2 mL acetic acid anhydride were added and samples were incubated at 40 °C in a water bath for 1 h. After cooling to room temperature, 4 mL ultrapure water and 1 mL dichloromethane was added and the solution mixed. After mixing and phase separation (centrifugation at 1,000 g for 5 min, 18/14, VWR) the organic phase containing the alditol acetates was collected and dried with $CaCl_2$.

Chromatographic separation was done using a CP-Sil 8 CB stationary phase column with a total length of 30 m and 2 mL min^{-1} helium as mobile phase. Injection volume was 1 µL (split 1:10), injector temperature was 200 °C. To enhance peak separation a linear temperature gradient starting from 150 °C (kept constant for 10 min after injection) with an increase of 4 °C min^{-1} until 200 °C was used. A flame ionization detector (FID) using a hydrogen (30 mL min^{-1}) and artificial air (300 mL min^{-1}) flame was used as detector. FID temperature was 275 °C. A 4-point calibration was performed ranging from 0 - 10 µM. A 20 µM multi-standard containing rhamnose, fucose, ribose, arabinose, mannose, glucose and galactose with erythritol as internal standard to calculate peak area correction was used for calibration. Peaks were annotated based on their relative retention times compared to the internal standard.

4 Results

4.1 Influence of relevant factors on growth of *L. discophora* SS-1

In the following experiments the generation time and maximal cell density of *L. discophora* SS-1 in 2 different growth media with and without supplementation of Mn(II) was investigated. Additionally, the influence of Mn(II) supplementation on the ATP content of stationary cell cultures was assessed. The experiments were conducted to gain new insight into the physiological processes and optimize growth conditions for subsequent EPS- and biofilm formation analysis.

4.1.1 Growth of *L. discophora* SS-1 without addition of manganese

The generation time of *L. discophora* SS-1 was tested in B12 medium (standard medium suggested by the CCM) and MSVP-2, a minimal salt and vitamin medium optimized for growth of *L. discophora* in minimal medium by El Gheriany (El Gheriany et al. 2009). The growth of *L. discophora* SS-1 in batch cultures without addition of Mn in B12 and MSVP-2 was monitored for up to 78 h. To increase the statistical population, time delayed batch cultures were set up (refer to chapter 3.7.1).

Figure 8 shows the combined results in B12-medium of the two cultures, the initial cell numbers were 9.4×10^5 cell mL^{-1} and 3.8×10^5 cells mL^{-1}, respectively.

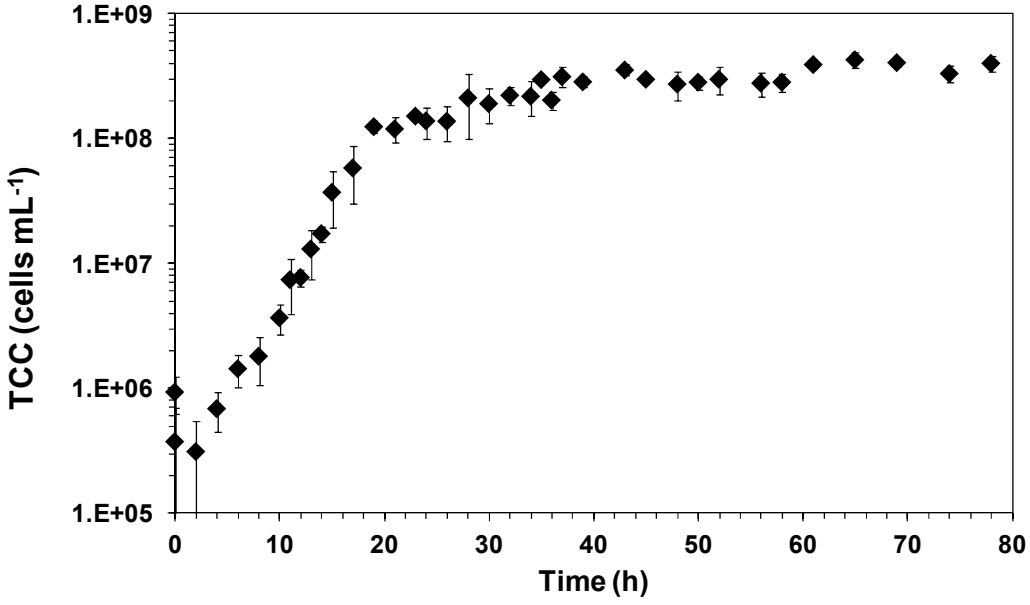

Figure 8: Growth of *L. discophora* SS-1 in B12-medium. 2 independent biological samples with 2 technical replicates each were grown in stirred (300 rpm) 500 mL flasks in B12-medium at 28 °C. Cell number (♦) was determined by total cell count (TCC).

After a 2 h lag phase, the cells entered the phase of logarithmic growth, which lasted from 4 h to 19 h. The specific growth rate *k* of *L. discophora* SS-1 was 0.35 h^{-1} and the doubling time was 2.0 h. Exponential growth stopped after 20 h and the cells entered the stationary phase. The maximum achieved cell number was $4.3x10^8$ cells mL^{-1}. Figure 9 shows the combined results in MSVP-2 medium of the two cultures, the initial cell numbers were $4.4x10^5$ cell mL^{-1} and $3.1x10^5$ cells mL^{-1}, respectively. After a 4 h lag phase, the cells entered the logarithmic growth phase, the stationary phase started after 23 h. The specific growth rate *k* of *L. discophora* SS-1 was 0.32 h^{-1} and the doubling time was 2.3 h. Exponential growth stopped after 20 h and the cells entered the stationary phase. The maximum achieved cell number was $2.7x10^8$ cells mL^{-1}.

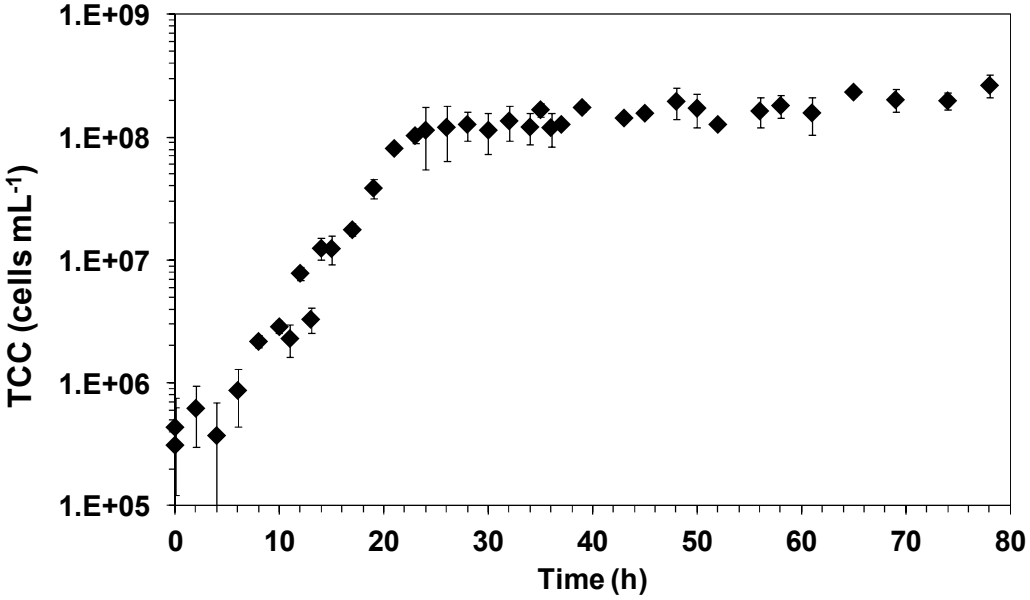

Figure 9: Growth of *L. discophora* SS-1 in MSVP-2 medium. 2 independent biological samples with 2 technical replicates each were grown in stirred (300 rpm) 500 mL flasks in MSVP-2 medium at 28 °C. Cell number (♦) was determined by total cell count (TCC).

4.1.2 Growth of *L. discophora* SS-1 in the presence of 0.2 mM Mn(II)

The generation time of *L. discophora* SS-1 was tested similarly to the process described in the chapter 4.1.1 but with the addition of 0.2 mM Mn(II) to each tested medium.

The growth of *L. discophora* SS-1 in batch cultures without the addition of Mn in B12 and MSVP-2 was monitored for up to 90 h. To increase the statistical population, time delayed batch cultures were setup (refer to chapter 3.7.1).

Figure 10 shows the combined results in B12-medium of the two cultures, the initial cell numbers were $1.4x10^6$ cells mL^{-1} and $2.7x10^6$ cells mL^{-1}, respectively.

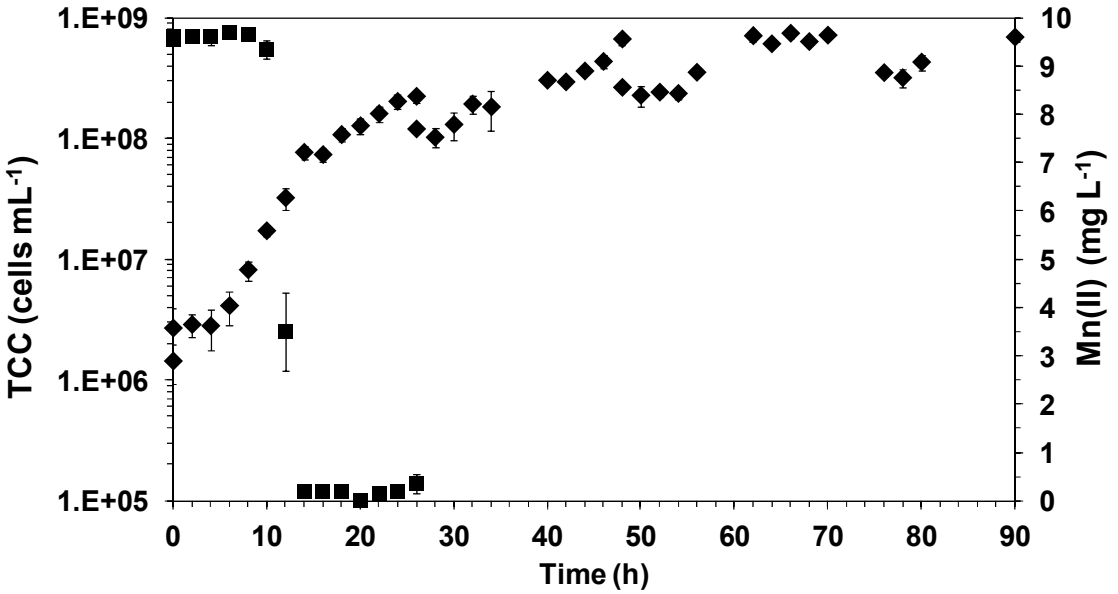

Figure 10: Growth and Mn oxidation of *L. discophora* SS-1 in B12-medium. 2 independent biological samples with 2 technical replicates each were grown in stirred (300 rpm) 500 mL flasks at 28 °C with addition of 0.2 mM Mn(II). Growth (♦) was determined by total cell count (TCC) and Mn oxidation (■) was monitored by AAS as decrease of the Mn(II) ion concentration.

After a 6 h lag phase, the cells entered the exponential growth phase which lasted until 26 h after inoculation. The specific growth rate *k* of *L. discophora* SS-1 was 0.23 h^{-1} and the doubling time was 3.0 h. Exponential growth stopped after 26 h and the cells entered the stationary phase. The maximum cell number reached $7.4x10^8$ cells mL^{-1}. Mn(II) concentration was monitored up to 24 h in 2 h-intervals. The initial concentration was 9.6 mg L^{-1} which remained constant for 10 h. Then, within 2 h (10 h to 12 h) the concentration dropped to 3.5 mg L^{-1} and reached near zero values after 14 h. Figure 11 shows the combined results in MSVP-2 medium of the two cultures, the initial cell numbers were $1.0x10^6$ cell mL^{-1} and $2.8x10^6$ cells mL^{-1}, respectively. The lag phase lasted for 8 h, afterwards, the cells entered the exponential growth phase which lasted until 26 h after inoculation. The specific growth rate *k* of *L. discophora* SS-1 was 0.22 h^{-1} and the doubling time was 3.2 h. Exponential growth stopped after 26 h and the cells entered the stationary phase. The maximum cell number reached $6.8x10^8$ cells mL^{-1}. Mn(II) concentration was monitored for 24 h in 2 h-intervals. The initial concentration was 9.5 mg L^{-1}, which remained constant for 8 h. Between 8 h and 16 h the concentration decreased to 0.7 mg L^{-1} and reached near zero values after 22 h.

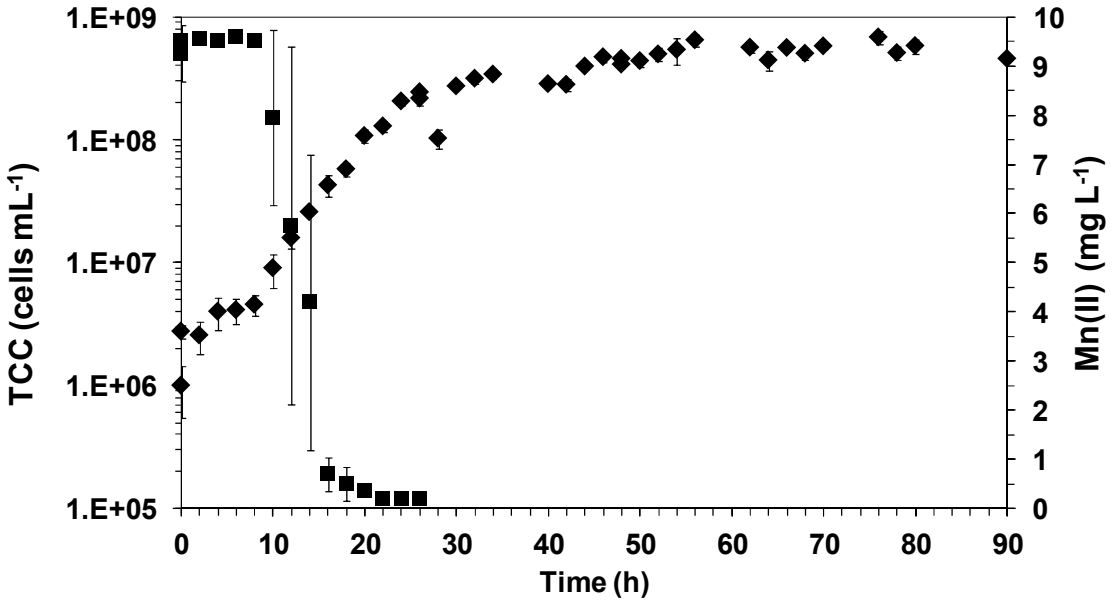

Figure 11 Growth and Mn oxidation of *L. discophora* SS-1 in MSVP-2 medium. 2 independent biological samples with 2 technical replicates each were grown in stirred (300 rpm) 500 mL flasks at 28 °C with addition of 0.2 mM Mn(II). Growth (♦) was determined by total cell count and Mn oxidation (■) was monitored by AAS as decrease of the Mn(II) ion concentration.

Cells of *L. discophora* SS-1 in medium B12 and MSPV-2 showed a fast oxidation of Mn(II) (i.e. decline in Mn(II) concentration) during early- to mid-logarithmic growth phase. Oxidation of manganese was accompanied by the formation of visible brown particles after 12 h to 14 h within all batches. The particles appeared refractive under the bright field microscope and were associated mostly to cell aggregates. However, some particles appeared free of cells. Table 9 summarizes the specific growth rate, doubling time as well as the maximum cell numbers reached under the different growth conditions.

Table 9: Specific growth rates (k), specific doubling times (t) and maximum cell numbers for the growth of L. discophora SS-1. Cells were grown in 500 mL Schott-flasks in duplicates in B12 and MSVP-2 medium at 28 °C with addition of 0.02 % yeast, each with and without the addition of 0.2 mM Mn(II)

Medium	k	t (h)	Maximum cell number (cells mL^{-1})
B12	0.35	2.0	$4.3x10^8$
MSVP-2 +0.02 % yeast	0.32	2.3	$2.7x10^8$
B12 + 0.2 mM Mn(II)	0.23	3.0	$7.4x10^8$
MSVP-2 +0.02 % yeast + 0.2 mM Mn(II)	0.22	3.2	$6.8x10^8$

The addition of Mn(II) to the growth medium resulted in an 1.0 h-increase of the doubling time in B12-medium and 0.9 h in MSVP-2 medium. Additionally, it lead to an increase in cell numbers in both media.

An additional experiment was performed to compensate for the relatively long sampling interval during the time period of manganese oxidation leading to a poor resolution due to insufficient set of data points (Figure 11). The experiment was repeated with an increased sampling rate (0.5 h) during the respective time period of manganese oxidation. The results are shown in Figure 12. The cultures were monitored continuously (no time delayed batch cultures). The start concentration of Mn(II) was 10.2 mg L^{-1} and remained constant throughout the lag phase until 6 h. Shortly after the initial cell growth started, a steep decrease in Mn(II) concentration was evident (manganese oxidation) until 11 h to 0.8 mg L^{-1}. After 15 h near zero values were reached. The maximal cell number was $3.1x10^8$ cell mL^{-1}.

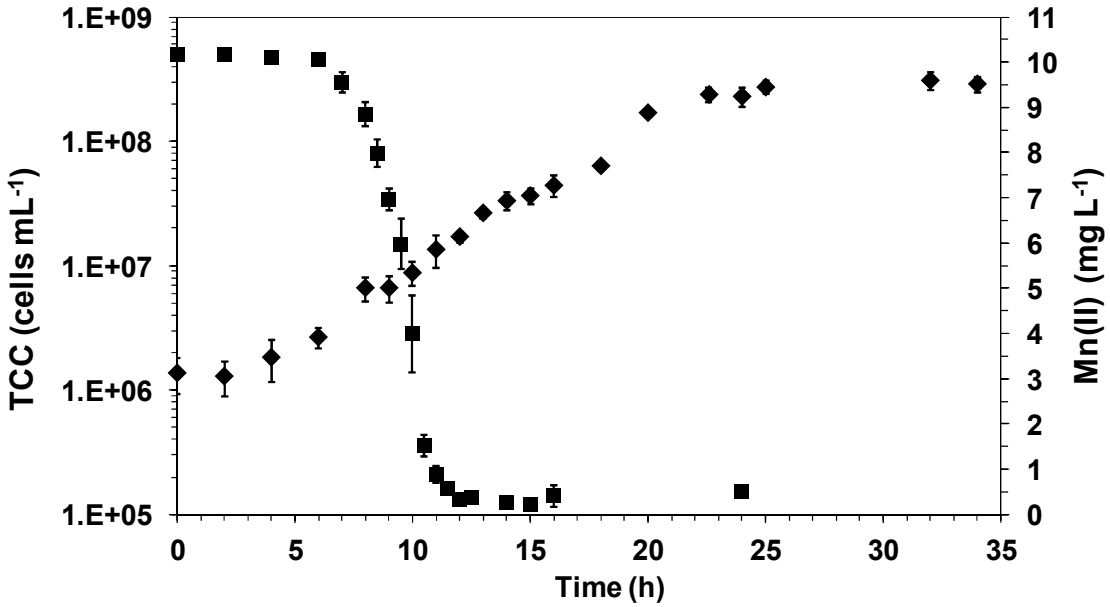

Figure 12: Growth and Mn oxidation of *L. discophora* SS-1 in MSVP-2 medium. 2 independent biological samples with 2 technical replicates each were grown in stirred (300 rpm) 500 mL flasks at 28 °C with addition of 0.2 mM Mn(II). Growth (♦) was determined by total cell count and Mn oxidation (■) was monitored by AAS as decrease of the Mn(II) ion concentration.

4.1.3 Influence of Mn(II) on the ATP content of cultures of *L. discophora* SS-1

Despite the influence of Mn(II) on the maximal cell number, generation time and specific growth rate, Mn(II) supplementation has also potentially influence on the ATP content of cultures of *L. discophora* SS-1. Therefore, the ATP and protein content of cultures of *L. discophora* SS-1 were analyzed. The results are shown in Figure 13.

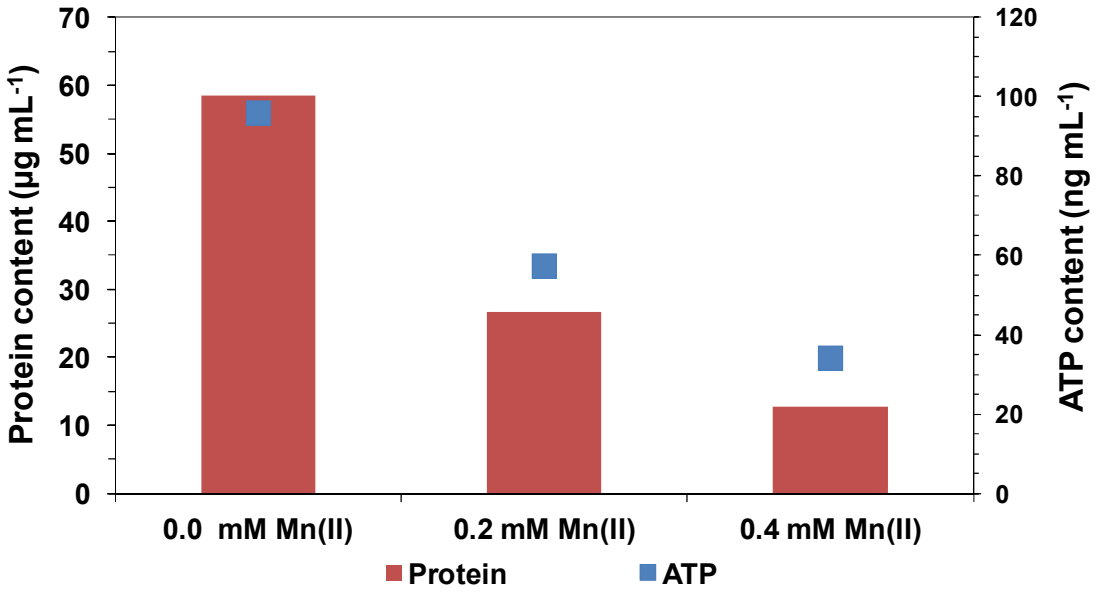

Figure 13: ATP and protein content of cultures of *L. discophora* SS-1 with different concentrations of Mn(II). The protein and ATP content of cultures of *L. discophora* SS-1 were determined at concentrations of 0.0, 0.2 and 0.4 mM Mn(II) supplementation. 2 independent biological samples with 2 technical replicates each were grown on a rotary shaker (120 rpm) in 100 mL flasks at 28 °C, SD (ATP) ≤ 5.8 ng mL^{-1}, SD (protein) ≤ 3.7 µg mL^{-1}. Sampling was done during the early stationary growth phase after 24 h. Cultures were homogenized before ATP measurement; protein measurement was done from the crude cell extract after cell lysis.

24 h after inoculation (in the early stationary phase), whole cultures of *L. discophora* SS-1 were homogenized (the entire culture flasks were homogenized, two individual culture flasks represent one data point), the ATP content measured and after additional bead beading of aliquots to get the crude cell extract the protein content was analyzed. Additionally, the cell numbers were determined. Comparative measurements with and without homogenization and cell lysis indicated that this is crucial to obtain reproducible results (data not shown). Cultures without the addition of Mn(II) showed an average content of 96.1 ng mL^{-1} ATP (SD 5.3 %), 58.6 µg mL^{-1} protein (SD 6.4 %) and a TCC of $3.8x10^8$ cells mL^{-1} (SD 11.5 %). The addition of 0.2 and 0.4 mM Mn(II) to the growth medium lead to a reduction of the ATP amount to 57.6 (SD 10.0 %) and 34.3 ng mL^{-1} (SD 6.8 %). Concomitantly, the protein content decreased to 26.8 (SD 7.7 %) and 12.8 µg ml^{-1} (SD 9.9 %) as well as the TCC to $2.1x10^8$ (SD 17.3 %) and $9.7x10^7$ cell mL^{-1} (SD 12.9 %) respectively.

4.2 Analysis of extracellular polymeric substances

The influence of four different growth conditions on the composition of EPS of *L. discophora* SS-1 was analyzed to gain further insights into the role of EPS as well as to elucidate its potential effect on corrosion, manganese oxidation and biofilm formation: (I) MSVP-2 medium without any addition (-SS -Mn). (II) MSVP-2 medium with addition of 0.2 mM Mn(II) (-SS +Mn). (III) MSVP-2 medium without addition of 0.2 mM Mn(II) but in the presence of 2000 cm^2 of a SS surface (+SS -Mn). (IV) MSVP-2 medium with addition of 0.2 mM Mn(II) and in presence of 2000 cm^2 of a SS surface (+SS +Mn). The EPS were extracted, separated into the tightly and the loosely bound fraction and quantified with colorimetric assays. Subsequently, the yield was determined as the dry weight of the EPS and the colorimetric quantification was correlated to the total EPS yield. To ease comparability of the EPS yield, the dry weight was normalized to 10^{10} cells. Additionally, identification of fatty acids and carbohydrate monomers was done by gas chromatography.

Table 10 shows the EPS yielded from the extraction of EPS of *L. discophora* SS-1 grown under the 4 different culture conditions.

Table 10: EPS yield in µg, normalized to 10^{10} cells for the 4 different culture conditions. For details of growth conditions and replicates refer to Figure 14 and chapter 3.11.1.

Condition	EPS fraction	EPS yield in µg per 10^{10} cells
-SS -Mn	Tightly bound	272 ± 178
	Loosely bound	4110 ± 2916
-SS +Mn	Tightly bound	694 ± 160
	Loosely bound	3195 ± 1448
+SS -Mn	Tightly bound	315 ± 135
	Loosely bound	2113 ± 607
+SS +Mn	Tightly bound	852 ± 194
	Loosely bound	4338 ± 375

The highest amount of tightly bound EPS was found in presence of manganese ions and a SS surface (+SS +Mn; 852 µg), followed by the sole presence of manganese ions (-SS +Mn; 694 µg), the sole presence of a steel surface (+SS -Mn; 315 µg) and finally no addition to the MSVP-2 medium (-SS -Mn; 272 µg). The yield of tightly bound EPS extracted from growth conditions with addition of 0.2 mM Mn(II) is higher compared to EPS gained from growth

conditions without. The addition of a SS surface did not significantly change the yield of tightly bound EPS. While the EPS yield per cell is higher for both conditions with added manganese ions, the total amount is lower (-SS -Mn = 216 ± 154 µg; +SS -Mn = 173 ± 48 µg; -SS +Mn = 168 ±76 µg; +SS +Mn = 155 ± 13 µg). Also the total cell count in the PBS solution containing CER and 25 mg cell pellet mL^{-1} for extraction of the tightly bound EPS was 5 times lower if the cells were harvested from culture medium initially containing 0.2 mM Mn(II). Manganese oxides in these cell pellets were indicated by a positive leucoberbelin test and in total 27.8 ± 1.9 mg manganese dioxide (MnO_2) could be quantified by AAS in the extraction solution. The highest amount of loosely bound EPS was found in presence of manganese ions and a SS surface (+SS +Mn; 4338 µg), followed by the MSVP-2 medium without additions (-SS -Mn; 4110 µg), the sole presence of manganese ions (-SS +Mn; 3195 µg) and the sole presence of a steel surface (+SS -Mn; 2113 µg). There is no trend for loosely bound EPS. The addition of both, 0.2 mM Mn(II) or a stainless steel surface reduces the EPS yield. However, the addition of both increases the yield compared to the pure MSVP-2 medium. Remarkably, the variations in-between the biological replicates is considerably high, especially for the loosely bound EPS -SS -Mn and -SS +Mn. Even after dialysis and filtration (0.2 µm) of the EPS extracts, particles with a higher refractive index than the surrounding medium, but lower than e.g. cells of *L. discophora* SS-1 with sharp and distinct edges were found by bright field microscopy.

Table 11 shows the amounts of identified compounds while Figure 14 shows the relative amounts of identified compounds (% compounds identified in relation to the dry weight) in the EPS of *L. discophora* SS-1 grown under different culture conditions.

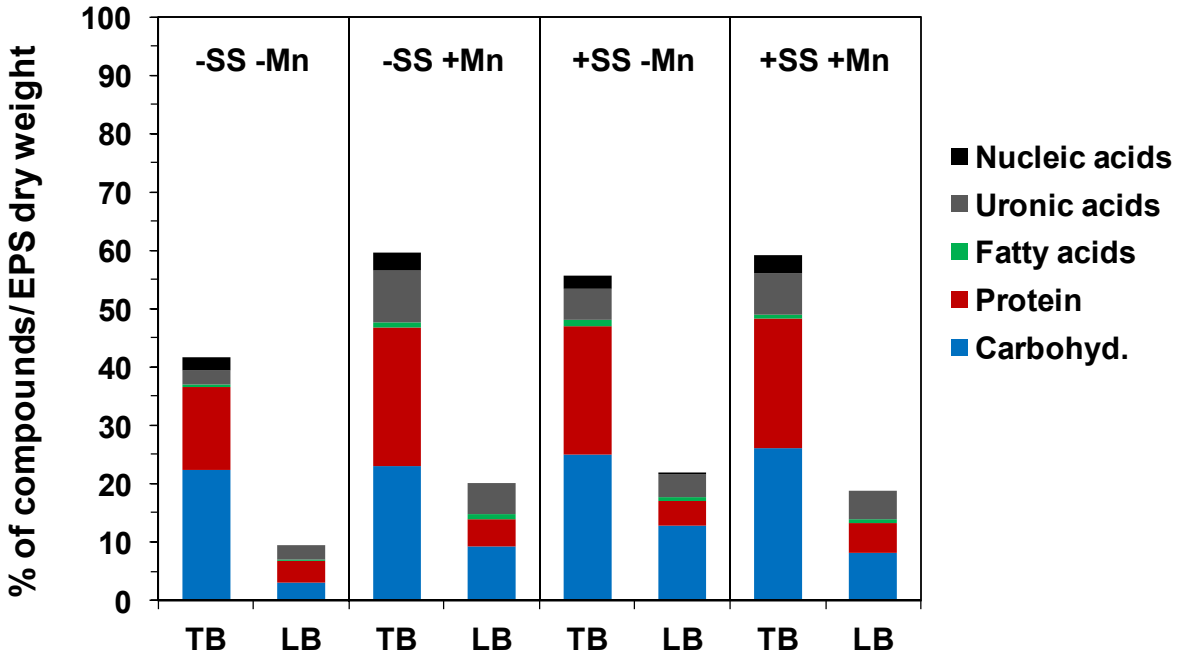

Figure 14: Relative amounts of the identified EPS compounds in proportion to the EPS dry weight. Bars indicate the relative composition of tightly and loosely bound EPS extracted from cultures of *L. discophora* SS-1, harvested in the late exponential phase (typically after 72 h) and grown under 4 different culture conditions. All cultures were grown in MSVP-2 medium at 28 °C, stirred (300 rpm) and supplied with compressed air. Culture conditions: grown in MSVP-2 medium without any additions (-SS -Mn), with addition of 0.2 mM Mn(II) (-SS +Mn), without addition of 0.2 mM Mn(II) but in presence of 2000 cm^2 of a SS surface (+SS -Mn) and with addition of 0.2 mM Mn(II) and in presence of 2000 cm^2 of a SS surface (+SS +Mn). Results for culture conditions without and with addition of 0.2 mM Mn(II) were determined from 3 respectively 2 independent biological samples with 2 technical replicates each.

Table 11: Amounts of identified compounds in EPS of *L. discophora* SS-1 grown under different growth conditions. For details of growth conditions and replicates see Figure 14 and chapter 3.11.1. Values are given as **µg mg^{-1}** EPS dry weight with SD. Values in brackets are given as percentage.

Condition	Fraction of EPS	Carbohydrates	Proteins	Nucleic acids
-SS -Mn	Tightly bound	222.6 (22.3) ± 98.2	142.7 (14.3) ± 80.6	22.0 (2.2) ± 15.4
	Loosely bound	30.9 (3.1) ± 24.1	36.1 (3.6) ± 34.9	0.0 (0) ± 0.0
-SS +Mn	Tightly bound	229.9 (23.0) ± 12.1	238.4 (23.8) ± 55.5	31.9 (3.2) ± 5.7
	Loosely bound	92.5 (9.3) ± 60.8	46.1 (4.6) ± 16.4	0.0 (0) ± 0.0
+SS -Mn	Tightly bound	250.8 (25.1) ± 75.4	218.1 (21.8) ± 97.8	19.1 (1.9) ± 6.4
	Loosely bound	127.2 (12.7) ± 30.2	43.5 (4.4) ± 47.3	0.0 (0) ± 0.0
+SS +Mn	Tightly bound	261.3 (26.1) ± 72.1	222.1 (22.2) ± 78.0	30.9 (3.1) ± 13.4
	Loosely bound	81.6 (8.2) ± 53.5	50.7 (5.1) ± 6.3	0.0 (0) ± 0.0
Condition	**Fraction of EPS**	**Uronic acids**	**Fatty acids**	**Total manganese**
-SS -Mn	Tightly bound	23.5 (2.4) ± 2.3	5.3 (0.5) ± 0.4	0.0 (0) ± 0.0
	Loosely bound	24.6 (2.5) ± 3.9	3.1 (0.3) ± 2.1	0.0 (0) ± 0.0
-SS +Mn	Tightly bound	90.0 (9.0) ± 35.3	7.1 (0.7) ± 0.8	0.0 (0) ± 0.0
	Loosely bound	52.6 (5.3) ± 33.8	9.7 (1.0) ± 4.4	0.0 (0) ± 0.0
+SS -Mn	Tightly bound	52.9 (5.3) ± 28.2	12.1 (1.2) ± 7.4	0.0 (0) ± 0.0
	Loosely bound	43.7 (4.4) ± 2.9	6.1 (0.6) ± 1.4	0.0 (0) ± 0.0
+SS +Mn	Tightly bound	72.4 (7.2) ± 33.2	6.0 (0.6) ± 0.6	0.0 (0) ± 0.0
	Loosely bound	48.8 (4.9) ± 5.5	6.8 (0.7) ± 0.6	0.0 (0) ± 0.0

Under all conditions carbohydrates, proteins and uronic acids constitute the major compounds in the tightly and loosely bound EPS. Carbohydrates represent the major compound in all loosely and tightly bound EPS fractions except the tightly bound fraction of -SS +Mn (proteins represent the major fraction). Fatty acids and nucleic acids represent minor fractions with 0.5 - 1.2 % and 1.9 - 3.2 %, respectively. There is no trend for fatty acids. Nucleic acids are increased in the tightly bound EPS in the presence of 0.2 mM Mn(II) (-SS +Mn and +SS +Mn), while being absent in all loosely bound fractions. Uronic acids were increased in presence of a SS surface (+SS -Mn) compared to EPS extracted from cultures grown in pure MSVP-2 medium (-SS -Mn). The amount of uronic acids continues to increase in presence of 0.2 mM Mn(II) (-SS +Mn). However, a combination of both (+SS +Mn) does not lead to even higher amounts of uronic acid. There is a similar, albeit weaker, trend for uronic acids in the loosely bound fraction. Manganese, determined as Mn(II)-ions as well as humic substances were not detected in either loosely or tightly bound EPS. G6PDH as a marker of cell lysis could not be detected in all scenarios.

The carbohydrate to protein ratios were calculated for all EPS fractions to evaluate EPS extraction efficiency and assess possible cell lysis. The results are given in Table 12.

Table 12: Carbohydrate to protein ratio. Numbers were calculated from values presented in Table 11. For details of growth conditions and replicates see Figure 14 and chapter 3.11.1.

Condition	Fraction of EPS	Carbohydrates to Protein ratio
-SS -Mn	Tightly bound	1.56
	Loosely bound	0.86
-SS +Mn	Tightly bound	0.96
	Loosely bound	2.01
+SS -Mn	Tightly bound	1.15
	Loosely bound	2.92
+SS +Mn	Tightly bound	1.18
	Loosely bound	1.61

The carbohydrate to protein ratio for tightly bound EPS varies between 0.96 and 1.56 and is under all conditions but -SS +Mn above 1. The carbohydrate to protein ratio for loosely bound EPS varies significantly more and is between 0.86 and 2.92.

The cell lysis marker G6PDH was tested for the tightly and loosely bound EPS fractions to exclude contribution of cell lysis to the quantified substances. To ensure correctness of the test, the residual cell pellet after the last (3rd) extraction was lysed and tested to show G6PDH activity after the extraction procedure. Additionally, a positive control (with added G6DPH) and a blank were tested. The G6PDH activity was tested regularly. Figure 15 shows exemplarily the G6PDH activity of the loosely and tightly bound EPS (gained from +SS -Mn), the residual cell pellet after the 3rd extraction, a positive control and a blank. There was no G6PDH activity, neither in the loosely no in the tightly bound EPS. The (lysed) residual cell pellet after the 3rd EPS extraction, however, showed distinct G6PDH activity. The positive control also showed a distinct activity while the blank was negative.

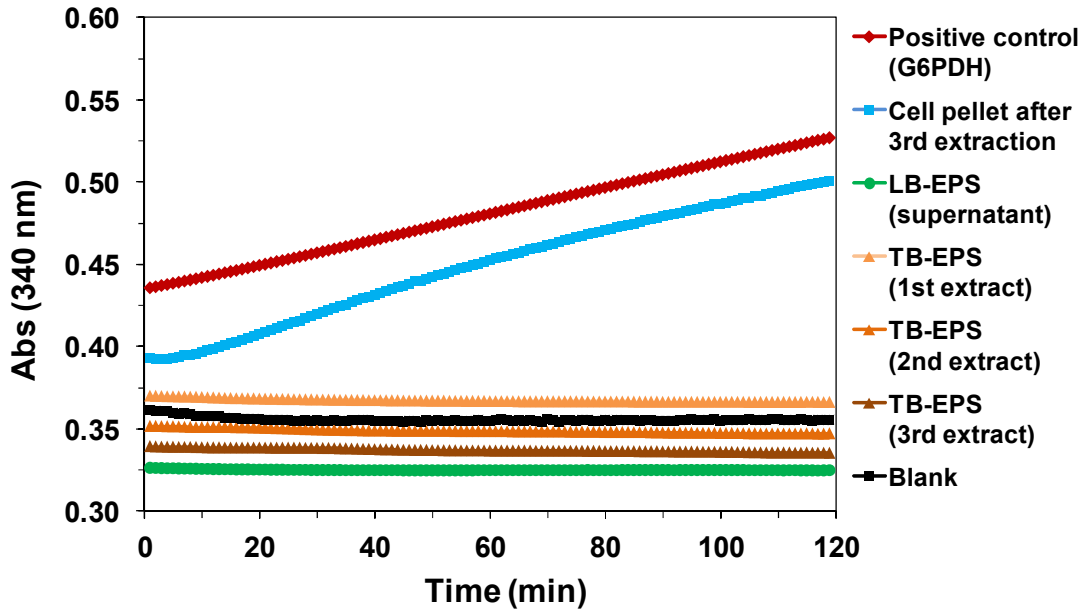

Figure 15: G6PDH test as a marker for cell lysis. Exemplary measurement of the G6PDH activity in the loosely bound EPS fraction, the 1st to 3rd tightly bound EPS fraction and the residual (lysed) cell pellet after the 3rd extraction. Additionally, a positive control with added G6PDH and a blank without G6PDH was tested.

Table 13 shows the fatty acids and carbohydrate monomers in tightly and loosely bound EPS of cells of *L. discophora* SS-1 grown under different growth conditions.

Table 13: Fatty acids and carbohydrate monomers in tightly and loosely bound EPS fractions of cells of *L. discophora* SS-1 grown under different growth conditions (chapter 3.11.1). Numbers represent single measurements from 3 merged EPS extracts (chapter 3.11.3).

	Condition and EPS fraction							
	-SS-Mn		**-SS+Mn**		**+SS-Mn**		**+SS+Mn**	
	TB	**LB**	**TB**	**LB**	**TB**	**LB**	**TB**	**LB**
Saturated fatty acids								
C8:0	16.0	100.0	3.2	100.0	13.6	100.0	5.4	100.0
C10:0	2.5	0	6.3	0	5.2	0	4.8	0
C12:0	12.0	0	19.2	0	10.9	0	22.4	0
C16:0	20.1	0	14.6	0	20.3	0	15.7	0
(Poly)unsaturated fatty acids								
C16:1	49.4	0	53.6	0	50.1	0	49.2	0
C18:1	0	0	3.0	0	0	0	2.5	0
Carbohydrates								
Rhamnose	48.9	14.0	33.4	19.9	29.6	14.7	36.3	15.5
Fucose	11.8	6.7	34.1	12.7	25.7	6.5	28.5	5.8
Arabinose	0	0	0	0	0	0	0	0
Ribose	0	0	0	0	0	0	0	0
Xylose	17.4	0	15.9	0	21.7	0	5.2	0
Mannose	13.7	21.7	16.6	24.9	9.9	22.4	0	21.7
Sorbitol	6.9	52.0	0	42.5	11.9	42.9	30.0	42.1
Galactose	1.3	1.2	0	0	1.2	13.5	0	14.9

In the loosely bound EPS the only identified fatty acid was C8:0. The unsaturated fatty acid C16:1 was in all tightly bound fractions the major component (49.2 - 53.6 %) with only minor variations in-between the different growth conditions. Tightly bound EPS from cells grown in MSVP-2 with 0.2 mM Mn(II) show a reduced amount of the fatty acid C8:0 and C16:0, while C12:0 is increased compared to cells grown in MSVP-2 without 0.2 mM Mn(II). A major difference is the unsaturated fatty acid C18:1 which is only present in tightly bound EPS from cells grown in MSVP-2 with 0.2 mM Mn(II). In general, the addition of a SS surface did not show a strong change in the fatty acid composition of tightly or loosely bound EPS. The proportion of identified peaks in the chromatogram of tightly bound EPS gained from cells grown in the absence of manganese ions but with our without a SS surface was 64 % and 66 %, while in presence of manganese ions with or without a SS surface it was 92 and 93 %.

The proportion of identified peaks in the chromatogram of loosely bound EPS gained from cells grown in the absence of manganese ions but with or without a SS surface was 72 % or 62 %, while in the presence of manganese ions with or without a SS surface 48 % or 97 % were identifiable.

In all loosely bound EPS sorbitol is the dominant carbohydrate followed by mannose, rhamnose, fucose and galactose. Only in the loosely bound EPS gained from cells grown in presence of a SS surface and 0.2 mM Mn(II) galactose is more frequent than fucose. Xylose, contrary to tightly bound EPS is absent under all conditions. In all tightly bound EPS except EPS from cells grown in pure MSVP-2 rhamnose and fucose represent major carbohydrates followed by varying amounts of xylose, mannose, sorbitol and galactose. In presence of a SS surface and 0.2 mM Mn(II) sorbitol represents also a major carbohydrate constituent. The amount of fucose is reduced in EPS from cells grown in pure MSVP-2 compared to all other conditions. Even though, galactose is only a minor constituent of the tightly bound EPS, it only present in EPS from cells grown without addition of manganese ions. There are no other discernible trends among the different conditions. For loosely bound EPS 30 - 35 % of all peaks in the chromatograms could be identified, while the identified amounts were considerably higher in tightly bound EPS with 85 - 100 %.

4.3 Biofilm formation of *L. discophora* SS-1

Biofilm formation is the preferred lifestyle of almost all bacterial communities and well known for the genus *Leptothrix*. However, it is still necessary to improve our understanding of biofilm formation, EPS composition and the influence on stainless steel corrosion in general and especially for *L. discophora* SS-1. To understand biofilm formation, it is necessary to address the role of EPS in detail. Therefore, biofilm formation was analyzed with FLBA (as a marker of EPS) with a set of 13 fluorescent lectins on (I) floating filters, (II) SS coupons without the addition of 0.2 mM Mn(II) and (III) SS coupons with the addition of 0.2 mM Mn(II). The floating filter method is a simple and fast tool to develop and investigate mature biofilms in situ, to address the structure as well as the glycoconjugate distribution and therefore investigate the polysaccharide proportion of the EPS. Stainless steel coupons are used as a model for real life scenarios, where MOMOs attach, grow and may cause biocorrosion on stainless steel. All results of the respective lectins were replicated twice (n = 3). Selected lectins were also replicated with different microscopic techniques since a technical malfunction of the CLSM (which could not be solved throughout this thesis) resulted in the necessity to use the EFM for the last set of samples (Biofilms on SS coupons +Mn). While the CLSM is superior in visualizing thick biofilms, both techniques produce comparable results for monolayer- or thin biofilms on SS coupons. Comparability is discussed later on

and demonstrated exemplarily (see Figure 25 and Figure 33). The possibility to use a different CLSM was also taken into consideration. However, an alternative CLSM was not readily available. Therefore, the use of the EFM was the best solution and scientific validity of the results was proven in this study.

In the following chapters, representative images of the results are shown and described in detail. Table 14 summarizes the ability or non-ability of 13 lectins to bind to glycoconjugate residues in the EPS of biofilms of cells of *L. discophora* SS-1.

Table 14: A Set of 13 lectins was tested for the ability of the lectins to bind to glycoconjugate residues in the EPS of *L. discophora* SS-1 biofilms grown in MSVP-2 medium. The lectins were tested on floating filters and additionally on SS coupons with and without addition of 0.2 mM Mn(II) to the medium. Lectins which resulted in a discernible signal are marked with "Yes" others with "No".

Lectin	Biofilms on floating filter	Biofilms on SS coupon –Mn	Biofilms on SS coupon +Mn
ConA	Yes	Yes	Yes
GS-I	No	Yes	Yes
GS-II	Yes	Yes	Yes
WGA	No	No	No
BPA	Yes	No	No
SBA	No	Yes	Yes
UEA-I	No	No	Yes
DBA	No	Yes	Yes
PWM	Yes	Yes	Yes
PHAE-I	No	Yes	Yes
PNA	No	Yes	Yes
MPA	No	Yes	Yes
LPA	Yes	Yes	Yes

The following glycoconjugate residues were identified by lectins within the EPS matrix: mannose, glucose (ConA), melibiose (GS-I), galactose (GS-I, SBA, PNA, MPA), fucose (UEA-I), N-acetylglucosamine (GS-II, PWM, PHAE-I), N-acetylgalactosamine (SBA, PHAE-I, MPA, BPA), Methyl-2-acetamido-2-deoxy-D-galactose (DBA), N-acetyllactosamine (PWM) and sialic acids (LPA). These findings are partially supported due to the identification of mannose, galactose and fucose in EPS of *L. discophora* SS-1 cells by gas-chromatographic carbohydrate monomer analysis (Table 13).

4.3.1 Biofilm formation on floating filters

Biofilms on floating filters were grown as described (3.8.1) and stained with nucleic acid stain Syto61 and additionally labeled with lectins (3.8.2). Biofilms were examined by CLSM and the nucleic acid as well as the lectin stains were visualized. Exemplary images of the 5 positive lectins ConA, GS-II, BPA, PWM and LPA are shown in Figure 16 to Figure 20.

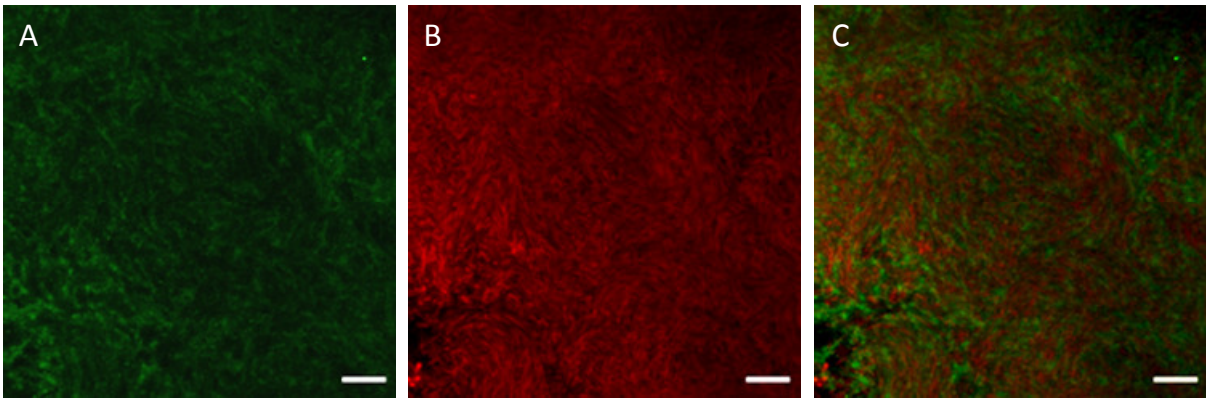

Figure 16: Biofilm formation of *L. discophora* SS-1 on a membrane filter. CLSM images of cells of *L. discophora* SS-1 stained with **SYTO61** and FITC-**ConA** grown on MSVP-2 medium for 12 d at 28 °C. (A) green: FITC-**ConA** (B) red: SYTO61 signal (C) merged image of (A) and (B). Bar 10 µm.

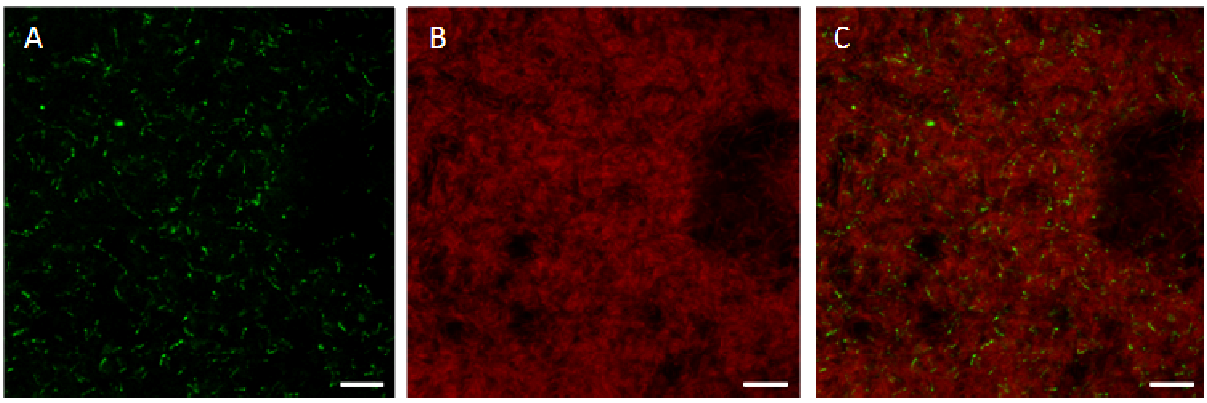

Figure 17: Biofilm formation of *L. discophora* SS-1 on a membrane filter. CLSM images of cells of *L. discophora* SS-1 stained with **SYTO61** and FITC-**GS-II** grown on MSVP-2 medium for 12 d at 28 °C. (A) green: FITC-GS-II (B) red: SYTO61 signal (C) merged image of (A) and (B). Bar 10 µm.

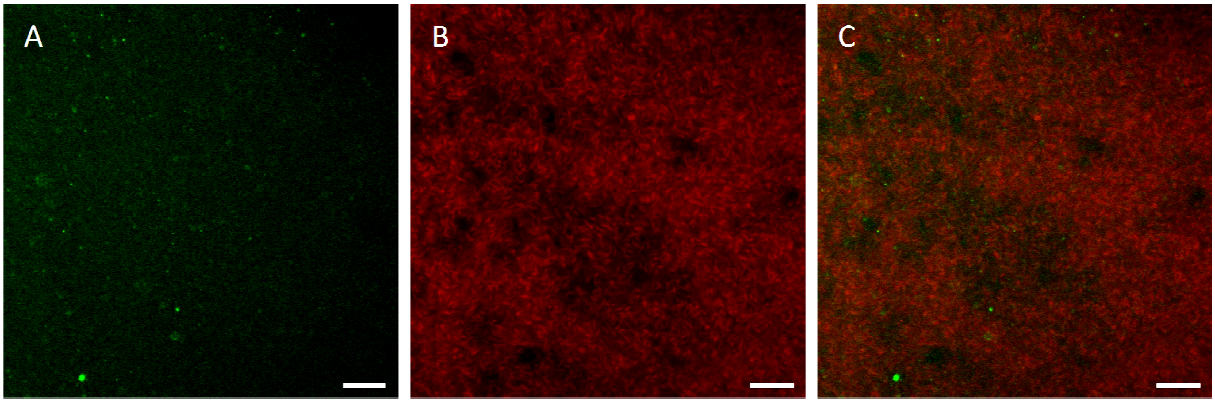

Figure 18: Biofilm formation of *L. discophora* SS-1 on a membrane filter. CLSM images of cells of *L. discophora* SS-1 stained with **SYTO61** and FITC-**BPA** grown on MSVP-2 medium for 2 d at 28 °C. (A) green: FITC-BPA (B) red: SYTO61 signal (C) merged image of (A) and (B). Bar 10 µm.

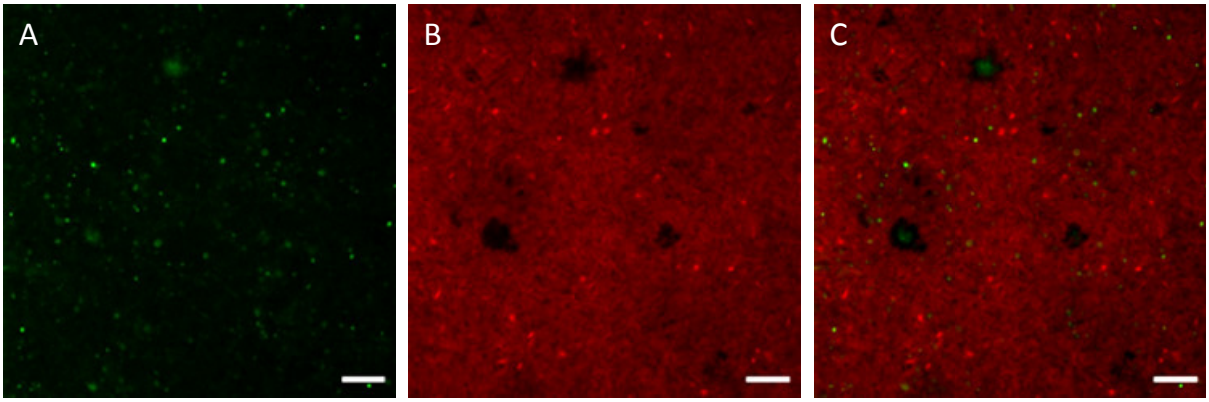

Figure 19: Biofilm formation of *L. discophora* SS-1 on a membrane filter. CLSM images of cells of *L. discophora* SS-1 stained with **SYTO61** and FITC-**PWM** grown on MSVP-2 medium for 2 d at 28 °C. (A) green: FITC-PWM (B) red: SYTO61 signal (C) merged image of (A) and (B). Bar 10 µm.

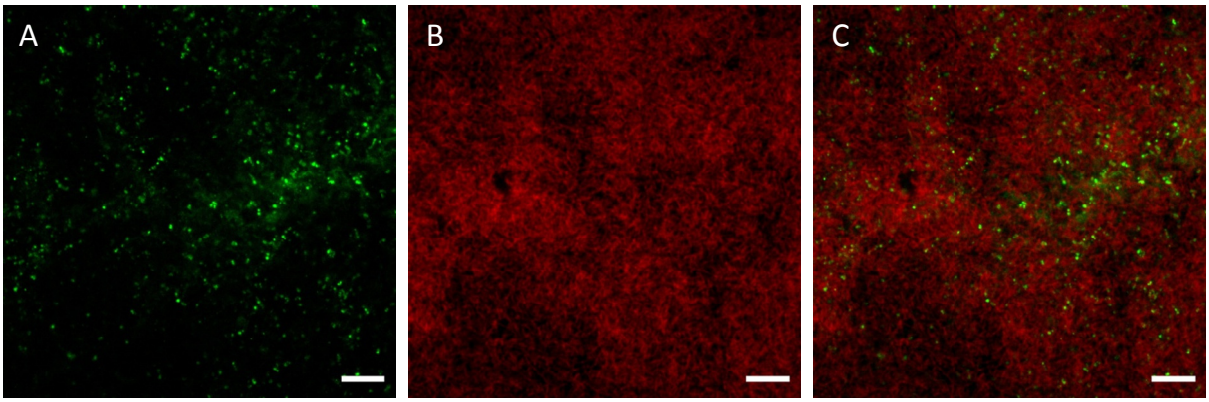

Figure 20: Biofilm formation of *L. discophora* SS-1 on a membrane filter. CLSM images of cells of *L. discophora* SS-1 stained with **SYTO61** and FITC-**LPA** grown on MSVP-2 medium for 2 d at 28 °C. (A) green: FITC-LPA (B) red: SYTO61 signal (C) merged image of (A) and (B). Bar 10 µm.

Biofilms on floating filters were yellowish, densely populated and consisted of several layers of cells. ConA showed to be the most suitable lectin to stain biofilms of *L. discophora* SS-1 cells. It stained the cells and presumably labeled also the biofilm matrix (EPS). This is indicated by a green signal in-between the cells (red nucleic acid stain) and/or a green stain surrounding the microcolonies. The lectin GS-II stained parts of the presumed EPS and some but not all of the cells themselves. The lectins BPA, PWM and LPA showed a lower signal compared to ConA but also stained presumably the biofilm matrix (EPS). By comparison of the lectin signals with their respective specificity for glycoconjugate residues the presence of the following carbohydrates is indicated: mannose or glucose (ConA), N-acetylglucosamine (GS-II, PWM), N-acetyllactosamine (PWM), N-acetylgalactosamine (BPA) and sialic acids (LPA).

To gain a deepened insight into the structure of *L. discophora* SS-1-biofilms and the distribution of ConA as a marker of EPS within the biofilm, 3-dimensional images of a mature 2 day old biofilm were recorded by CLSM (Figure 21).

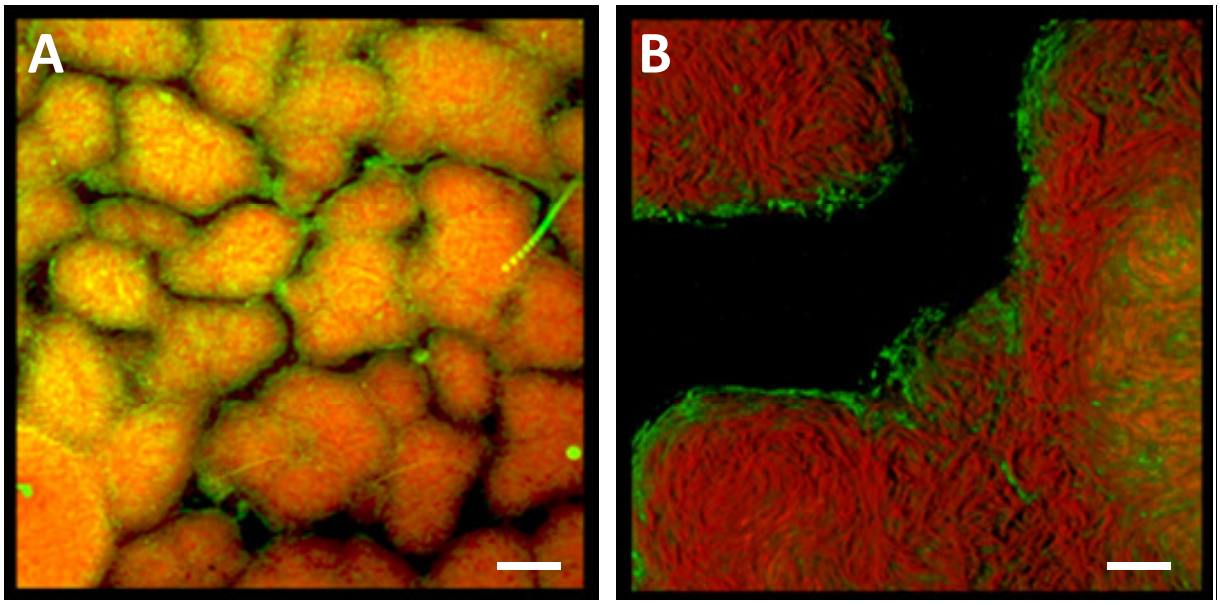

Figure 21: Biofilm formation of *L. discophora* SS-1 on a membrane filter. A: 3D projection of merged images of cells of *L. discophora* SS-1 stained with SYTO61 (red) and FITC-ConA (green) grown on a floating filter in MSVP-2 medium for 2 d at 28 °C, bar 50 µm. B: 3D projection of the same filter depicting two separated microcolonies in detail, bar 10 µm.

Figure 21 shows two merged CLSM images of the red and the green channel (images are top view projections). On image A, colonies of *L. discophora* SS-1 cells (indicated by the red nucleic acid stain) with a strong surrounding green ConA signal (ConA is used as a marker of EPS) can be seen. Some, but not all colonies are separated by distinguishable borders forming in between a channel-like structure. The colonies are generally closely associated to

the ConA-signal surrounding the respective colonies. On image B, two separated colonies and the channel like structure in between are shown. It is evident that the green signal (presumably EPS) mainly appears in the interspace of the cells and encloses the colonies.

Incorporation of manganese oxides into the biofilm was evident, if cells of *L. discophora* were grown on floating filters on top of MSVP-2 medium supplemented with 0.2 mM Mn(II). Manganese incorporation could be seen with the naked eye as a brownish discoloration of the previously yellowish biofilm. Figure 22 shows the merged image of the green and of the reflection channel. Cells of *L. discophora* SS-1 appear in green (Syto9 nucleic acid stain) and the surface is depicted in white (reflection).

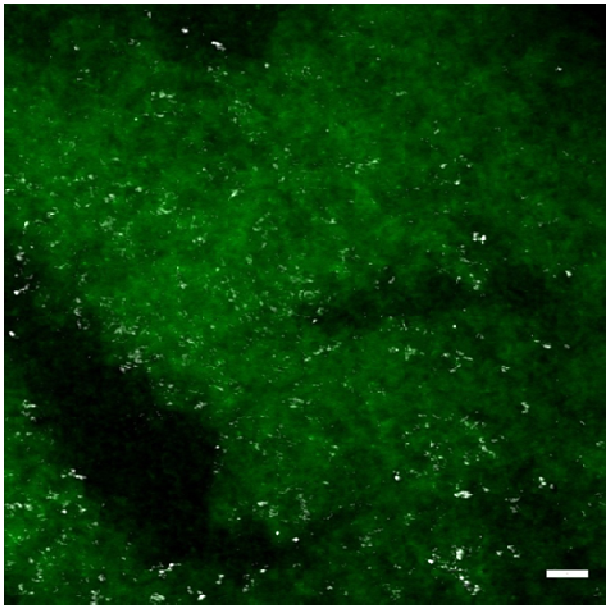

Figure 22: Biofilm formation of *L. discophora* SS-1 on a membrane filter. Merged CLSM image of cells of *L. discophora* SS-1 stained with SYTO9 (green) and visualization of the surface in reflection mode (white) grown on MSVP-2 medium with 0.2 mM Mn for 9 d at 28 °C. Bar 10 µm.

The reflectance correlates well with the brownish discoloration; dark spots in this image also correlate with strong brownish precipitates seen in reflected light microscopy (data not shown). The biofilm was positive for manganese oxides identified with the leucoberbelin assay.

4.3.2 Biofilm formation on stainless steel coupons

Biofilms on stainless steel coupons without addition of Mn(II)

Biofilms on SS coupons were grown as described (3.8.1) and stained with nucleic acid stain Syto83 and labeled with lectins (3.8.2). *L. discophora* SS-1 biofilms formed on the SS surface without incorporation of manganese oxides were examined by CLSM. The nucleic acid as well as lectin stains were visualized. Exemplary images of the 9 positive lectins ConA, GS-I, GS-II, SBA, DBA, PWM, PHAE-I, MPA and LPA are shown in Figure 23 to Figure 32 and described afterwards.

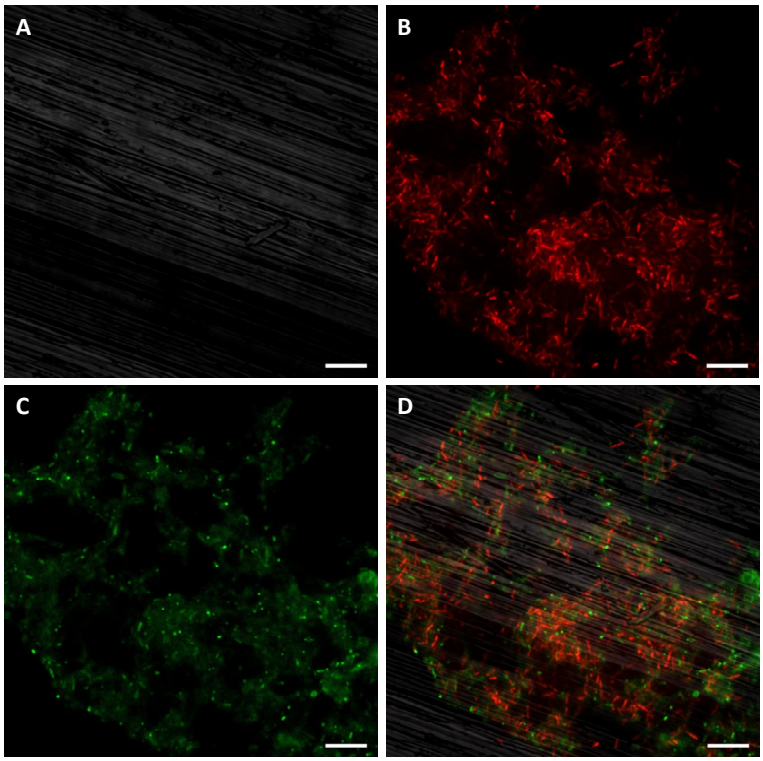

Figure 23: Biofilm formation of *L. discophora* SS-1 on a stainless steel coupon. CLSM images of cells of *L. discophora* SS-1 stained with **SYTO83** and **ConA** grown in MSVP-2 medium for 10 d at 28 °C. (A) white: reflection (B) red: SYTO83 signal (C) green: FITC-ConA signal (D) merged image of (A)-(C). Bar 10 µm.

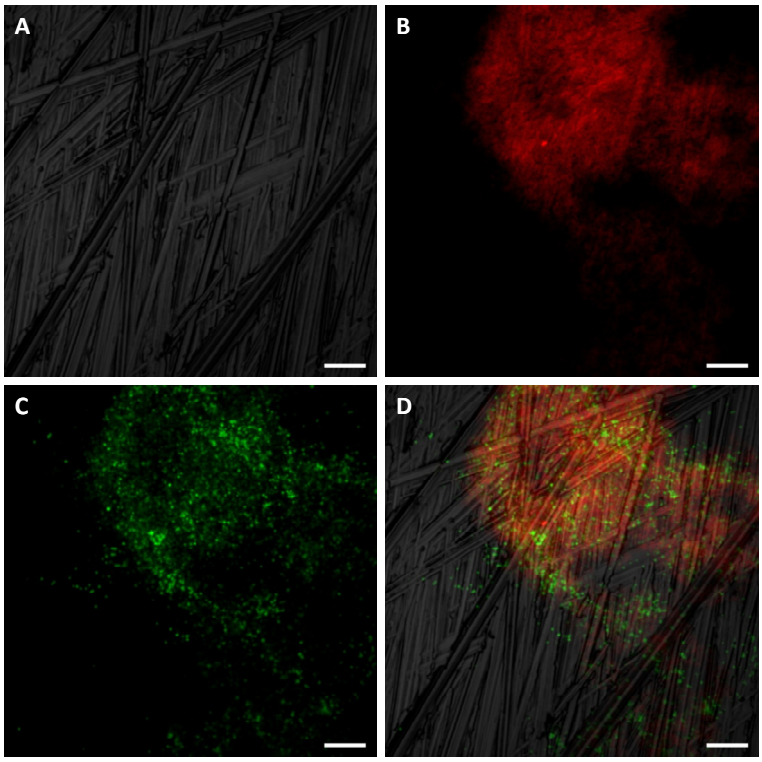

Figure 24: Biofilm formation of *L. discophora* SS-1 on a stainless steel coupon. CLSM images of cells of *L. discophora* SS-1 stained with **SYTO83** and **GS-I** grown in MSVP-2 medium for 5 d at 28 °C. (A) white: reflection (B) red: SYTO83 signal (C) green: FITC-GS-I signal (D) merged image of (A)-(C). Bar 10 µm.

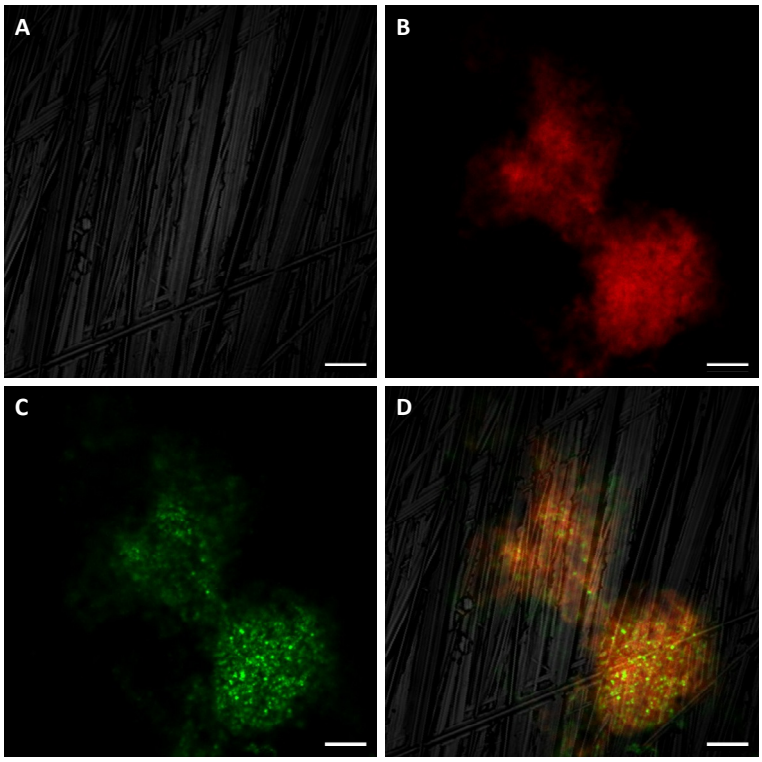

Figure 25: Biofilm formation of *L. discophora* SS-1 on a stainless steel coupon. CLSM images of cells of *L. discophora* SS-1 stained with **SYTO83** and **GS-II** grown in MSVP-2 medium for 5 d at 28 °C. (A) white: reflection (B) red: SYTO83 signal (C) green: FITC-GS-II signal (D) merged image of (A)-(C). Bar 10 µm.

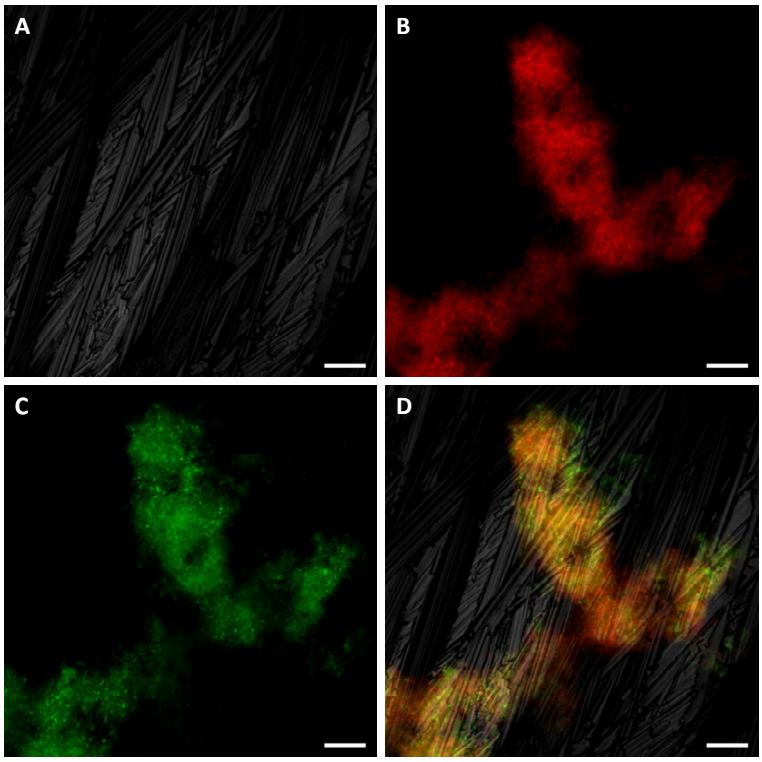

Figure 26: Biofilm formation of *L. discophora* SS-1 on a stainless steel coupon. CLSM images of cells of *L. discophora* SS-1 stained with **SYTO83** and **SBA** grown in MSVP-2 medium for 4 d at 28 °C. (A) white: reflection (B) red: SYTO83 signal (C) green: FITC-SBA signal (D) merged image of (A)-(C). Bar: 10 µm.

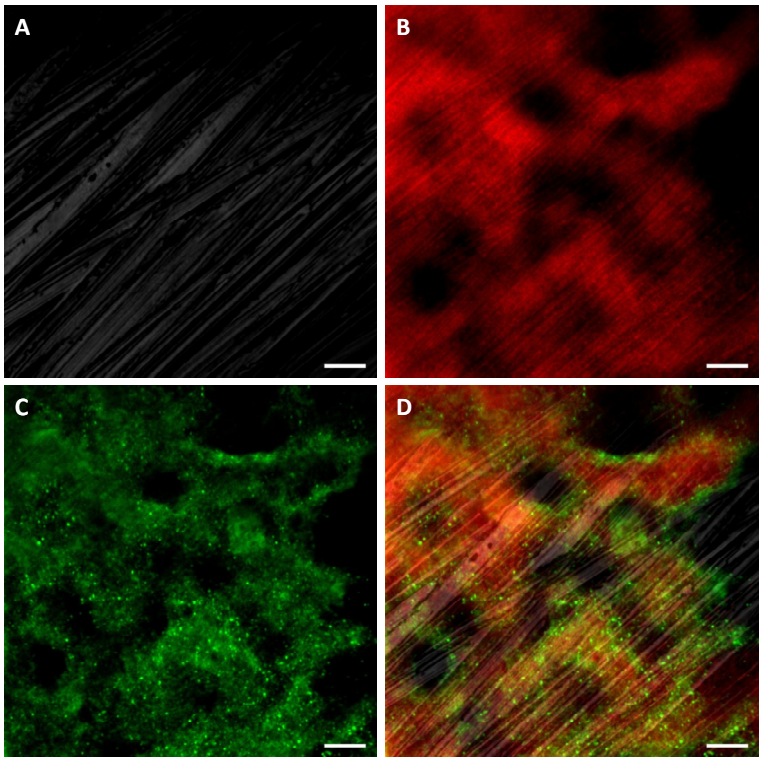

Figure 27: Biofilm formation of *L. discophora* SS-1 on a stainless steel coupon. CLSM images of cells of *L. discophora* SS-1 stained with **SYTO83** and **DBA** grown in MSVP-2 medium for 4 d at 28 °C. (A) white: reflection (B) red: SYTO83 signal (C) green: FITC-DBA signal (D) merged image of (A)-(C). Bar 10 µm.

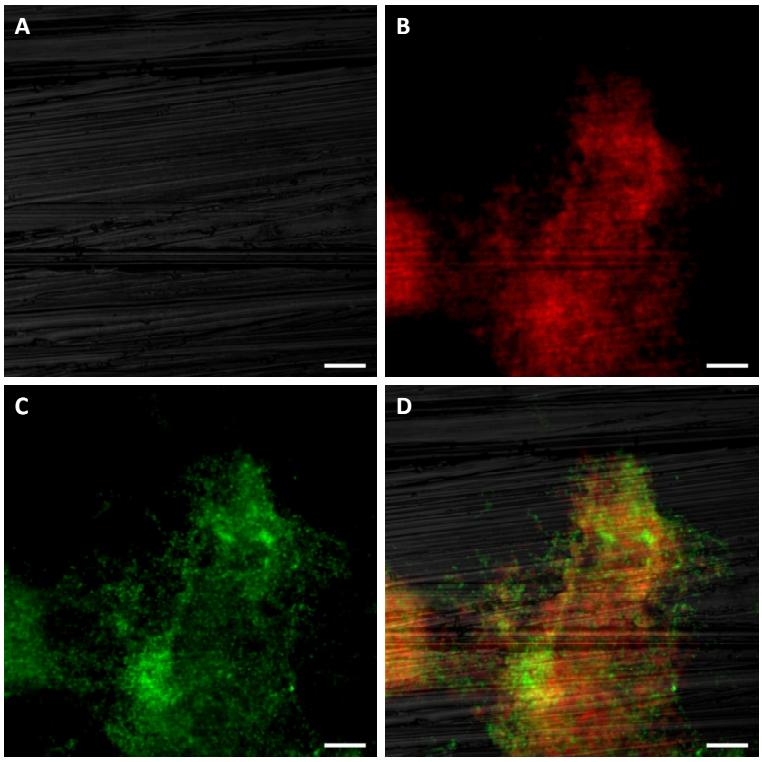

Figure 28: Biofilm formation of *L. discophora* SS-1 on a stainless steel coupons. CLSM images of cells of *L. discophora* SS-1 stained with **SYTO83** and **PWM** grown in MSVP-2 medium for 5 d at 28 °C. (A) white: reflection (B) red: SYTO83 signal (C) green: FITC-PWM signal (D) merged image of (A)-(C). Bar 10 µm.

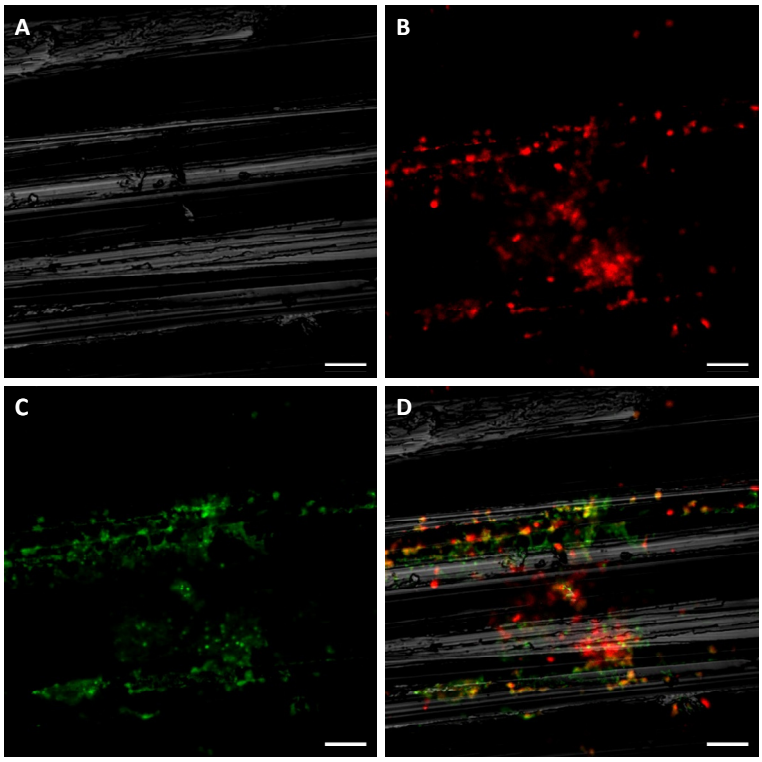

Figure 29: Biofilm formation of *L. discophora* SS-1 on a stainless steel coupon. CLSM images of cells of *L. discophora* SS-1 stained with **SYTO83** and **PHAE-I** grown in MSVP-2 medium for 5 d at 28 °C. (A) white: reflection (B) red: SYTO83 signal (C) green: FITC-PHAE-I signal (D) merged image of (A)-(C). Bar 10 µm.

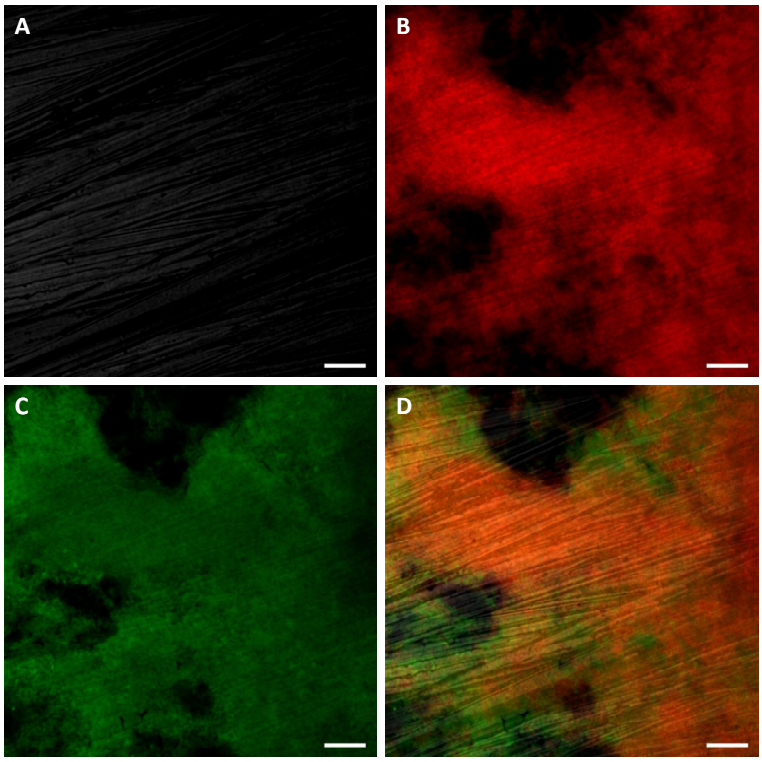

Figure 30: Biofilm formation of *L. discophora* SS-1 on a stainless steel coupon. CLSM images of cells of *L. discophora* SS-1 stained with **SYTO83** and **PNA** grown in MSVP-2 medium for 6 d at 28 °C. (A) white: reflection (B) red: SYTO83 signal (C) green: FITC-PNA signal (D) merged image of (A)-(C). Bar 10 µm.

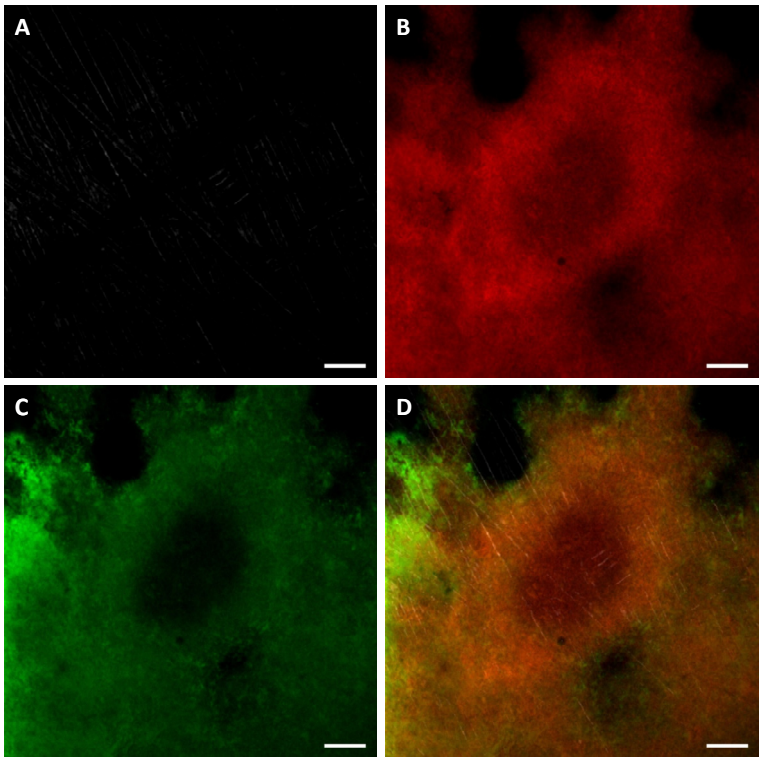

Figure 31: Biofilm formation of *L. discophora* SS-1 on a stainless steel coupon. CLSM images of cells of *L. discophora* SS-1 stained with **SYTO83** and **MPA** grown in MSVP-2 medium for 6 d at 28 °C. (A) white: reflection (B) red: SYTO83 signal (C) green: FITC-MPA signal (D) merged image of (A)-(C). Bar 10 µm.

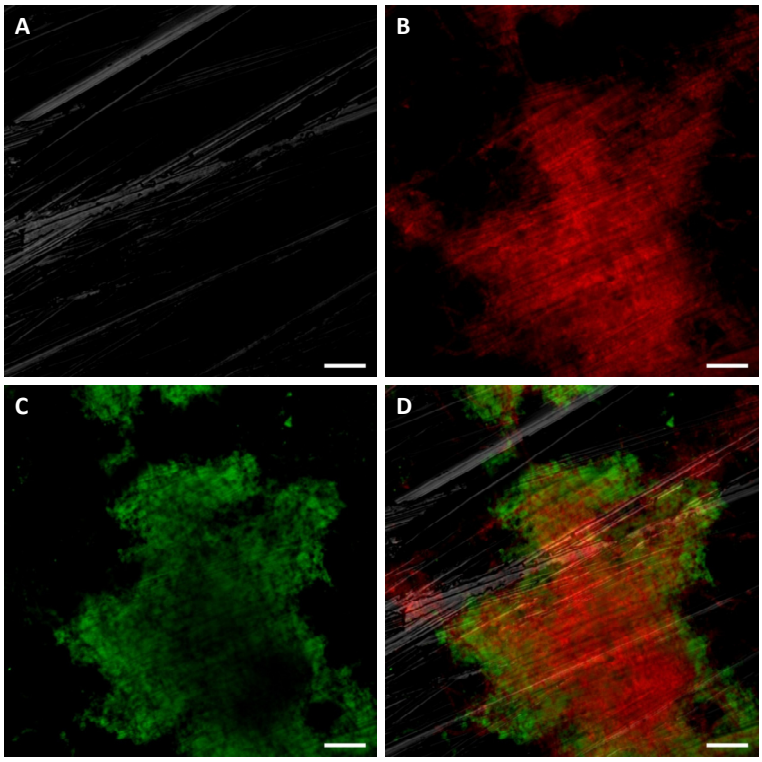

Figure 32: Biofilm formation of *L. discophora* SS-1 on a stainless steel coupon. CLSM images of cells of *L. discophora* SS-1 stained with **SYTO83** and **LPA** grown in MSVP-2 medium for 6 d at 28 °C. (A) white: reflection (B) red: SYTO83 signal (C) green: FITC-LPA signal (D) merged image of (A)-(C). Bar 10 µm.

Biofilms on SS coupons were less dense compared to biofilms on floating filters and there were certain differences in the binding pattern of the lectins. GS-I, GS-II, SBA, PHAE-I, PNA and MPA mainly labeled the biofilm (presumably cells and EPS) similarly to the nucleic acid stain. The lectins ConA, DBA, PWM and LPA showed a significantly different staining pattern. These lectins presumably mainly labeled the biofilm matrix (EPS). This is indicated by a green signal in-between the cells (red nucleic acid stain) and/or a green stain surrounding the microcolonies. By comparison of the lectin signals with their respective specificity for glycoconjugate residues the presence of the following carbohydrates is indicated: mannose or glucose (ConA), melibiose (GS-I), galactose (GS-I, SBA, PNA, MPA), N-acetylglucosamine (GS-II, PWM, PHAE-I), N-acetylgalactosamine (SBA, PHAE-I, MPA), methyl-2-acetamido-2-deoxy-D-galactose (DBA), N-acetyllactosamine (PWM) and sialic acids (LPA).

Biofilms on stainless steel coupons with addition of Mn(II)

Biofilms on SS coupons with Mn(II) were grown as described (3.8.1) and stained with nucleic acid stain Syto83 and labeled with lectins (3.8.2). *L. discophora* SS-1 biofilms formed on the SS surface with incorporation of manganese oxides were examined and the nucleic acid as well as the lectin stains were visualized. Due to technical malfunction of the CLSM (which

could not be solved throughout this thesis) all images were taken by EFM. Care was taken to ensure comparability of the results gained by both microscopic techniques. Exemplarily, the results obtained for SS coupons with the lectin GS-II without addition of manganese were repeated to ensure both instruments produce similar data (Figure 33).

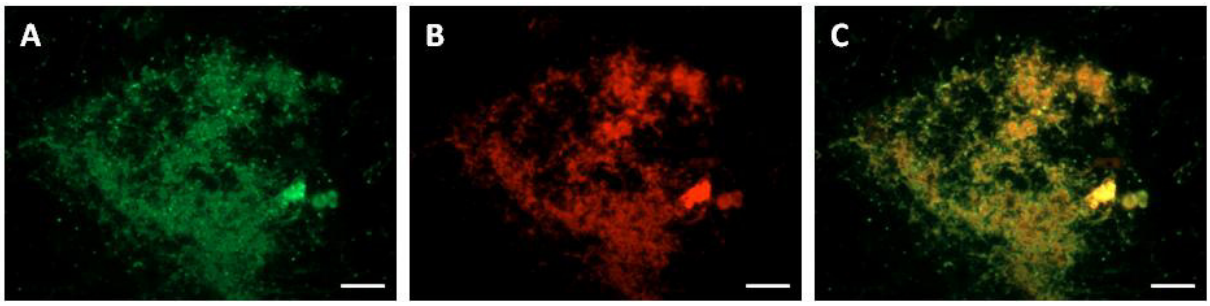

Figure 33: Biofilm formation of *L. discophora* SS-1 on a stainless steel coupon. EFM images of cells of *L. discophora* SS-1 stained with **SYTO83** and **GS-II** grown in MSVP-2 medium for 3 d at 28 °C. (A) green: FITC-GS-II signal (B) red: SYTO83 signal (C) merged image of (A) and (C). Bar 10 µm.

By comparison of Figure 25 (GS-II, CLSM) and Figure 33 (GS-II, EFM) it becomes obvious that the lectin GS-II produces a similar staining pattern of the biofilm, comparable to the nucleic acid stain. This indicates that results of the same lectin are reproducible with both microscopical techniques. However, reflection imaging to visualize the surface is not possible with EFM. Additionally, all lectins were tested with and without the use of a red nucleic acid stain to prove that the green lectin stain is not a result of a false positive signal due to signal crossing from a red stain to the green EFM filter (results of lectin stains without nucleic acid stain are not shown). Furthermore, two red TRITC labeled lectins were selected (SBA and UEA) to be tested with a green nucleic acid stain (Syto9). This was done to ensure repeatability with different stains and to omit false positive results. The staining patterns were identical, the colors were inverted (see exemplary image of the lectin SBA in Figure 34 compared to Figure 38).

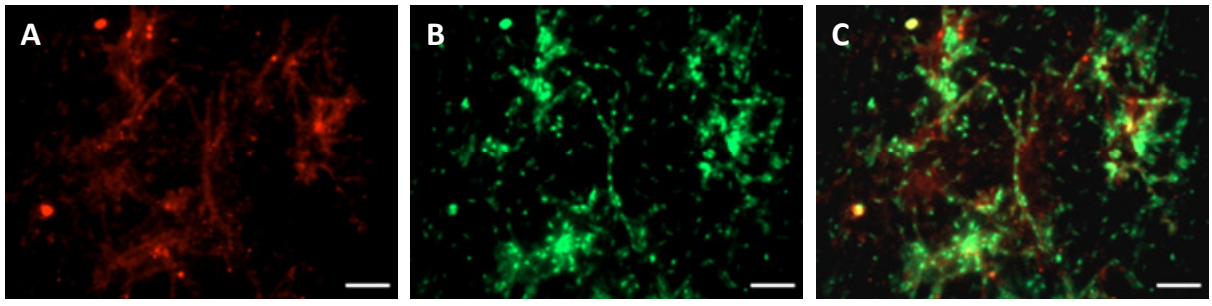

Figure 34: Biofilm formation of *L. discophora* SS-1 on a stainless steel coupon. EFM images of cells of *L. discophora* SS-1 stained with **SYTO9** and **SBA** grown in MSVP-2 medium for 3 d at 28 °C. (A) red: TRITC-SBA signal (B) green: SYTO9 signal (C) merged image of (A) and (C). Bar 10 µm.

Exemplary images of the 11 positive lectins ConA, GS-I, GS-II, SBA, UEA-I, DBA, PWM, PHAE-I, PNA, MPA and LPA are shown in Figure 35 to Figure 45 and described afterwards.

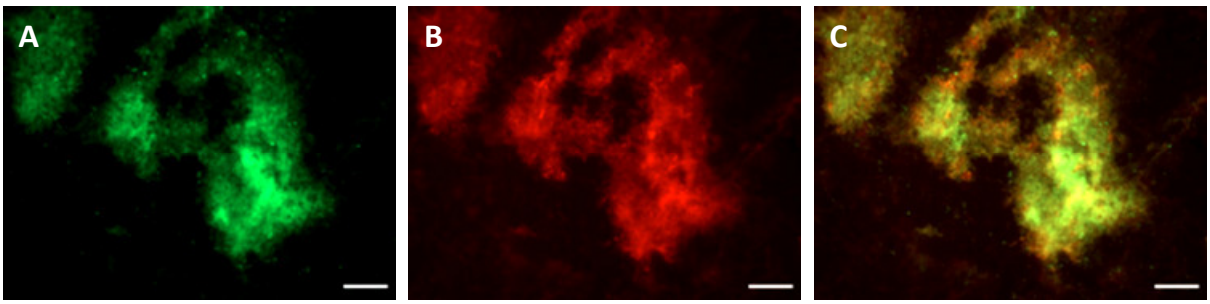

Figure 35: Biofilm formation of *L. discophora* SS-1 on a stainless steel coupon. EFM images of cells of *L. discophora* SS-1 stained with **SYTO83** and **ConA** grown in MSVP-2 medium supplemented with 0.2 mM Mn(II) for 3 d at 28 °C. (A) green: FITC-ConA signal (B) red: SYTO83 signal (C) merged image of (A) and (C). Bar 10 µm.

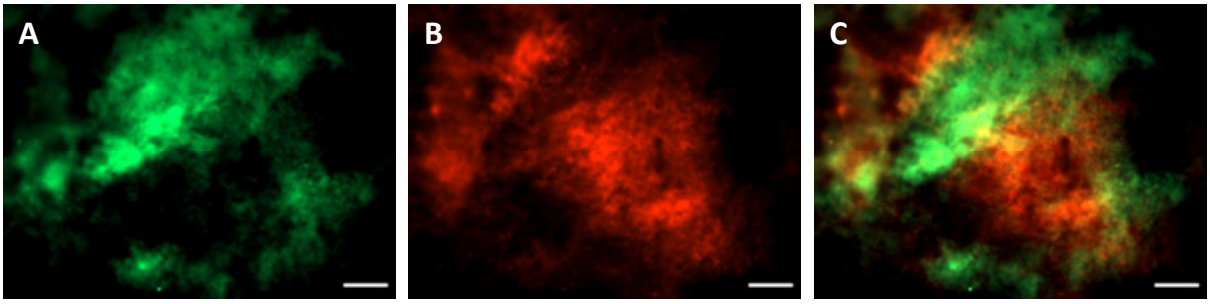

Figure 36: Biofilm formation of *L. discophora* SS-1 on a stainless steel coupon. EFM images of cells of *L. discophora* SS-1 stained with **SYTO83** and **GS-I** grown in MSVP-2 medium supplemented with 0.2 mM Mn(II) for 3 d at 28 °C. (A) green: FITC-GS-I signal (B) red: SYTO83 signal (C) merged image of (A) and (C). Bar 10 µm.

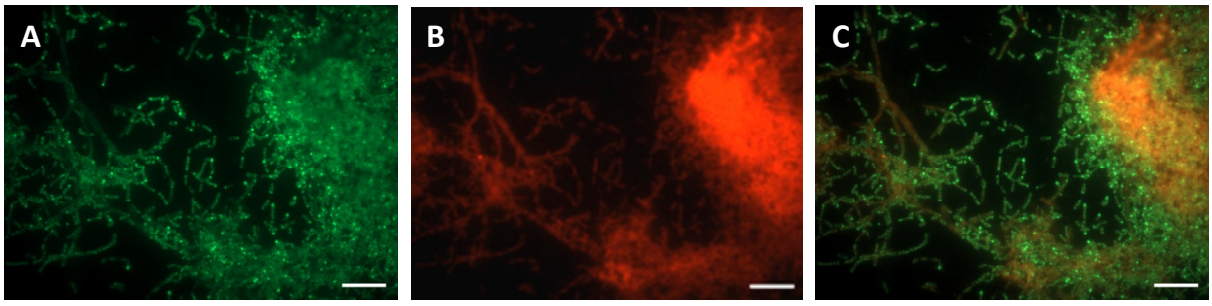

Figure 37: Biofilm formation of *L. discophora* SS-1 on a stainless steel coupon. EFM images of cells of *L. discophora* SS-1 stained with **SYTO83** and **GS-II** grown in MSVP-2 medium supplemented with 0.2 mM Mn(II) for 3 d at 28 °C. (A) green: FITC-GS-II signal (B) red: SYTO83 signal (C) merged image of (A) and (C). Bar 10 µm.

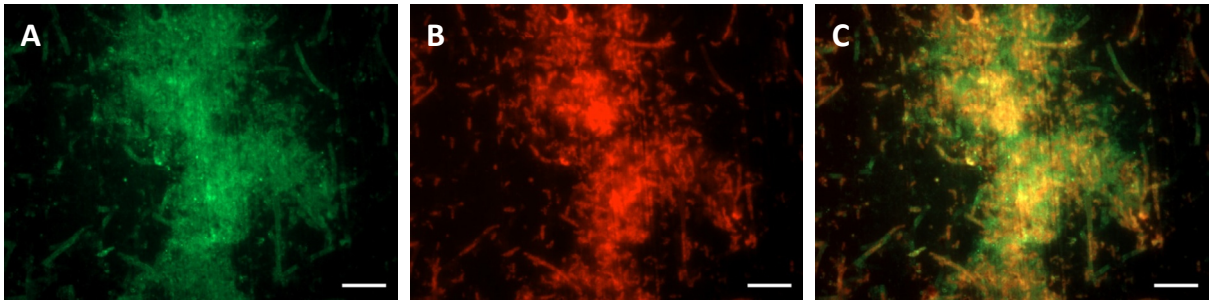

Figure 38: Biofilm formation of *L. discophora* SS-1 on a stainless steel coupon. EFM images of cells of *L. discophora* SS-1 stained with **SYTO83** and **SBA** grown in MSVP-2 medium supplemented with 0.2 mM Mn(II) for 3 d at 28 °C. (A) green: FITC-SBA signal (B) red: SYTO83 signal (C) merged image of (A) and (C). Bar 10 µm.

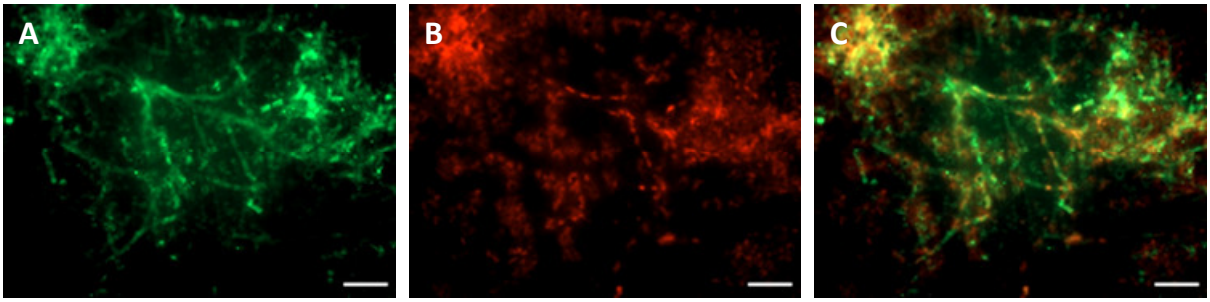

Figure 39: Biofilm formation of *L. discophora* SS-1 on a stainless steel coupon. EFM images of cells of *L. discophora* SS-1 stained with **SYTO83** and **UEA-I** grown in MSVP-2 medium supplemented with 0.2 mM Mn(II) for 3 d at 28 °C. (A) green: FITC-UEA-I signal (B) red: SYTO83 signal (C) merged image of (A) and (C). Bar 10 µm.

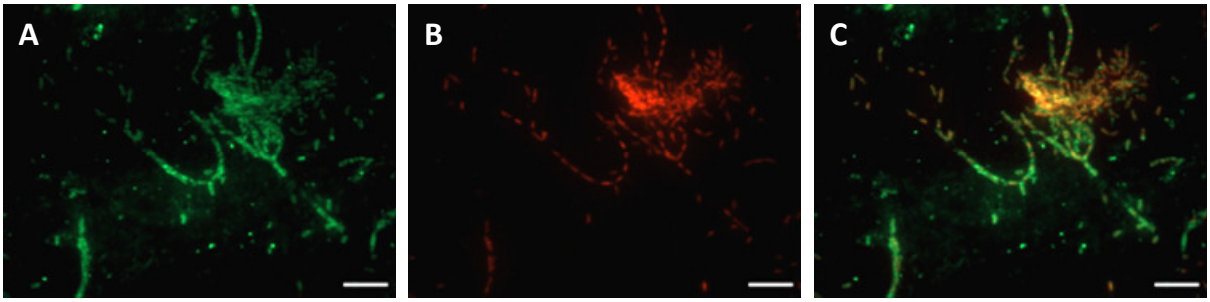

Figure 40: Biofilm formation of *L. discophora* SS-1 on a stainless steel coupon. EFM images of cells of *L. discophora* SS-1 stained with **SYTO83** and **DBA** grown in MSVP-2 medium supplemented with 0.2 mM Mn(II) for 3 d at 28 °C. (A) green: FITC-DBA signal (B) red: SYTO83 signal (C) merged image of (A) and (C). Bar 10 µm.

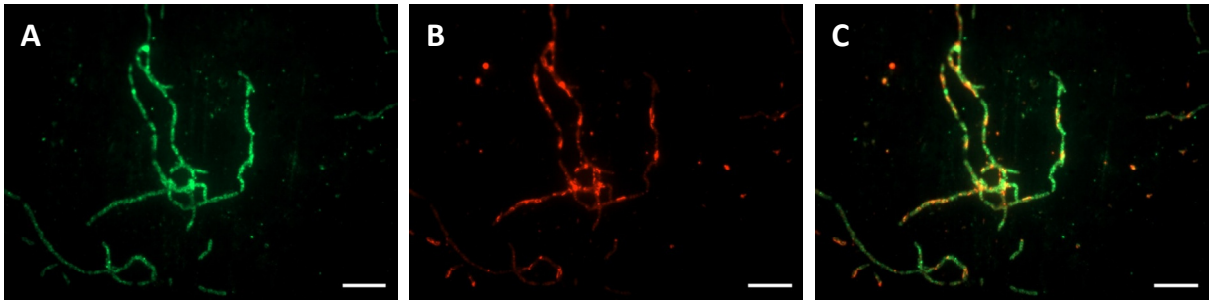

Figure 41: Biofilm formation of *L. discophora* SS-1 on a stainless steel coupon. EFM images of cells of *L. discophora* SS-1 stained with **SYTO83** and **PWM** grown in MSVP-2 medium supplemented with 0.2 mM Mn(II) for 3 d at 28 °C. (A) green: FITC-PWM signal (B) red: SYTO83 signal (C) merged image of (A) and (C). Bar 10 µm.

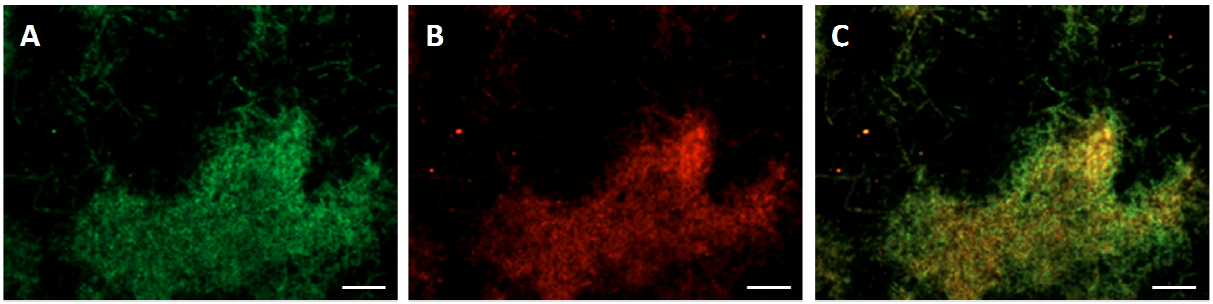

Figure 42: Biofilm formation of *L. discophora* SS-1 on a stainless steel coupon. EFM images of cells of *L. discophora* SS-1 stained with **SYTO83** and **PHAE-I** grown in MSVP-2 medium supplemented with 0.2 mM Mn(II) for 3 d at 28 °C. (A) green: FITC-PHAE-I signal (B) red: SYTO83 signal (C) merged image of (A) and (C). Bar 10 µm.

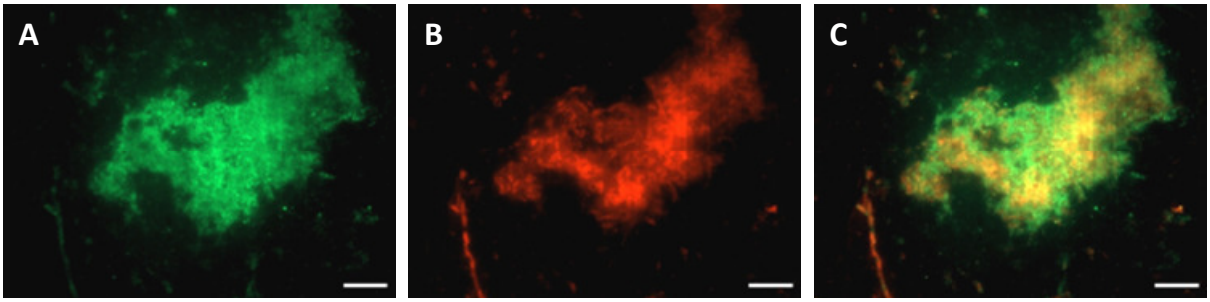

Figure 43: Biofilm formation of *L. discophora* SS-1 on a stainless steel coupon. EFM images of cells of *L. discophora* SS-1 stained with **SYTO83** and **PNA** grown in MSVP-2 medium supplemented with 0.2 mM Mn(II) for 3 d at 28 °C. (A) green: FITC-PNA signal (B) red: SYTO83 signal (C) merged image of (A) and (C). Bar 10 µm.

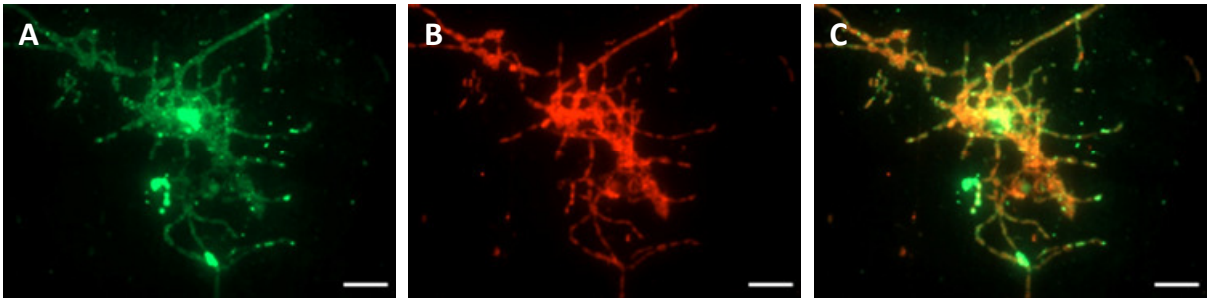

Figure 44: Biofilm formation of *L. discophora* SS-1 on a stainless steel coupon. EFM images of cells of *L. discophora* SS-1 stained with **SYTO83** and **MPA** grown in MSVP-2 medium supplemented with 0.2 mM Mn(II) for 3 d at 28 °C. (A) green: FITC-MPA signal (B) red: SYTO83 signal (C) merged image of (A) and (C). Bar 10 µm.

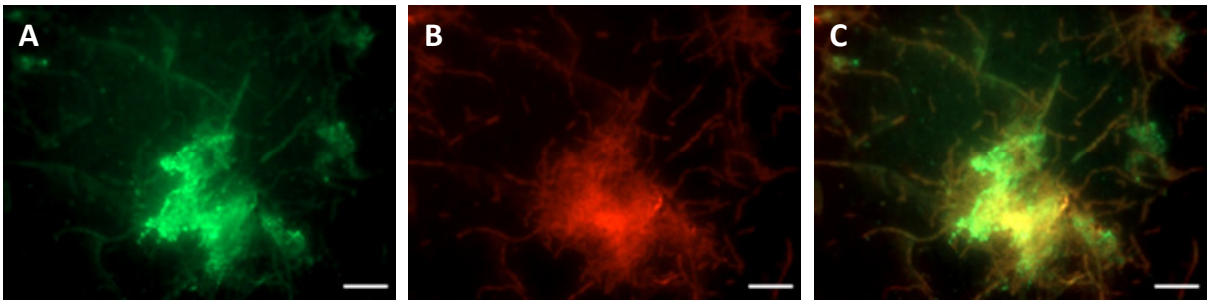

Figure 45: Biofilm formation of *L. discophora* SS-1 on a stainless steel coupon. EFM images of cells of *L. discophora* SS-1 stained with **SYTO83** and **LPA** grown in MSVP-2 medium supplemented with 0.2 mM Mn(II) for 3 d at 28 °C. (A) green: FITC-LPA signal (B) red: SYTO83 signal (C) merged image of (A) and (C). Bar 10 µm.

Biofilms on SS coupons grown with MSVP-2 medium supplemented with 0.2 mM Mn(II) were brownish in color compared to SS coupons grown in MSVP-2 medium without addition of Mn(II). The leucoberbelin test for manganese oxides was positive in all cases. The lectins ConA, PHAE-I and GS-II mainly labeled the biofilm comparable to the staining pattern of the nucleic acid stain. ConA, however, also stains presumably the biofilm matrix (EPS). Especially GS-II mainly stains the cells themselves and outlines the cells precisely as indicated by the nucleic acid stain. Even more, it is sometimes stronger in fluorescence than the nucleic acid stain. The lectins GS-I, SBA, UEA-I, DBA, PWM, PNA, MPA and LPA presumably mainly stained parts of the EPS in-between the cells and EPS covering and/or surrounding the microcolonies. However, the staining pattern of the lectins in some parts is very similar to the staining pattern of the nucleic acid stain, especially if single cells or thin biofilms are present. By comparison of the lectin signals with their respective specificity for glycoconjugate residues the presence of the following carbohydrates is indicated: mannose or glucose (ConA), melibiose (GS-I), galactose (GS-I, SBA, PNA, MPA), fucose (UEA-I), N-acetylglucosamine (GS-II, PWM, PHAE-I), N-acetylgalactosamine (SBA, PHAE-I, MPA), methyl-2-acetamido-2-deoxy-D-galactose (DBA), N-acetyllactosamine (PWM) and sialic acids (LPA).

The lectins SBA, PNA, MPA, PWM, DBA and UEA-I showed for some parts of the biofilm a particular staining pattern: they labeled a shell-like structure surrounding the cells. This structure outlines the red nucleic acid stain very precisely and follows the filament-like growth structure, which spreads over the surface. Figure 46 shows an exemplary image of the shell-like structure with cells. The cells are stained in red (Syto83) and the structure in green (FITC-PNA).

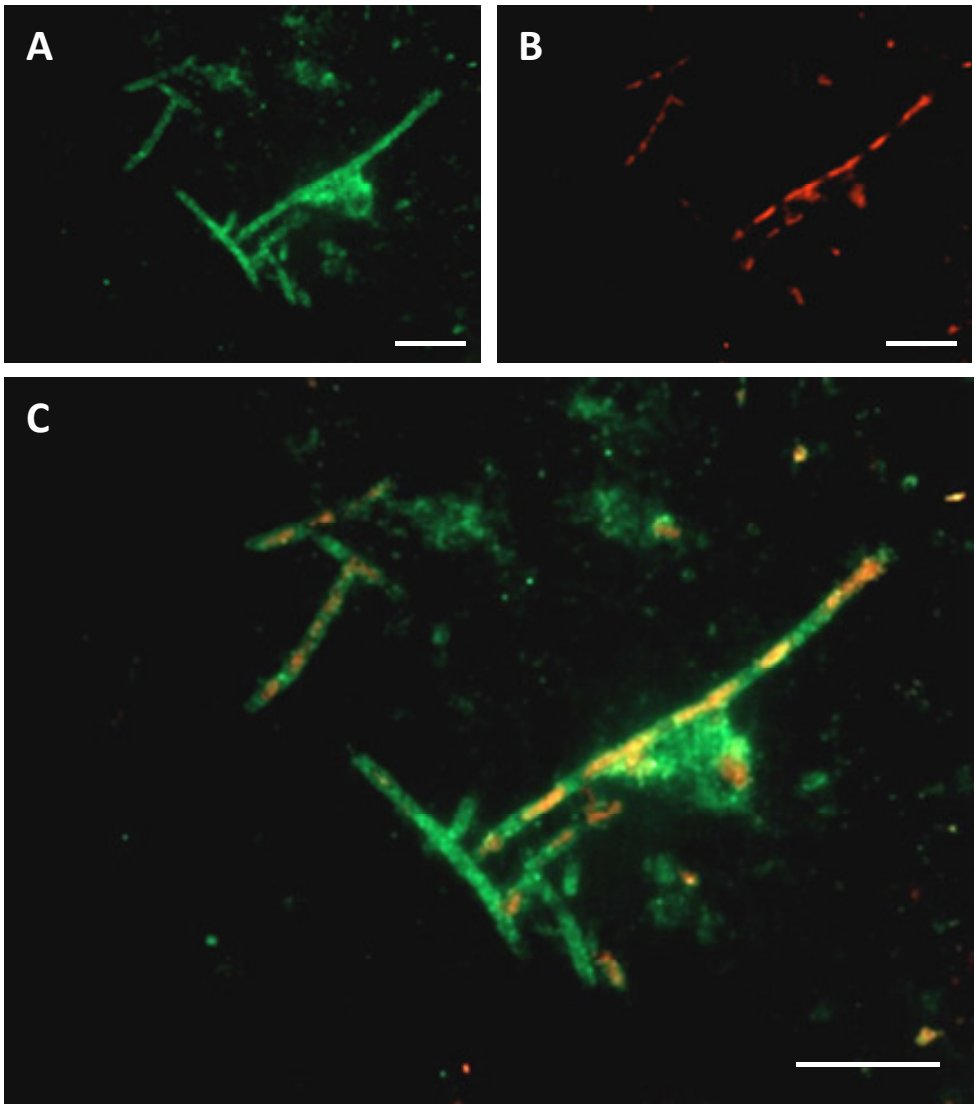

Figure 46: Image of *L. discophora* SS-1 cells on a stainless steel coupon grown with Mn(II). EFM images (cropped) of cells of *L. discophora* SS-1 stained with **SYTO83** and **PWM** grown in MSVP-2 medium supplemented with 0.2 mM Mn(II) for 3 d at 28 °C. (A) green: FITC-PWM signal (B) red: SYTO83 signal (C) merged image of (A) and (C). Bar 10 µm.

The cells are separated from each other but connected by a continuous filament-like (possibly sheaths) green structure. However, some of these filaments are free of cells. The lectins SBA, PNA, DBA and MPA are specific for a galactose-type carbohydrate, while PWM and UEA-I are specific for N-acetyllactosamine and fucose, respectively. Other lectins did not

stain these structure. This indicates the possible importance of galactose and in part N-acetyllactosamine and fucose for these presumed sheaths. Throughout the study it was evident that cells of *L. discophora* SS-1 do not exclusively appear on surfaces with shell- or filament-like structures. Some cells were even not stainable by lectins at all or only showed a thin green stain by various FITC labeled lectins (data not shown).

4.4 Open circuit- and pitting potential determination

The OCP of SS 1.4301 (18/10 austenitic chrome nickel alloy) was monitored to evaluate, whether biofilm formation of *L. discophora* SS-1 and manganese oxide precipitation lead to a shift of the OCP compared to sterile and manganese free controls. Additionally, the E_{pit} was determined to elucidate, whether a potential shift of the OCP would lead to an increased probability of chloride induced pitting (OCP is above E_{pit}; E_{pit} is in a potential range of 420 to 510 mV vs. SHE under the given conditions).

Therefore, the OCP was monitored in a 3 electrode setup (3.10.1), a SS 1.4301 cylinder served as working electrode, mercury/mercurous-sulfate was used as a reference electrode and a 2 cm^2 platinum sheet served as a counter electrode. The OCP was monitored in sterile MSVP-2 medium with and without addition of 0.2 mM Mn(II) and in inoculated MSVP-2 medium with and without addition of 0.2 mM Mn(II). The OCP after 96 h is shown in Figure 47. Afterwards the E_{pit} was determined (Figure 48 and Table 15).

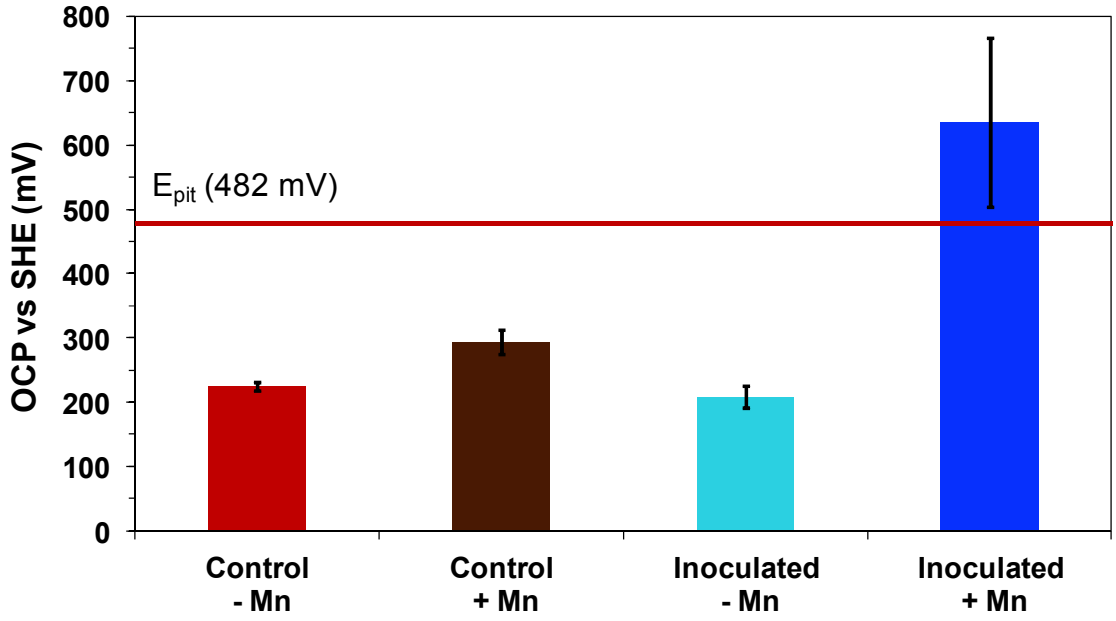

Figure 47: Average values of open circuit potential measurements of stainless steel in MSVP-2 medium. OCP values (SHE) of SS (1.4301) after 96 h in MSVP-2 medium at 28 °C supplemented with or without 0.2 mM Mn(II) (± Mn), inoculated with *L. discophora* SS-1 or sterile (control), n = 3. The average OCP of SS is: 225 mV (Control -Mn), 294 mV (Control +Mn), 208 mV (Inoculated -Mn) and 635 mV (Inoculated +Mn). The red line indicates the mean Epit (482 mV) of the data presented in Table 15. Stainless steel (1.4301) was used as working electrode, mercury/mercurous-sulfate was used as a reference electrode and a 2 cm^2 platinum sheet served as a counter electrode.

The mean OCP (SHE) of SS after 96 h in sterile MSVP-2 medium without addition of 0.2 mM Mn(II) accounted to 225 mV, with addition of 0.2 mM Mn(II) to 294 mV, inoculated but without addition of 0.2 mM Mn(II) to 208 mV and inoculated with supplementation of 0.2 mM Mn(II) to 635 mV. All samples were tested for the presence of manganese oxides on the surface (leucoberbelin test). Only the surface of the SS incubated in MSVP-2 medium inoculated with *L. discophora* SS-1 and supplemented with 0.2 mM Mn(II) was positive for manganese oxides. However, a distinct biofilm was also visible on the SS cylinder incubated in inoculated MSVP-2 medium without addition of 0.2 mM Mn(II). The OCP of the SS with manganese oxides and *L. discophora* SS-1 cells on the surface is approximately 400 mV higher compared to the mean value of all OCP´s without manganese oxides on the surface. This anodic shift leads to an OCP, which is well above the average E_{pit} for this SS under the given conditions. For all other conditions (without manganese oxides on the surface) the OCP is well below the E_{pit}. The potentiodynamic polarization curves and E_{pit} values for a set of 6 samples (2 controls; 4 inoculated samples) are given in Figure 48 and Table 15, respectively. The E_{pit} values range from 416 to 511 mV (SHE) with an average E_{pit} of approx. 482 mV.

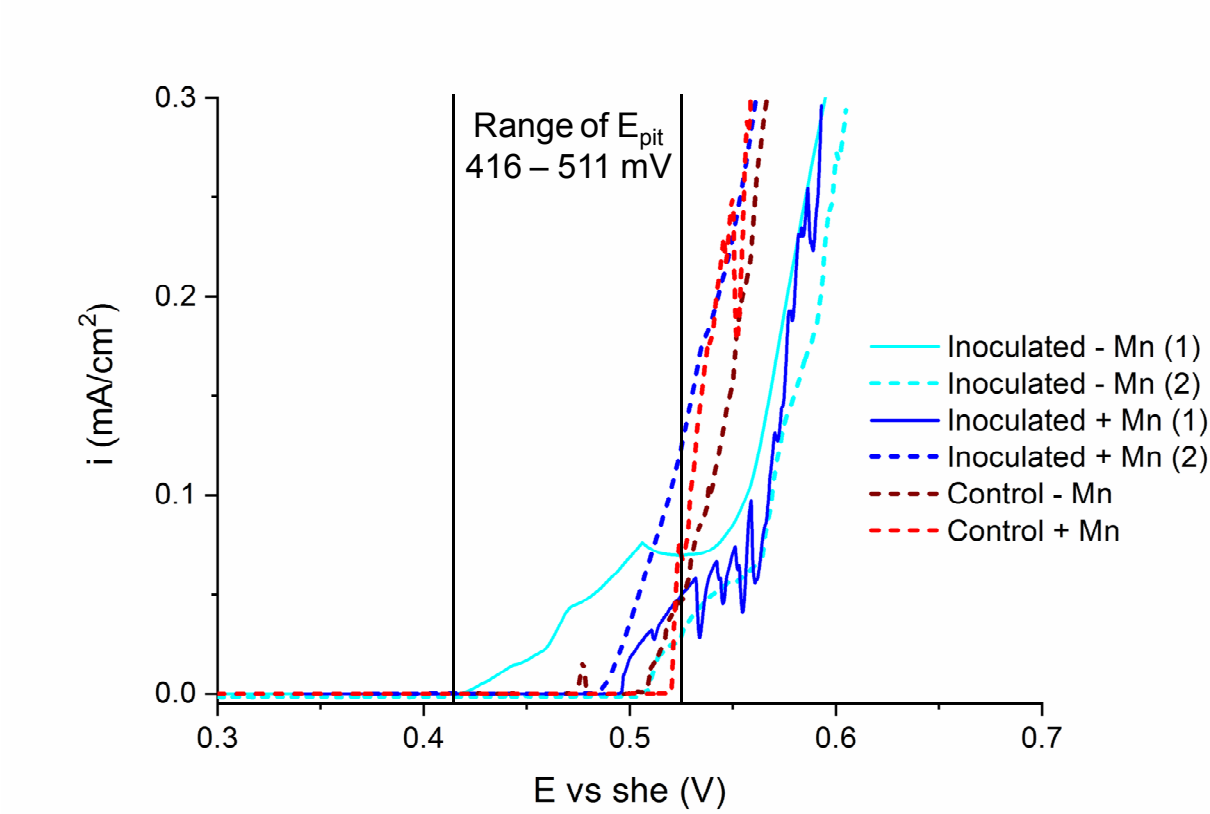

Figure 48: Current density-potential curves (I vs. U) of stainless steel (1.4301) in sterile (control) and inoculated (*L. discophora* SS-1) MSVP-2 medium supplemented with or without (±) 0.2 mM Mn(II). Single measurements from potentiodynamic polarization in anodic sweep direction (scan rate 0.01 mV sec^{-1}) after OCP monitoring. Start of measurement at E = OCP - up to 300 mV. Stop of measurement at a given current density of 2 mA cm^{-2}. Stainless steel (1.4301) was used as working electrode, mercury/mercurous-sulfate was used as a reference electrode and a 2 cm^2 platinum sheet served as a counter electrode. The range of E_{pit} is indicated in-between the two vertical black bars.

Table 15: Pitting potential values of stainless steel (1.4301) in sterile (control) and inoculated MSVP-2 medium supplemented with or without (±) 0.2 mM Mn(II). Single measurements, determined from potentiodynamic polarization in anodic sweep direction (scan rate 0.2 mV sec^{-1}) after OCP monitoring.

Sample	**E_{pit} (mV)**
Control – Mn	504
Control + Mn	511
Inoculated – Mn	509
Inoculated – Mn	416
Inoculated + Mn	491
Inoculated + Mn	465

4.5 Scanning Kelvin probe studies of *L. discophora* SS-1

In the previous experiments the growth and manganese oxidation, the EPS, the biofilm formation and their global effect (ennoblement) on the electrochemical degradation of stainless steel was analyzed subsequently. Finally, a combination of EFM and an AFM equipped with a scanning Kelvin probe module (SKPFM) was used to gain further insights into the influence of *L. discophora* SS-1 cells and manganese oxides on the surface potential of stainless steel and to elucidate the electrochemical processes.

To analyze and visualize attachment and biofilm formation, cells of *L. discophora* SS-1 were allowed to colonize vertically submerged stainless steel coupons for 1 h. Afterwards, adhering cells were stained with DAPI and samples were processed with EFM and SKPFM (see Figure 49).

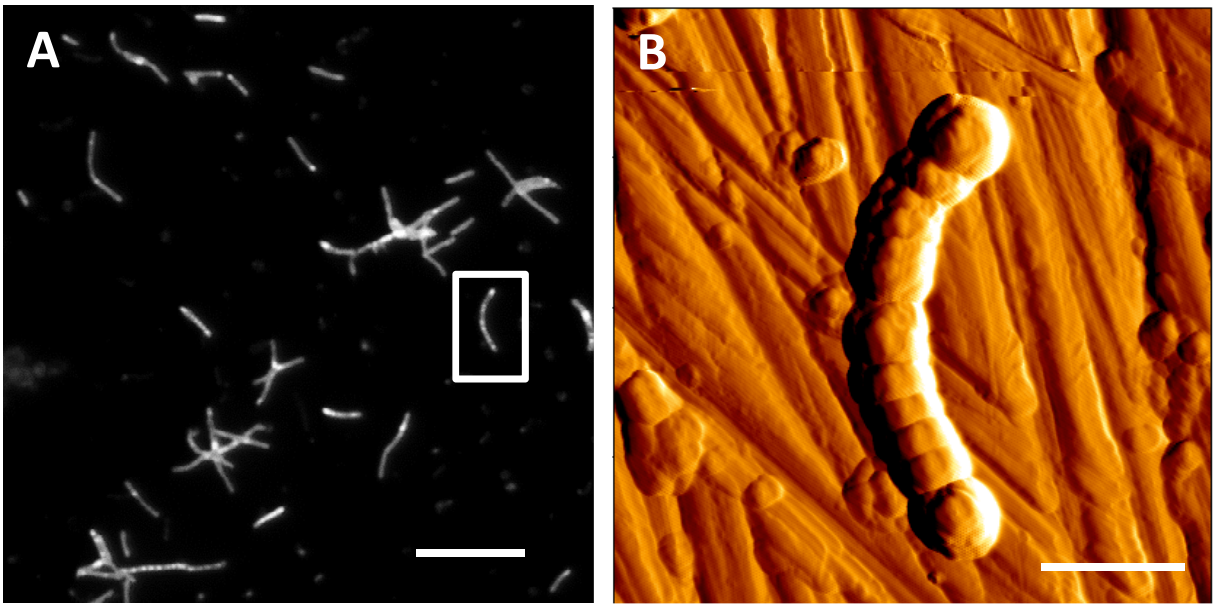

Figure 49: EFM and AFM images of cells of *L. discophora* SS-1 attached to stainless steel. Cells were incubated with vertically submerged SS coupons for 1 h in MSVP-2 medium at 28°C. A: EFM image of *L. discophora* SS-1 cells labeled with DAPI. Bar 10 µm. B: AFM image of the single cell which is visible in image A in the white rectangle. Bar 2 µm. Intermittent Contact, Line rate 0.3 Hz, target amplitude 5 V.

Cells of *L. discophora* SS-1 attached to the steel surface are shown in Figure 49 A. Figure 49 B shows a high resolution AFM image of an attached cell, the original location is indicated by a white rectangle in Figure 49 A. In contrast to pictures of densely populated surfaces, the blank steel is still visible, similar to freshly ground coupons without precipitations or biomolecules (for comparison see Figure 53 and Figure 54).

It is necessary to understand the effects of single cells and manganese oxides (without cells) to the surface of SS individually, before the complex system of a manganese encrusted biofilm is investigated. Therefore, *L. discophora* SS-1 cells and manganese(IV)-oxides were measured separately to identify their individual influence on the CPD towards the steel surface (see Figure 50, Figure 51 and Figure 52).

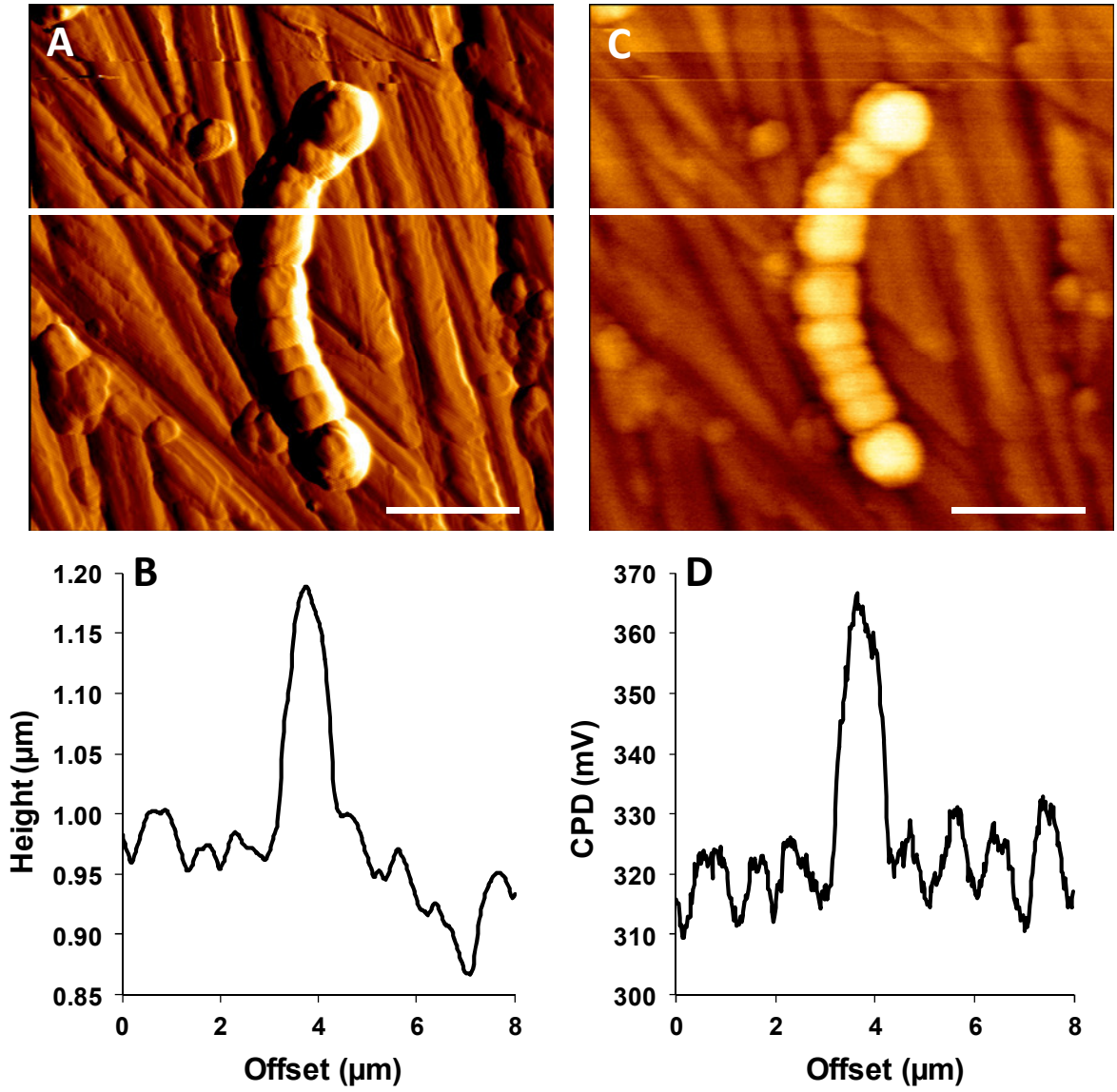

Figure 50: AFM and SKPFM images of cells of *L. discophora* SS-1 attached to stainless steel. A: AFM image of a single cell; B: Corresponding height profile. C: SKPFM image of the same cell; D: Corresponding contact potential difference (CPD) profile. The white lines in A and C indicates the areas of height (B) and CPD profile (D). Intermittent Contact, Line rate 0.3 Hz, target amplitude 5 V. Bar 2 µm. Cells were incubated with vertically submerged SS coupons for 1 h in MSVP-2 medium at 28°C.

AFM and SKPFM measurements were performed on dried samples. Nevertheless, surface topography (Figure 50; left) and CPD mapping (Figure 50; right) correlate well. The imaged cell is approximately 0.2 µm in height and has a CPD of approximately + 50 mV (difference

from baseline value (316.88 mV) to peak maximum (366.62 mV)), compared to the plain steel surface. In contrast, the CPD mapping of manganese oxides reveals a negative potential of up to approximately - 226 mV (difference of baseline value (323.15 mV) to the average of the two peak maximum values (71.53 and 122.06 mV)) compared to the steel surface (Figure 51 C&D). Also in this case surface topography and CPD correlate well (Figure 51).

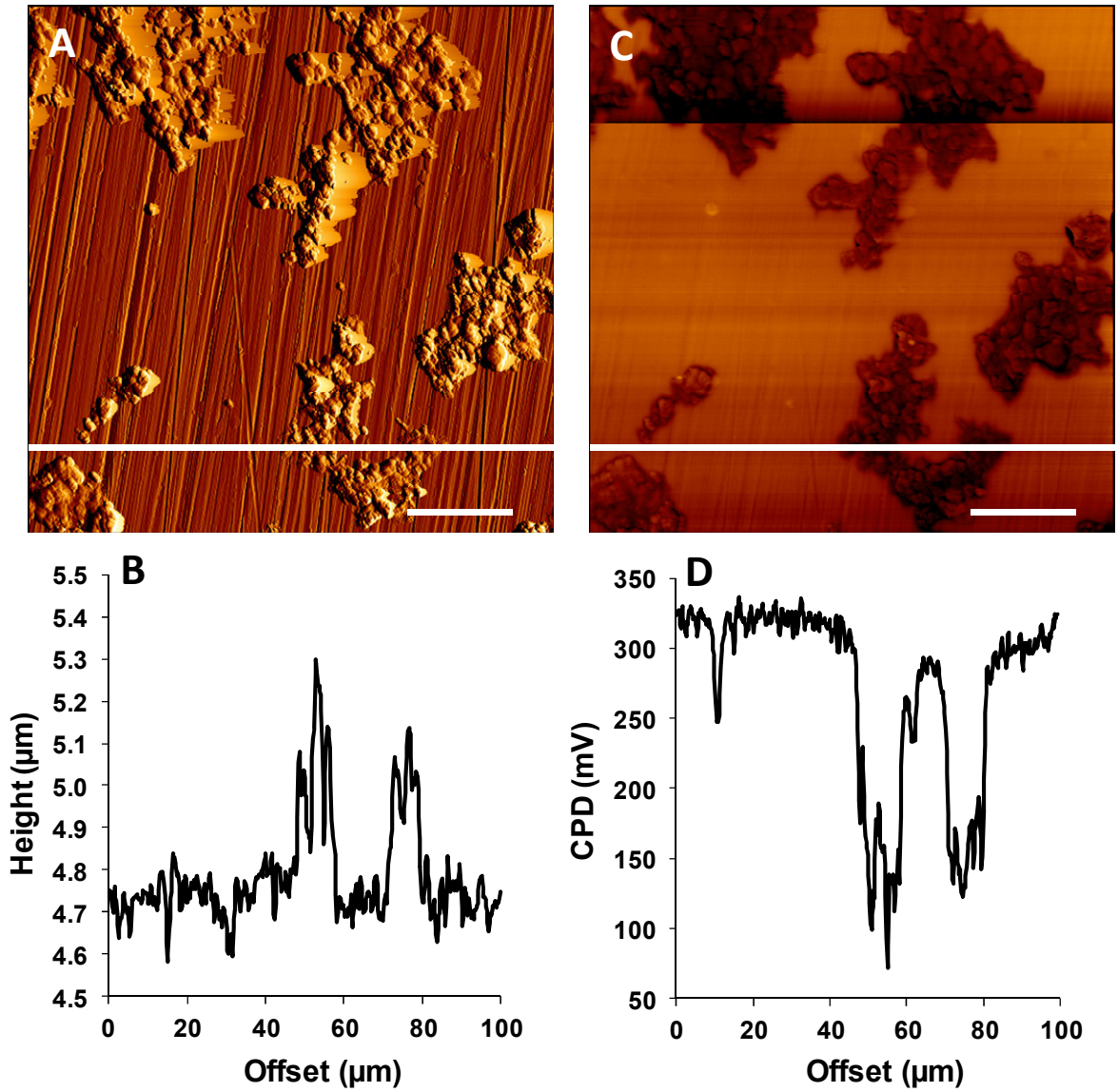

Figure 51: AFM and SKPFM images of biologically produced manganese oxides deposited on stainless steel. A: AFM image of manganese oxides; B: Corresponding height profile. C: SKPFM image of the same manganese oxides; D: Corresponding contact potential difference (CPD) profile. The white lines in A and C indicates the areas of height (B) and CPD profile (D). Intermittent Contact, Line rate 0.3 Hz, target amplitude 5 V. Bar 20 µm. For details of manganese oxide appliance see chapter 3.10.2.

These results are supported by similar findings with electrodeposited manganese oxides on the steel surface (Figure 52). Figure 52 A&B show the surface topography with the

corresponding height profile, while Figure 52 C&D show the SKPFM image with the corresponding CPD profile. The electrochemically deposited manganese can be seen in the upper part of the topographic surface image as a layer on top of the steel surface (leucoberbelin positive). This layer is also visible in the SKPFM image as a strongly negative (dark part) CPD. The average CDP of the manganese surface is - 204 mV and the average CPD of the plain steel surface is 412 mV. The CPD between the manganese oxides and the steel surface is therefore approximately -616 mV.

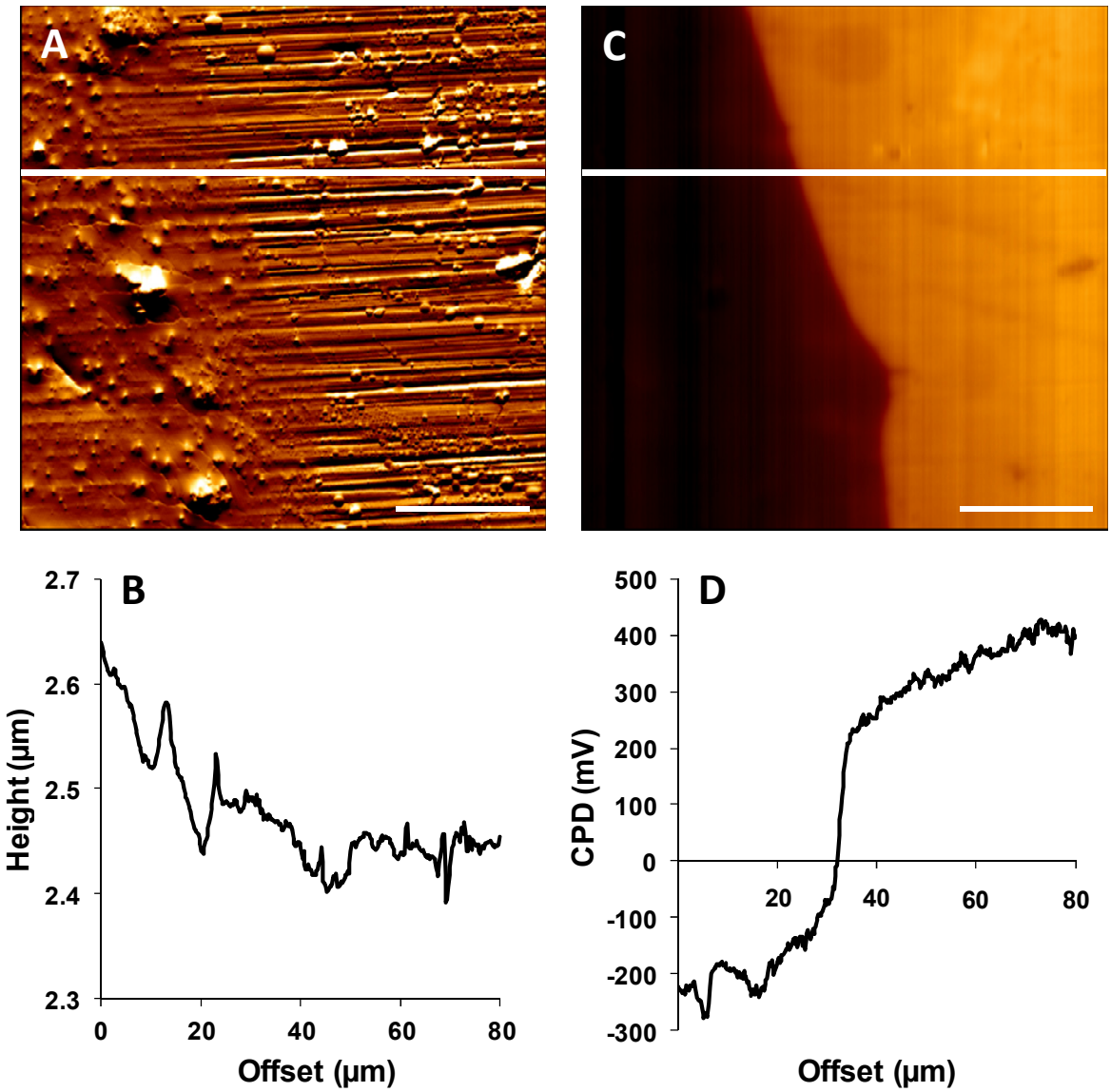

Figure 52: AFM and SKPFM images of electrodeposited manganese oxides on stainless steel. A: AFM image of manganese oxides; B: Corresponding height profile. C: SKPFM image of the same manganese oxides; D: Corresponding contact potential difference (CPD) profile. The white lines in A and C indicates the areas of height (B) and CPD profile (D). Intermittent Contact, Line rate 0.3 Hz, target amplitude 5 V. Bar 20 µm. For details of manganese oxide appliance see chapter 3.10.2.

After elucidating the effect of cells and manganese oxides individually on the SS surface, the complex system of a mature biofilm (7 d) was analyzed with EFM, bright field microscopy and SKPFM (Figure 53 and Figure 54). Bacteria were grown on vertically submerged stainless steel coupons in MSVP-2 medium with the addition of 0.2 mM Mn(II). Brownish, leucoberbelin positive precipitates were visible on the SS surface.

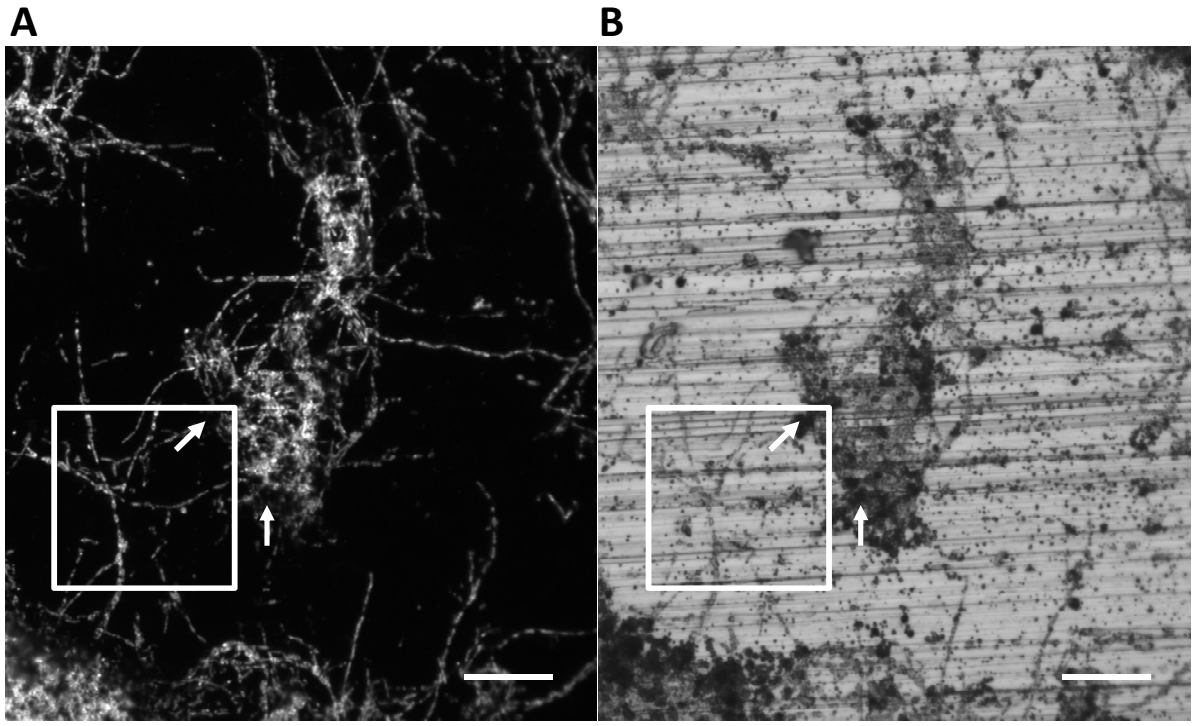

Figure 53: EFM and bright field images of a biofilm of *L. discophora* SS-1 on stainless steel. A: EFM image of Syto 9 labeled *L. discophora* cells. B: Bright field image of the same area. Arrows indicate dark spots and the white square indicates the position of the AFM and SKPFM images in Figure 54. Colonies and precipitates are visible. Cells were grown on vertically submerged SS coupons for 7 d in MSVP-2 medium with 0.2 mM Mn(II) at 28°C. Bar 20 µm.

The EFM image shows filaments of bacteria, overgrowing the surface and partly stretching from one microcolony to another (Figure 53). Parts of the microcolonies are covered with dark structures, which appear brownish in bright field microscopy (see arrows in Figure 53). The dark spots proved to be not stainable by Syto9 and further investigations with the SKPFM showed a CPD of up to – 220 mV compared to the steel surface (Figure 54). Figure 54 shows the excerpt highlighted in Figure 53 with the white rectangle. Figure 54 A shows a topographic surface image with filamentous, chain like structures which can mostly be related to bacterial cells. They were also identified with a nucleic acid stain in the corresponding EFM image (Figure 53). Figure 54 B shows the corresponding CPD image. Arrow 1 points to a cathodic area. This area has a CPD of up to - 220 mV towards the steel surface. The steel surface is indicated by arrow 2. Arrow 3 points to an anodic area with a CPD of up to + 200 mV towards the steel surface. The total difference between cathodic and

anodic areas has a maximum of 420 mV (cathodic area - 220 mV; steel surface 0 mV; anodic area + 200 mV). A freshly ground stainless steel incubated under similar but sterile conditions did not show any significant variation in the CPD (data not shown).

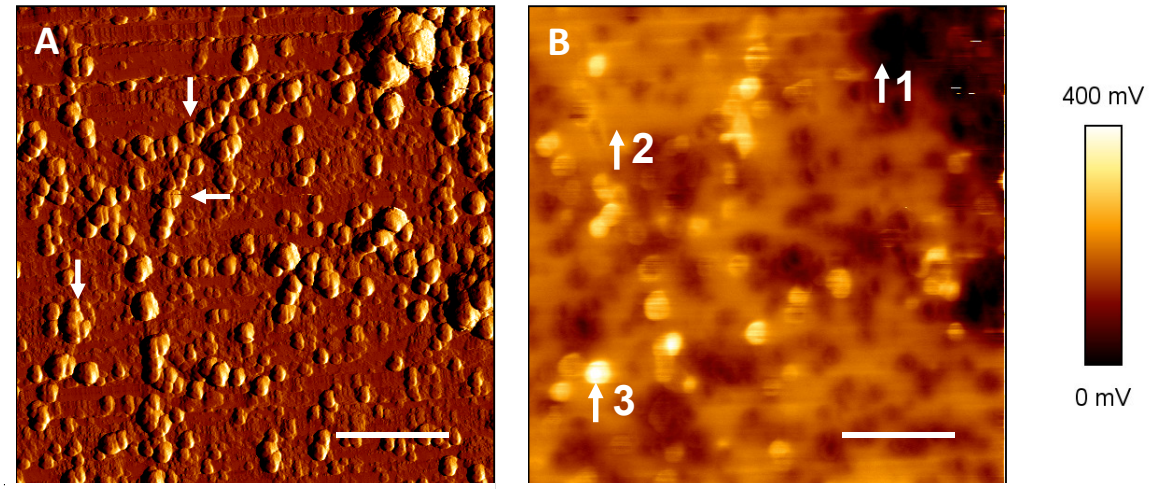

Figure 54: AFM and SKPFM images of a biofilm of *L. discophora* SS-1 on stainless steel. A: AFM image of the area highlighted in Figure 53 with the white square. Arrows indicate chain like structures of bacterial cells. B: Corresponding SKPFM image. Arrow 1 indicates a cathodic area (0 mV), arrow 2 indicates the steel surface (+ 220 mV) and arrow 3 indicates an anodic area (+ 420 mV). Intermittent contact, Line rate 0.3 Hz, target amplitude 5 V. Cells were grown on vertically submerged SS coupons for 7 d in MSVP-2 medium with 0.2 mM Mn(II) at 28°C. Bar 10 µm.

5 Discussion

5.1 Growth and manganese oxidation of *L. discophora* SS-1

The growth of cells of *L. discophora* SS-1 was analyzed with 2 different media with or without an addition of 0.2 mM Mn(II). Additionally, the effect of supplementation of 0.2 or 0.4 mM Mn(II) on the protein and ATP content of stationary cell cultures was assessed. The experiments resulted in new insights into the response of cells of *L. discophora* SS-1 to the afore mentioned factors. Furthermore, they delivered fundamental information for subsequent mass culturing for EPS analysis as well as for formation and analysis of biofilms.

The generation time and maximum cell density in B12 or MSVP-2 medium with 0.02 % yeast extract were comparable (2.0 h to 2.3 h and $4.3x10^8$ to $2.7x10^8$ cells mL^{-1}). However, the lag phase for cells grown in MSVP-2 medium increased two times (2 h to 4 h). This is likely due to the lack of high amounts of complex carbon sources in the MSVP-2 medium (Nelson et al. 1999) compared to the B12 medium. The B12 medium contains complex carbon sources (1 % yeast extract and 1.5 % peptone), whereas MSVP-2 is a minimal medium containing only salts, vitamins, pyruvate and 0.02 % yeast extract. The growth of cells of *L. discophora* SS-1 in MSVP-2 medium without addition of yeast extract is also possible, however, cells tend to form long filaments (Nelson et al. 1999) rendering the determination of the generation time difficult. To test the influence of manganese ion supplementation on the generation time as well as on the protein and ATP content the MSVP-2 medium was supplemented for the particular experiments with 0.02 % yeast extract. Since growth and manganese oxidation are still possible without addition of yeast extract, all other experiments were carried out without yeast extract. This was done to eliminate possible effects of yeast extract on the attachment of cells of *L. discophora* SS-1 as well as on the corrosion behavior of the SS. The later has been discussed in a review by Little & Ray (Little and Ray 2002) as a possibility for serious mistakes. The manganese oxidation was concomitant with cell growth and started approximately 2 h thereafter. The addition of 0.2 mM Mn(II) to B12 or MSVP-2 media resulted in an approximately 50 % increase of the generation time (3.0 h and 3.2 h). This might be due to interferences of manganese ions with the physiological processes in *L. discophora* SS-1 (Adams and Ghiorse 1985). Other possible interfering effects are a substitution of other divalent cations like Mg^{2+} by manganese ions or non specific toxic effects related to heavy metals (Ehrlich 1978; Gadd and Griffiths 1977; Goodman et al. 1983). Despite an increase in the generation time, which was also found by Adams & Ghiorse (Adams and Ghiorse 1985), the lag phase was also prolonged in presence of manganese ions. This indicates the necessity of an upregulation of the protein synthesis responsible for

manganese oxidation in *L. discophora* SS-1 (Adams and Ghiorse 1987) before the growth started. The upregulation is time consuming and this might result in a prolonged lag phase. Manganese oxidation was always complete. All manganese ions were fully oxidized (determined by the decrease of manganese ions in the medium by AAS) to manganese oxides within 15 h to 20 h after inoculation and well before the end of the exponential growth phase. One the one hand, this explains why there were no manganese ions found in the EPS of cells of *L. discophora* SS-1. On the other hand this supports the assumption of interferences of manganese ions with physiological processes in *L. discophora* SS-1, since all manganese ions were removed from the aqueous phase before the end of growth.

The cell density increased in case of addition of manganese ions to the medium from $4.3x10^8$ to $7.4x10^8$ cells mL^{-1} in B12 medium and from $2.7x10^8$ to $6.8x10^8$ cells mL^{-1} in MSVP-2 medium. The increase in cell density cannot be attributed to manganese oxidation since it has been shown that *L. discophora* SS-1 does not derive energy from manganese oxidation (Ehrlich and Newman 2009). The higher TCC might be a result of a different dispersal of the cells due to manganese oxides present in the medium. It is known from literature that *L. discophora* grows in long chains and filaments during parts of its life cycle (Adams and Ghiorse 1985; Pringsheim 1949). The long chains might disperse into small chains or single cells due to shear forces that might occur with stirring together with the manganese particles. Another possibility is that *L. discophora* SS-1 grew in short chains or filaments ab initio, thus resulting in increased microscopic counts. This assumption is supported by microscopic examinations, which showed a high number of brownish refractive particles (presumably manganese oxides) in cultures grown with addition of 0.2 mM Mn(II). Although differentiation between particles and cells might have affected cells counts, cells attached to these particles as well as short chains and single rod shaped cells were identified. The chains appeared to be shorter in cultures grown with manganese ions compared to cultures grown without. Additionally, measurement of the total ATP and protein content of homogenized stationary phase (24 hours after inoculation) cell cultures of *L. discophora* SS-1 point to a lower cell mass in cultures grown with manganese ions. Cell cultures grown in MSVP-2 without addition of 0.2 mM Mn(II) showed a total ATP and protein content of 96.1 ng/mL (± 5.1) and 58.6 µg/mL (± 3.7), while cell cultures grown in MSVP-2 with addition of 0.2 mM Mn(II) showed a reduced total ATP and protein content of 57.6 ng/mL (± 5.8) and 26.8 µg/mL (± 2.1). Addition of 0.4 mM Mn(II) further reduced the ATP and protein contents. Additionally, the total cell counts decreased alongside with the ATP and protein content with increasing concentration of manganese ions. Microscopic examinations showed a high number of cells attached to manganese particles, elongated chains of cells and less single cells compared to microscopic examination of cultures grown with manganese ions for the determination of the

generation time. While the decrease of the TCC is contradictory to the earlier findings in this study, it is in agreement with literature reports. Adams and Ghiorse (Adams and Ghiorse 1985) stated that levels higher than 0.055 mM Mn(II) lead to a decrease in total cell numbers. The TCC in the experiments for determination of total ATP and protein content was lower compared to the TCC from experiments of the determination of the generation time. This might be a result of different shear forces due to different growth conditions. Cultures for determination of the generation time were stirred, while cultures for determination of ATP and protein content were shaken.

Although manganese oxidation in *L. discophora* SS-1 does not contribute to cell mass, there are beneficial effects. Tebo et al. (Tebo et al. 2005) pointed out that bacteria precipitate extracellular manganese oxides in order to coat themselves as a protective mechanism against environmental stress factors like UV-irradiation, predation, viral attack and heavy metal toxicity. Protection to UV-irradiation might be beneficial e.g. in surface waters, protection from predation or viral attack might be beneficial in environments with high number of protozoan grazers or viruses, while the absorptive capacities of manganese oxides might deliver protection from other divalent cations (heavy metals).

5.2 Analysis of the effect of different growth conditions on the EPS of *L. discophora* SS-1

The potential effect of 4 different growth conditions on the composition of the loosely and tightly bound EPS of cells of *L. discophora* SS-1 was examined in detail with different analytical methods. This was done to draw conclusions on the potential effects of the presence of Mn(II) and/or a SS surface on EPS and, consequently, on biofilm formation, manganese oxidation and finally corrosion

Several authors report that the extraction procedure has a significant influence on the biochemical composition of the EPS extracts (Comte et al. 2006; D'Abzac et al. 2010; Frølund et al. 1996; Michalowski 2012). Therefore, a suitable method should extract the different components equally and avoids the enrichment of certain substance classes. Additionally, it should not interfere with the subsequent analysis and cause minimal cell lysis. There are various extraction procedures described in literature: extraction by chemical agents such as NaOH, formaldehyde, EDTA, or crown ether, physical methods like centrifugation, sonication, filtration or heating and combinations of both such as the use of a CER (e.g. Dowex) and shear force (Brown and Lester 1980; Frølund et al. 1996; Michalowski 2012; Nielsen and Jahn 1999; Wingender et al. 1999; Wingender et al. 2001). Several authors suggest the use of the CER method since it causes minimal cell lysis, does not give

preference to certain substances or interfere with the subsequent analysis (D'Abzac et al. 2010; Michalowski 2012; Takahashi et al. 2010; Wingender et al. 1999). The study by Michalowksi (Michalowski 2012) focused on the comparison of various extraction procedures and their influence on the subsequent analysis with spectrophotometrical methods and possible cell lysis. Only the use of a CER combined both attributes. For example, formaldehyde and NaOH treatment resulted in interference with the carbohydrate determination, EDTA interfered with the protein and carbohydrate determination as well as the dialysis of the EPS, heating might result in impairment of cells indicated by a decreased culturability. Although advanced methods like FLBA as well as identification of lipids and carbohydrate monomers were applied in this study, the quantification of EPS components depends on the use of spectrophotometrical methods. Therefore, the CER method was chosen as the most promising technique for this study. A careful developed and evaluated method from Wikiel (Wikiel 2013) for the corrosion relevant class of SRP was adapted for this study with only minor modifications. To evaluate, if the CER method interferes with the subsequent analysis, a continuous set of controls was performed. The control (PBS-Control) contained amounts of CER and PBS comparable to the amounts of the extraction solution with CER, PBS and cells. An individual control was performed for every single time a EPS extraction was performed and treated the same way. No interferences of the extraction procedure were observed for the identification of lipids and carbohydrate monomers (no peaks in the respective chromatograms). Interferences with the spectrophotometric methods were minimal. In average the false positive signal due to the extraction procedure amount to 1.5 % (carbohydrates), 1.8 % (proteins) and 3.1 % (uronic acids) of the signal (amount) of the respective tightly bound EPS extract, no interferences were shown for DNA and lipid determination (data not shown). The signal of the control was subtracted from the respective result of the TB-EPS. For loosely bound EPS, di. water was used as a control. No interferences were observed. This indicates minimal to no interference of the CER extraction method with the subsequent analysis. Additionally, cell lysis was negligible, this matter will be discussed later in detail. All parameters were kept constant for reproducibility of the results (e.g. glass vessels, magnetic stirring, time, buffer). Especially the growth phase was monitored by TCC. Cell harvest and EPS extraction were always started in the late exponential phase (usually 72 h after inoculation). Since the extraction protocol was kept constant, the variations of the EPS composition shown in this study are a result of the presence of manganese ions and/or a SS surface. Additionally, carbohydrate to protein ratios were calculated as they can be used as an indicator for cell lysis and EPS extraction efficiency (Lewandowski and Beyenal 2013). Ratios above 4.2 indicate inefficient EPS extraction and below 0.2 indicate contamination from cell lysis for laboratory-cultivated biofilms. The ratios in this study are non critical in the sense of cell lysis as well as efficiency

and range from 0.86 to 2.92. Summarized, this indicates that the EPS extraction in this study with CER caused minimal to no cell lysis, was sufficiently efficient and did not interfere with the analysis. Yet, approximately only 40 – 60 % of the tightly bound EPS and approximately 10 – 20 % of the loosely bound EPS were identified by spectrophotometric determinations compared to the EPS dry weight. It is well known from literature that a large amount of EPS (based on dry weight) is not quantifiable (D'Abzac et al. 2010; Kuklinski 2017; Michalowski 2012; Takahashi et al. 2010; Teubner 2018; Wikiel 2013) with commonly applied methods. This is especially true for loosely bound EPS. Because of this limitation and to gain a deeper knowledge, the EPS of cells of *L. discophora* SS-1 were additionally analyzed with FLBA and by gas chromatographic analysis. Several studies implicate that the large unidentified part of the EPS is a result of inorganic compounds, interferences with the analytical methods or unspecific interferences with e.g. the dry weight determination (D'Abzac et al. 2010; Kuklinski 2017; Teubner 2018; Wikiel 2013). Interferences with the analytical methods can be neglected (as described above). However, inorganic compounds might interfere especially with the dry weight determination and might result in an over estimation of the dry weight. The EPS extraction in this study was performed in three consecutive extraction steps. With each extraction step the released amounts of organic compounds (carbohydrates, proteins, uronic acids, lipids and DNA) decreased gradually. However, the EPS dry weight did not decreased in the same way. Presumably, this is a result of inorganic compounds. This might be residual salts from the growth medium or inorganic compounds introduced into the EPS extract by the extraction procedure (CER). The final dialysis obviously could not quantitatively eliminate these inorganic compounds from the EPS. To test this hypothesis, an exemplary set of EPS extracts (all 4 growth conditions) was analyzed for the TOC content (see appendix 8.1). For loosely bound EPS (independent from which growth condition the EPS was extracted from), approximately 25 % of the dry weight was identified as organic carbon (TOC). Based on this, the identified amount of loosely bound EPS might be 4-fold underestimated. Manganese was not identified in these EPS extracts. This would also be consistent with the high dry weight of loosely bound EPS (about 5 to 15 times higher compared to the tightly bound EPS). Such a clear trend was not found for the tightly bound EPS. Here, approximately 21 % of the EPS dry weight could be recovered as TOC if cells were grown in MSVP-2 medium without addition of manganese ions, and 18 %, if cells were grown in presence of a SS surface but still without manganese ions. For the tightly bound EPS from cells grown in MSVP-2 medium with manganese ions, only approximately 1.5 % of the EPS dry weight could be recovered as TOC and 5 % for tightly bound EPS from cells grown in presence of manganese ions and a SS surface. While this might indicate an interference of manganese oxides or residual manganese ions with the TOC analysis or a contribution to the dry weight, manganese was also not found in the tightly EPS (determined

by AAS). The low recovery was in part a result of high TOC values in the control (data not shown, controls were subtracted from samples). This indicates an interference of the CER method with the TOC analysis by e.g. leakage of organic contaminants. A possible interference of the manganese oxides or residual manganese ions on the TOC analysis could be resolved in future studies by determining the TOC of a defined sample with and without manganese ions. This could be done by determining the TOC form the difference of potassium hydrogen phthalate (total carbon) and sodium carbonate (total inorganic carbon) with and without addition of manganese ions. However, this was not done in this study, since neither manganese oxides nor manganese ions were identified in any of the EPS extracts after dialysis. Nevertheless, TOC values were also generally lower, if EPS was extracted from cells grown with manganese ions compared to EPS extracted from cells grown without manganese ions. This shows that inorganic compounds might contribute to the dry weight of EPS and, therefore, result in lower quantified amounts of EPS components when based on the dry weight. While TOC analysis impressively shows that inorganic compounds contribute to a significant proportion to the EPS dry weight, TOC analysis did not proved to be a valid basis to base quantification of identified EPS components up on. On the one hand this is due to interferences of the CER method with the TOC analysis and on the other hand quantification based on TOC repeatedly lead to a significant overestimation of the identified compounds (up to 140 % of the TOC were identified by spectrophotometric determinations).
A possible inorganic contribution to the dry weight was found with bright field microscopy. Even after dialysis and filtration (0.2 µm) of the EPS extracts presumed inorganic particles were found. These particles had sharp and distinct edges and resembled the appearance of crystals or inorganic precipitates. These precipitates may have been formed during or after the extraction procedure and were not eliminated by dialysis and filtration. Presumably, they contributed to the dry weight of the EPS but were not analyzed with the applied methods in this study. Although the most probable inorganic compound, manganese was analyzed in this study, future studies need to evaluate the nature and origin of these particles using elemental analysis with e.g. inductively coupled plasma optical emission spectrometry (D'Abzac et al. 2010).

The EPS yield as dry weight per 10^{10} cells is approximately 2.5 x higher for both growth conditions, if cells of *L. discophora* SS-1 have oxidized actively manganese ions. This is probably related to the fact that within the extraction mixture 5 times less cells mL^{-1} were present. This might be caused by manganese oxides (identified by leucoberbelin test) present in the harvested cell pellet (cell pellet was harvested from the liquid growth medium by centrifugation, and 1 g of the pellet was used for extraction). Therefore, the manganese oxides contributed to the wet weight, resulting in less cells per g of the wet weight pellet.

Contradictory, the identified amount was minimal (27.8 mg) per 1 g of wet weight cell pellet. However, biologically oxidized manganese oxides are amorphous with a high surface area and can bind various cations and water (Ehrlich and Newman 2009; Najafpour et al. 2012; Zhu et al. 2012). Thereby they may increase the influence of the manganese oxides on the wet weight of the cell pellet. Additionally, *L. discophora* grows in long chains and filaments during parts of its life cycle (Adams and Ghiorse 1985; Pringsheim 1949). It seems plausible that the chain length increased, or flocks were formed in the liquid medium. Therefore, the TCC might be lower compared to growth conditions without manganese oxides. However, this was not observed in stirred 500 mL glass vessels used to determine the generation time, but the growth conditions differ significantly compared to the large 5 L glass vessels. Nevertheless, based on these observations each cell of *L. discophora* SS-1 produced more EPS, if manganese ions were present in the growth medium. Manganese ions are therefore considered to be a trigger for an increase of EPS production. This seems plausible since it was reported for *L. discophora* sp6 that manganese ions in the medium, concomitant with the oxidation of manganese ions, lead to increased biofilm formation on SS (Dickinson et al. 1997). EPS can be assumed to be more abundant in the EPS of the biofilm population than in the EPS of the planktonic cells. Several authors reported that EPS are increased for the biofilm population (Bellenberg et al. 2012), show that EPS production starts after biofilm formation (Bryers and Ratner 2004) or the various general benefits of EPS for biofilm cells (Flemming et al. 2007; Flemming 2011b; Flemming and Wingender 2010). An increased biofilm formation of *L. discophora* SS-1 was also apparent in this study. Even though cells of *L. discophora* SS-1 always formed a loosely attached biofilm (not only on the metal substrate, but also on the glass at the water/air interface and at the silicone tube used for ventilation), the biofilm formation was visibly increased (already by the naked eye) in presence of manganese ions in the growth medium with concomitant manganese oxidation. However, these biofilms were very loosely attached and detached readily into the medium. It was not possible to separate the biofilm from the planktonic subpopulation. Therefore, the harvested cell pellet from the different growth conditions always contained both, the biofilm and the planktonic subpopulation.

Among the identified substances, carbohydrates and proteins always represent the major fraction in both loosely and tightly bound EPS. In all tightly bound EPS fractions (except -SS +Mn) carbohydrates represent the major constituent, whereas proteins were the main component in tightly bound EPS extracted from cells of *L. discophora* SS-1 grown in presence of manganese ions without a SS surface (-SS +Mn). Although there is only limited information on the EPS of *Leptothrix* species available (and, to the author's knowledge, nothing particular for *L. discophora* SS-1), the high abundance in general is well described in

literature. Carbohydrates and proteins play a pivotal role in the adhesive and cohesive properties of biofilms (Czaczyk and Myszka 2007; Flemming and Wingender 2010; Higgins and Novak 1997; Laspidou and Rittmann 2002; Lewandowski and Beyenal 2013). Carbohydrates are often considered to be water soluble or at least hydrophilic due to large amounts of functional groups such as carboxyl-, keto- or hydroxyl groups. The contribution of carbohydrates to the hydrophobic properties of EPS is also often reported in literature (Flemming 2011b; Jorand et al. 1998; Sutherland 2001; Wingender et al. 1999). However, there is only limited information available on which functional groups might be responsible for their hydrophobic properties. Sutherland (Sutherland 1999; Sutherland 2001) as well as Neu and co-workers (Neu et al. 1992) point to localized hydrophobic regions like O-acetylated carbohydrates or the methyl group in rhamnose. Therefore, carbohydrates may promote adhesion to hydrophilic as well as hydrophobic surfaces. The same is true for proteins. Even though they are often considered as external digestive system (Wingender et al. 1999), they may also have hydrophobic properties (Dignac et al. 1998) due to amino acids like leucine or phenylalanine (Betts and Russell 2003) and hydrophilic properties due to e.g. carboxyl groups (Dignac et al. 1998; Poncin-Epaillard et al. 2012; Rubio et al. 2002). The type of SS surface used in this study shows contact angles (θ) from 80° (freshly polished) to 60° (after 24 h at ambient temperature in a desiccator) (Hedberg et al. 2014). In general, such surfaces with static water contact angles (θ) < 90° are considered to be hydrophilic (Law 2014). Carbohydrates and proteins posses anionic (e.g. carboxyl groups (Rubio et al. 2002; Sutherland 2001)) as well as cationic features (N-acetylglucosamine in carbohydrates (Mack et al. 1996) or positively charged amines in proteins (Poncin-Epaillard et al. 2012)). The isoelectric point (IEP) and the pH of the surrounding medium contribute to electrostatic attraction forces. The IEP determines the pH at which the sum of all positive and negative surface charges results in a net zero charge (McNaught and Wilkinson 1997). For SS grade 1.4301 and comparable grades the IEP is between 3.4 and 4.2, if the surface is prepared as described in this study (Boulangé-Petermann et al. 1995; Lefèvre et al. 2009). Lefèvre and co-workers (Lefèvre et al. 2009) tested SS of the grade 304L (a comparable alloy to SS 1.4301) in an aqueous solution of functionalized polystyrene spheres with a negative surface charge and monitored, if these spheres adsorb to the SS as a function of varying pH. The spheres did not adsorb at a pH of the aqueous solution of 4 or higher. This indicates a negative surface charge of the SS at pH of 4 or higher, since it repelled the negatively charged spheres. At a pH below 4, the spheres adsorb, indicating a positive surface charge of the SS. The passive layer of the SS 1.4301 used in this study mainly consists of chromium and nickel oxides. Most oxides are amphoteric and their charge is a function of the pH of the surrounding solution (Brunelle 1978). In a medium below the IEP of the oxide (more acidic), the oxide is positively charged. However, the principle of electroneutrality implies the

presence of a negatively charged layer of ions near the oxide surface. If the pH of the surrounding medium is above the IEP of the oxide (more basic), the reverse is true (Brunelle 1978; Schwertmann 1991). The MSVP-2 medium used in this study has a pH of around 7, which is above the IEP of SS 1.4301 (IEP = 3.4 to 4.2). Considering that and the findings by Lefèvre and co-workers (Lefèvre et al. 2009) it can be assumed that the SS was negatively charged in MSVP-2 medium with positively charged ions adsorbed to the surface. However, only the net average charge was negative, positively charged metal species might have been also present on the surface and electrostatic interactions of EPS components with the positively charged layer of ions near the SS surface were also possible. Consequently, cationic and to a minor extent anionic features of carbohydrates and proteins in the EPS play a significant role in the electrostatic adhesion of cells of *L. discophora* SS-1 to SS. This is particularly valid for proteins. In all conditions presenting an external stimulus in the MSVP-2 medium (-SS +Mn, +SS -Mn and +SS +Mn) the protein amount is increased by approximately 60 % over the pure salt medium. In loosely bound EPS, carbohydrates as well as proteins were upregulated and increased amounts were found under all conditions except for -SS -Mn. This indicates that *L. discophora* SS-1 excretes EPS to its surrounding medium as a direct reaction to external stimuli. These results are also in agreement with reports for SRP, where proteins were found to be crucial in attachment to and biofilm formation on iron surfaces (Kuklinski 2017; Wikiel 2013; Wikiel et al. 2014) and play a significant role in the corrosion process (Beech 2002). Additionally to promoting adhesion, proteins can also act as chelating agents due to carboxyl groups (Rubio et al. 2002). Interestingly, it was shown that *L. discophora* SS-1 excretes a polysaccharide-linked protein involved in manganese oxidation (Adams and Ghiorse 1987; Adams and Ghiorse 1986). The results presented here strongly indicate that proteins might possess the possibility to bind manganese ions, bring them in close contact to the cells and participate in the manganese oxidation. The second and probably more important class of chelating agents addressed in this study are sugar acids with terminal carboxyl groups: uronic acids. Although EPS analyses with manganese ions were carried out only in duplicate and the deviation among replicates is up to approximately 50 %, it can be concluded that the amounts of uronic acids still are significantly increased by up to approximately 4 times in EPS extracted from cells grown in the presence of manganese ions. These findings were supported by two independent studies (Walter 2015; Wiggers 2015). In both studies deviations among replicates were comparably high like in the present study. This might indicate that this is a feature of the uronic acid determination (although the experiments were carefully scrutinized) or dependant on physiological variations among the EPS extracted from cells of *L. discophora*. Nevertheless, it is obvious that the trend of an increased amount of uronic acids in loosely and tightly bound EPS extracted from cells grown in the presence of manganese ions is existing in all these three

independent studies. The increased amount of uronic acid indicates their importance for manganese oxidation. Presumably, uronic acid–manganese ion complexes are formed through the functional carboxyl groups. This might increase the availability for the subsequent oxidation analog to the chelating ability of proteins. A comparable upregulation of uronic acids has already been shown for the EPS of *Acidithiobacillus ferrooxidans* grown on pyrite (a sulfide mineral) compared to sulfur grown cells (Gehrke et al. 1998). It was discussed that Fe(III)-ions were retained in the EPS in close proximity to the surface by formation of glucuronic acid-iron ion complexes. Therefore, the availability of Fe(III) for the oxidation of the metal-sulfide is increased (Gehrke et al. 2001; Gehrke et al. 1998). Yet, no manganese ions were found in the EPS of *L. discophora* SS-1 in this study. Manganese ions, however, attached to the steel surface are not involved in the corrosion process, but manganese oxides are. *L. discophora* SS-1 presumably oxidizes manganese ions for detoxification, as a byproduct or to shield itself from environmental stress. Therefore, it can be speculated that manganese ions only need to be retained within the EPS until complete oxidation. The quantitative oxidation of manganese(II) ions to manganese(IV) oxides by *L. discophora* SS-1 is shown in this study.

The amount of nucleic acids is upregulated in the assays -SS +Mn and +SS +Mn compared to the other two ones. One might speculate that nucleic acids, despite increasing stability and rigidity of the biofilm matrix (Das et al. 2013; Whitchurch et al. 2002), play an important role in binding manganese ions via ionic interactive forces induced by the negatively charged phosphate groups of the polar back bone (Saenger 2013; Watson and Crick 1953). However, they might play only a minor role in adhesion to the SS surface, since the net charge of the SS is considered negative in this study. This is also in agreement with the findings, since nucleic acids are not upregulated in presence of a SS surface compared to assays without a SS surface. The structural importance and postulated role in manganese ion binding is also supported by a lack of nucleic acids excreted into the medium (no nucleic acids where found in any loosely bound EPS). Lipids and phospholipids presumably play an important part as a wetting agent for hydrophobic surfaces, to overcome repulsive effects and to facilitate attachment to hydrophobic surfaces (Flemming and Wingender 2010; Gehrke et al. 2001; Gehrke et al. 1998). This has been shown in particular for the acidophilic leaching organisms *Acidithiobacillus* (*A*.) *ferrooxidans* and *A. thiooxidans*. In *A. ferrooxidans,* fatty acids (Gehrke et al. 1998) and in *A. thiooxidans,* phospholipids (Shively and Benson 1967) seem to function as an emulsifying agents for elemental sulfur. Both might facilitate attachment to sulfur surfaces (Gehrke et al. 1998). It was also shown that fatty acids were upregulated in EPS of sulfur (hydrophobic surface) grown cells compared to cells grown on pyrite or ferrous iron ions (Gehrke et al. 1998). This is in agreement with the present results, since neither the

hydrophilic SS surface nor the manganese ions seem to trigger any upregulation or trend among the different culture conditions in both loosely and tightly bound EPS. However, a closer look into the qualitative fatty acid content revealed that in tightly bound EPS manganese ions or the oxidation of them triggers a reduction in the saturated fatty acids C8:0 and C16:0, an upregulation of C12:0 and the advent of the unsaturated fatty acid C18:1. Generally, the unsaturated fatty acid C16:1 represents the major fatty acid among all conditions followed by C16:0 for conditions without manganese ions and C12:0 for conditions with manganese ions. This is in agreement with fatty acid markers reported in literature (Spring 2006) for the *Leptothrix* group. Here, C16:0, C16:1 and C18:1 represent the major fatty acids. Interestingly, the only identified fatty acid in loosely bound EPS under all conditions was C8:0. In loosely bound EPS the carbohydrate compositions were comparable. No significant up- or downregulation was detected. Sorbitol and mannose represent the major carbohydrate monomers followed by mannose and rhamnose with minor amounts of fucose and galactose. In tightly bound EPS also no significant up- or downregulation was evident. However, rhamnose and in part fucose represent the major carbohydrate monomers. Both are 6-deoxyhexoses and are associated with hydrophobic functions in the biofilm matrix (Sutherland 1999; Sutherland 2001). This indicates that not only hydrophilic but also hydrophobic interactions may play a significant role in the biofilm matrix of *L. discophora* SS-1.

The strictly intracellular enzyme G6PDH was used as a marker for cell lysis (Ng and Dawes 1973; Platt et al. 1985). The values were below the detection limit in residual cell pellets obtained after the 3rd and final extraction step. However, a lysed cell pellet after the 3rd extraction produced a positive result for G6PDH. G6PDH is regularly used to determine cell lysis during EPS extraction (Aguilera et al. 2008; Michalowski 2012; Platt et al. 1985; Ras et al. 2008). However, periplasmic proteins might have contaminated the EPS extract since an intracellular enzyme marker does not answer the question whether or not periplasmic proteins might have gone into solution. Nevertheless, the CER method is considered as a very gentle method by several authors (D'Abzac et al. 2010; Frølund et al. 1996; Jahn and Nielsen 1995; Wu and Xi 2009). Additionally, carbohydrate to protein ratios indicate no cell lysis, as discussed before. Summarized, this indicates that the EPS extraction in this study with CER caused minimal to no cell lysis.

Overall, it can be concluded that the EPS of cells of *L. discophora* SS-1 possess all abilities to facilitate the attachment and biofilm formation on various surfaces and possibly retain manganese ions by chelation with uronic acids for subsequent oxidation to manganese oxides. This indicates the importance of EPS characterization, since it is the EPS which

promote the biofilm formation on SS and the formation of manganese oxides, which are involved in the corrosion process.

5.3 Fluorescent lectin binding analysis (FLBA)

FLBA was used to gain insight into the spatial structure and the distribution of lectin binding groups in biofilms of *L. discophora* SS-1 grown on filters, SS coupons or SS coupons with addition of manganese ions to the medium. Lectins are commonly used in biofilm analysis, because of their specific interaction with glycoconjugate residues in the EPS. Therefore they are used as a marker of EPS, more precisely of polysaccharides (Bellenberg et al. 2012; Neu and Lawrence 1999; Neu et al. 2001; Zhang et al. 2015).

Biofilms of *L. discophora* SS-1 on floating filters are considered here as artificial biofilms, since the polycarbonate membrane doesn't represent a natural habitat. The cells were filtered onto the membrane and the filter floats on top of a liquid medium. However, the floating filter method delivers a fast and easy applicable method for analysis of the 3-dimensional structure of a biofilm (de Bruyn et al. 1990). SS coupons with and without addition of 0.2 mM Mn(II) to the MSVP-2 medium were used to simulate corrosion relevant scenarios. In general, the biofilm formation on both, filters and SS coupons, was successful. On floating filters the 3-dimensional structure with channels allowing for exchange of nutrients and metabolites was evident. It was shown that the whole biofilm was covered with polysaccharides (indicated by the green stain with the lectin ConA). Additionally, each single microcolony was outlined by polysaccharides and, therefore, possibly by EPS. This indicates that *L. discophora* SS-1 is covered by polysaccharides. This presumably provides beneficial functions like increased stress resistance, reduced desiccation, increased rigidity and adhesiveness (Flemming 2011b; Flemming and Wingender 2010; Sutherland 2001; Wingender et al. 1999). The biofilms formed on the floating filters were analyzed with 13 different lectins of which 5 gave a positive signal. However, no distinct glycoconjugate distribution was found. Only ConA (as a marker for glucose and mannose) stained both single cells as well as microcolonies. While there was no evident 3-dimensional structure (the biofilms typically consisted of only a few bacterial layers) for biofilms on SS coupons, there was a distinct binding pattern of the lectins. On SS coupons without manganese 10 out of 13 lectins gave a positive signal. This impressively shows that the structural complexity of EPS increases, if bacteria attach to a surface and form biofilms. The lectins GS-I, GS-II, SBA, PHAE-I mainly labeled the cells and, presumably, the tightly bound (in some cases called capsular) part of the EPS directly associated to the bacterial cell wall. This can be attributed especially to the lectins GS-II and PHAE-I with a specificity to N-acetylglucosamine (part of

the peptidoglycan layer in the cell wall (Meroueh et al. 2006)). GS-I is specific to melibiose and galactose, SBA is specific to N-acetylgalactosamine and galactose. These findings are supported by the common denominator galactose. Galactose was detected by gas chromatographic analysis in this study as a part of the carbohydrate monomers of the EPS of *L. discophora* SS-1. On SS coupons (without addition of manganese ions to the medium), ConA mainly stained the biofilm matrix, rather than the cells themselves. The microcolonies on these SS coupons were significantly less dens (larger areas between individual cell), compared microcolonies on floating filters. The space in-between the cells appeared in green because of the signal of the lectin ConA, indicating EPS. This supports the assumption of an upregulation of EPS production in "real" biofilms, since mannose and glucose might be excreted into the biofilm matrix. This is also true for the lectins DBA, PNA and LPA, which distinctively stained the biofilm matrix. Microcolonies on the SS surface were well outlined by their lectin signal and the signals were usually stronger on the border or on top than "inside" the microcolony. THE CLSM con visualize microcolonies layer by layer, differentiating between the top and the "inside" of the microcolony. This finding indicate that *L. discophora* SS-1 embeds itself in EPS. The evaluation of biofilms on SS coupons grown in the presence of manganese ions revealed additional information. 11 out of 13 lectins produced a positive signal. Due to a malfunction of the CLSM, it needs to be emphasized that these biofilms were analyzed with an EFM. The experiments were carefully scrutinized and previous results gained for the lectins with the CLSM were repeated with the EFM gaining similar results. This indicates comparability of the information obtained with the two different microscopic techniques.

UEA-I, specific for fucose solely bound to such biofilms on SS coupons grown in presence of manganese ions. However, carbohydrate monomer analysis identified fucose in EPS under all conditions. GS-II and PHAE-I stained mainly the cells, analog to their previously discussed staining pattern. ConA was proven to be a well-suited lectin to stain the EPS as well as some cells of *L. discophora* SS-1. The lectins GS-I, SBA, UEA-I, DBA, PWM, PNA, MPA and LPA, however, mainly stained the biofilm matrix. These findings are supported by gas chromatographic analysis of the carbohydrate monomers for the lectins ConA, GS-I, SBA, UEA-I, PNA and MPA. Interestingly, 4 lectins gave a positive signal for all biofilms in this study: ConA, GS-II, PWM and LPA. These lectins seem to be specific for the EPS of *L. discophora* SS-1. A particularly striking staining feature was observed for the lectins SBA, PNA, MPA, PWM, DBA and UEA-I. These lectins stained filament-like structures, possibly sheaths connecting individual cells. The cells within this presumed filament network were separated from each other (as indicated by the nucleic acid stain), but clearly connected via a shared EPS sheath. The filamentous growth of *L. discophora* spp. is well documented in

literature (Adams and Ghiorse 1985; Adams and Ghiorse 1986; Pringsheim 1949; Rogers and Anderson 1976; Spring et al. 1996) To the author's knowledge this is the first time that parts of the carbohydrates in these structures were identified with FLBA. With regard to the carbohydrate specificity of these lectins, it can be assumed that a galactose-type carbohydrate (SBA, PNA, DBA and MPA) and in part N-acetyllactosamine (PWM) as well as fucose (UEA-I) play a major role in the structure of these presumed sheaths.

In general, the following glycoconjugate residues were identified by lectins within the EPS matrix: mannose, glucose (ConA), melibiose (GS-I), galactose (GS-I, SBA, PNA, MPA), fucose (UEA-I), N-acetylglucosamine (GS-II, PWM, PHAE-I), N-acetylgalactosamine (SBA, PHAE-I, MPA), Methyl-2-acetamido-2-deoxy-D-galactose (DBA), N-acetyllactosamine (PWM) and sialic acids (LPA). N-acetylglucosamine and N-acetylgalactosamine are discussed to be common in bacterial exopolysaccharides (Decho 1990) and might play a significant role in adhesion to surfaces (Nichols and Nichols 2008). The presence of N-acetylglucosamine is this study might be attributed to the peptidoglycan-layer that forms the cell wall of most bacteria, since the lectins specific for N-acetylglucosamine bind regularly direct to the cells themselves. That indicates that N-acetylglucosamine might be mostly associated with cells rather than with excreted EPS. Some lectins did not bind (like WGA) or only bound under specific conditions (like PHAE-I), even though they are specific for N-acetylglucosamine. This might be related to the structural complexity of bacterial cell walls, as they consist of various lipopolysaccharides, capsular polysaccharides, lipooligosaccharides and glycoproteins (Ristl et al. 2010). Other glycoconjugate residues like mannose, glucose, galactose and fucose were also identified by gas chromatography and by FLBA in the EPS and biofilms of *A. ferrooxidans* (Bellenberg et al. 2012; Gehrke et al. 1998). The potential role of the individual carbohydrates is discussed in detail later. Sialic acid, not commonly found but recently identified in the EPS of *Ferroplasma acidiphilum* (Zhang et al. 2015), was also identified in the EPS of *L. discophora* SS-1 under all growth conditions. It indicates that sialic acid might be a specific component of the EPS of *L. discophora* SS-1.

In summary, FLBA was successfully used to evaluate the binding pattern of lectins to EPS of biofilms of *L. discophora* SS-1. The data indicate the possible occurrence of carbohydrate components in the EPS. A major part of these findings are supported by gas chromatographic analysis of the carbohydrate monomers of EPS of *L. discophora* SS-1. However, lectin binding specificity needs to be reviewed critically. Despite their stated specificity, they might bind also unspecifically to di-, tri- and oligosaccharides (Böckelmann et al. 2002). Nevertheless, FLBA indicated that *L. discophora* SS-1 cells adapt their EPS to external stimuli like a SS surface and/or manganese ions.

5.4 Analysis of the contact potential (CDP) mapping and corrosion measurements

Up to date no SKPFM studies exist that visualize and analyze localized surface potential effects initiated by biofilm formation and manganese oxidation of MOMOs. In this study these data are supplemented with actual corrosion analysis (OCP and E_{pit} measurements) However, several studies exist that correlate biologically mediated manganese oxidation with ennoblement of SS (Campbell et al. 2004; Carpén et al. 2003; Dickinson et al. 1996; Dickinson et al. 1997; Geiser et al. 2001; Lewandowski et al. 2002; Linhardt 2004; Linhardt 2006; Olesen et al. 2001; Shi et al. 2002c). Yet, these studies did not target the surface potential effects initiated by biofilm formation and manganese oxide deposition.

Several studies are available focusing on SKPFM analyses. From these basic settings were derived (Guillaumin et al. 2001; Kuklinski 2017; Rohwerder and Turcu 2007; Stratmann and Streckel 1990; Stratmann et al. 1991; Zerweck et al. 2005). The study by Kuklinski (Kuklinski 2017) gave indications for the individual settings and were adapted to the current experimental set-up. The potential contrast (i.e. the minimal difference measurable between two surface features) largely depends on the tip to surface distance. This is due to the fact that the influence of the geometry of the cantilever tip on the potential contrast increases with increasing distance (Rohwerder and Turcu 2007). Zerweck and co-workers (Zerweck et al. 2005) showed that the maximum signal was achieved for tip to surface distances below 30 nm. This distance will result in a lateral resolution of approximately 50 nm. However, these results were achieved in ultrahigh vacuum and results may differ under ambient conditions. Rohwerder and Turcu (Rohwerder and Turcu 2007) pointed out that for a distance of 100 nm a lateral resolution below 500 nm for surface features can be expected. However, they indicated that several other factors influence the resolution. Zerweck (Zerweck et al. 2005) as well as Guillaumin (Guillaumin et al. 2001) showed that at distances below 30, respectively 50 nm the potential contrast did not significantly increase further. Similar observations were made in this study. The potential contrast did not increase with decreasing distances from 50 to 10 nm. Therefore, a 50 nm air gap was used throughout this study. The robustness of the experimental design is supported by these findings, since a low dependency of the tip to surface distance on the potential contrast indicates a low influence of stray capacities (Rohwerder and Turcu 2007). The second important influence on the potential contrast is the tip velocity (Rohwerder and Turcu 2007; Zerweck et al. 2005). The tip velocity had also a high impact during this study on the quality of the topographic images, especially for rough manganese oxide-covered surfaces. The topographic image is recorded first to maintain a constant air gap for the following CPD measurement. Therefore, the topographic image is of

utmost importance for both the visualization of the surface as well as the following CPD measurement. However, scanning speed and topographic quality had to be balanced to circumvent possible time effects on the surface potential. It has been demonstrated for ferric materials that original surface potential values (before the corrosion experiment) will be restored quickly (within hours) after the corrosion experiment ended (Kuklinski 2017; Rohwerder and Turcu 2007). This limits the time to evaluate the samples. This effect may be a result of the work function of ferric materials, which depends on the Fe(III)/Fe(II) ratio. It promptly re-equilibrates after emersion (Rohwerder and Turcu 2007) due to oxidation of Fe(II) by atmospheric oxygen. However, these experiments were carried out with actively corroding carbon steel and the fast relaxation of the surface potential must not necessarily be applicable to austenitic SS too. During this study the influence of time (and therefore possibly the influence of the oxidation of Fe(II) or other work function determining species) on the CPD between the tip and the surface was shown to be minimal within 5 h. The CPD between a manganese oxide surface and the surrounding steel surface changed from 209 mV (1 h after emersion from the MSVP-2 medium) to 217 mV (4 h after emersion). On another example it changed from 127 to 135 mV within 5 h after emersion (data not shown). Since ongoing time dependent CPD changes cannot be excluded fully, a scan rate of 0.3 Hz was chosen resulting in scanning durations of approximately 1 h per image.

After determining the basic settings, it was necessary to elucidate the effect of cells of *L. discophora* SS-1 and manganese oxides on the CPD of a SS surface individually. Therefore, cells of *L. discophora* were allowed to colonize on vertically submerged SS coupons for 1 h and manganese oxides were deposited by application of an aqueous solution followed by air drying as well as electrochemical deposition. Single cells showed a CPD of up to +50 mV compared to the steel surface. Up to date only limited data are available on high resolution surface potential mapping (with SKPFM) of cells on alloyed steels. However, Kuklinski (Kuklinski 2017) could show a CPD between cells of *Desulfovibrio (D.) vulgaris* and non-alloyed steel as well as alloyed steel (1.4301) of approximately +25 mV and +20 to +25 mV, respectively. Additionally, Birkenhauer and Neethirajan (Birkenhauer and Neethirajan 2014) estimated that the CPD of *Pseudomonas aeruginosa* and MRSA cells to SS were +100 mV and +10 to +20 mV, respectively. Similar findings were shown for pyrite. The surface potential of the pyrite surface (determined with a scanning Kelvin Probe, SKP) shifted approximately 200 mV (after 4 h) and 300 mV (after 18 h) in anodic direction (from approximately 690 mV to 890/990 mV), if cells of *A. ferrooxidans* actively grew on the pyrite surface (Gehrke et al. 1998). These results were attributed to the influence of the oxidation of Fe(II) to Fe(III) in the EPS by living bacteria. Therefore, the results of this study fit well into this literature context. Additionally, *L. discophora* SS-1 is an aerobic heterotrophic organism

using the Entner-Doudoroff pathway to generate energy from carbohydrate catabolism with oxygen as final electron acceptor (Adams and Ghiorse 1986; Entner and Doudoroff 1952; Zhang et al. 2002). During cultivation, the cells deliver electrons to oxygen and may become therefore electron depleted. This could lead to a positive CPD of the cells compared to the SS surface. The influence of manganese oxides on the CPD was also tested. The CPD of biologically produced manganese oxides was -226 mV against the SS surface. However, the CPD of electrodeposited manganese oxides was approximately -616 mV against the SS surface. Electrodeposition of manganese by cathodic electrosynthesis result in the formation of manganese oxides and hydroxides (Gong and Zangari 2002; Nagarajan et al. 2006) on the cathode. Due to electrogenerated bases (protons are consumed at the cathode) the local pH at the cathode is considerably higher than in the surrounding medium. This leads to the formation of colloidal non-stoichiometric manganese oxides/hydroxides (manganese ions precipitate at higher pH). The formed colloidal manganese species are then electrophoretically deposited at the cathode (Nagarajan et al. 2006). In these manganese oxides/hydroxides, manganese is almost exclusively present in the form Mn(II), Mn(III) and Mn(IV) (Gong and Zangari 2002). While it is not clear which species dominates, the positive leucoberbelin test indicates a considerable amount of manganese(IV) oxides. The CPD of the electrodeposited manganese oxides might be higher compared to the biological produced manganese oxides because of the different composition or because the biological produced manganese oxides are less pure due to co-precipitations from the growth medium. In general, manganese oxides act as an electron sink taking up electrons from steel causing corrosion (Linhardt 2004). Following the argumentation of cells with a positive CPD, manganese oxides appear negative towards the steel surface, as they accumulate electrons. AFM and SKPFM measurements were performed on dried samples. As an unwanted side effect of this, structure and texture of cells and manganese(IV)-oxides may have changed, if compared to fully hydrated systems. Nevertheless, surface topography and CPD mapping correlate well.

After elucidating the effect of cells and manganese oxides individually on the SS surface, the complex system of a mature biofilm (7d) was analyzed with EFM, bright field microscopy and SKPFM. Filamentous, chain like structures of *L. discophora* SS-1 were identified. The bacteria are spread over the surface connecting different microcolonies. Based on the experimental set-up it is assumed that the cells overgrow the surface forming colonies rather than aggregates of cells that attach to the surface. The ability of various *L. discophora* species to form biofilms is known (Campbell et al. 2004; Dickinson and Lewandowski 1996; Dickinson et al. 1997; Geiser et al. 2001). Also chain formation and filamentous growth is documented in the literature (Adams and Ghiorse 1985; Adams and Ghiorse 1986; Pringsheim 1949; Rogers and Anderson 1976; Spring et al. 1996). This make the

assumption of cells overgrowing the surface and forming colonies plausible. During the investigation, dark spots were identified in the microcolonies, which proved to be not stainable by Syto 9. Further investigation with the SKPFM showed a CPD of up to -220 mV against the steel surface. Bearing in mind the positive leucoberbelin test and considering the previous findings of a negative CPD for manganese oxides (against the steel surface) the spots are most likely manganese(IV)-oxides deposited in the microcolonies. In case of a corrosion process the cathodic area (manganese(IV) oxides) takes up electrons, while at anodic sites the metal dissolution happens (Lewandowski et al. 2002). Reddy and co-workers (Reddy et al. 2004), described (using an SKP setup) that cathodes exhibit a negative CPD and anodes a positive CPD. Since manganese(IV)-oxides may act as an electron sink within a corrosion process by taking up electrons from anodic sites (Linhardt 2004), it is presumed that the manganese(IV)-oxides function as cathodically active compounds due to their negative CPD (-220 mV) towards the steel surface. The filamentous, chain like structures could largely be related to CPD (up to +200 mV) positive areas in the SKPFM image. However, not all CPD positive areas where solely identical with identified bacteria, but they were always in close proximity to cells. Since anodes transfer electrons to the cathode thereby releasing Fe(II) in the corrosion process (Linhardt 2004), anodic areas could be identified due to their positive CPD (+200 mV) towards the steel surface. Overall, there is a difference of up to 420 mV between cathodic and anodic areas. A single cell, which is not influenced by any manganese precipitate, exhibits a positive CPD towards the steel surface of approximately +50 mV. However, anodic areas of up to +200 mV towards the steel surface were identified. This cannot be related to the sole presence of cells but must be related to the corrosion process itself. Thus, the ennoblement caused by the interaction between bacteria and Mn-oxides could be shown directly on the steel surface.

The previous findings are supported by OCP- and E_{pit} measurements, tools regularly used in corrosion studies and corrosion risk assessment (Campbell et al. 2004; Dickinson et al. 1996; Dickinson et al. 1997; Heitz et al. 1990; Linhardt 2004; Shi et al. 2002b) in a comparable set-up. NaCl (0.35 % w/v) was added to deliver a sufficient amount of chlorine ions to induce pit formation, since the original MSVP-2 medium contains only approximately 30 mg L^{-1} of chloride ions and 1.4301 type SS is considered as being resistant to chloride induced pitting and crevice corrosion up to 200 mg L^{-1} chloride in natural waters (pH neutral, aerated) under ambient conditions (Lewus et al. 1997; Linhardt 2004; Tuthill 1990; Tuthill and Avery 1994). The addition of 0.35 % NaCl (w/v) gives approximately 2000 mg L^{-1} chloride ions. Since several other factors like temperature, other anions or oxygen concentration strongly influence the susceptibility of SS 1.4301 to chloride induced pitting (Leckie and Uhlig 1966), a 10 times excess amount was chosen to ensure pit formation under the given conditions. In

retrospect, this supplementation seems unnecessary. The amount of chloride in the original MSVP-2 medium would have also resulted in pitting during potentiodynamic polarization in anodic sweep direction yet possibly at higher potentials. With regard to the relevant literature dealing with manganese oxide induced ennoblement of SS (Campbell et al. 2004; Dickinson et al. 1996; Dickinson et al. 1997; Lewandowski et al. 2002; Linhardt 1997; Linhardt 2004; Linhardt 2006; Olesen et al. 2001) the result of the experiment (ennoblement and increased susceptibility to pitting corrosion) is still plausible. The OCP of SS was well in range with the expected OCP of 144 to 344 mV_{she} (Davis 1987; Scotto et al. 1985) under all conditions without manganese oxides present on the surface. Without manganese oxides on the surface only the cathodical oxygen reduction is relevant for the OCP and, hence, the reaction kinetics are hindered (Linhardt 2004). The OCP of sterile MSVP-2 medium with addition of 0.2 mM Mn(II) is slightly higher (294 to 225 mV) compared to sterile MSVP-2 medium without addition of 0.2 mM Mn(II). This could be attributed to the increased salt content (Leckie and Uhlig 1966). However, the manganese were still present as Mn(II)-ions, since there were no cells of *L. discophora* SS-1 available to oxidize them. The OCP for the inoculated MSVP-2 medium without 0.2 mM Mn(II) was 208 mV, marginally lower compared to sterile MSVP-2. The formation of differential aeration or concentration cells might have resulted in an anodic increase of the OCP (Beech and Gaylarde 1999; Sand and Gehrke 2003; Thierry and Sand 2011). However, this was not demonstrated for the biofilm in this experiment. In general, differential aeration or concentrations cells evolve, if metabolic processes in biofilms e.g. respiration of oxygen (leading to oxygen depleted zones) or other metabolic processes result in concentration gradients. These gradients result in potential differences and lead, in consequence, to corrosion (Videla and Characklis 1992). The approximately 400 mV anodic shift of the OCP to 635 mV_{she} observed for a biofilm of *L. discophora* SS-1 precipitating manganese oxides on the SS surface is also well in agreement with the expected OCP of approximately 571 mV_{she} for the Mn(II)/Mn(IV)-redox system (Linhardt 2004). The pitting potential of the SS under the given conditions ranged from 416 to 511 mV_{she} and the manganese oxides, produced by microbiological oxidation processes, shifted the OCP of the SS from average 242 mV_{she} to 635 mV_{she} well beyond the determined pitting potential. This clearly shows the possible detrimental effect of MIC and support the previous findings of formation of anodic and cathodic areas on the SS surface due to biofilm formation and manganese oxidation by *L. discophora* SS-1.

In summary, the data collected during this work strongly indicate the influence on the corrosion of SS by biological oxidized manganese oxides deposited by *L. discophora* SS-1. The formation of a biofilm with incorporated manganese oxides leads to the formation of cathodic and anodic areas, which were not present on freshly ground steel incubated under

similar but sterile conditions. However, care must be taken, if interpreting SKPFM results. Rohwerder & Turcu (Rohwerder and Turcu 2007) showed a 10 times lower potential difference between Al inclusions in a pure Mg surface compared to expected values from SKP measurements. Additionally, they point out that corrosion analysis with SKPFM is difficult to interpret and one cannot necessarily draw direct conclusions from SKPFM measurements to real world scenarios. One frequent issue with SKPFM is the inversion of the Kelvin signal from positive to negative values and vice versa (Henning et al. 1995; Hochwitz et al. 1996; Rohwerder and Turcu 2007). In order to avoid such problems in this study, a gold sputtered SS surface was scanned prior to each experiment. The data show clearly that CPD was is all cases positive; indicating a valid interpretation of the data presented in this study.

6 Conclusion and Perspective

This study focused extensively on the influence of: (I) different growth conditions and especially manganese ions on the (bio)chemical composition of EPS; (II) the visualization of biofilm formation by DNA stains combined with FLBA and (III) the characterization of the localized electrochemical effects of cells, biofilms and manganese oxides on the surface potential of stainless steel with particular regard to its electrochemical corrosion exemplified with *L. discophora* SS-1 as a model organism.

The growth of *L. discophora* SS-1 cells in presence of manganese ions leads to an increase of the generation time and a reduction in the ATP and protein content. Dependant on the culture conditions the addition of manganese ions results in either an increase or a decrease of the cell density. This indicates a possible adaptation of the protein synthesis of *L. discophora* SS-1 to the production of proteins involved in the manganese oxidation prior to the start of the cell growth.

FLBA and characterization of the EPS prove to be a useful combination for biofilm studies. Several lectins identified genuine features of biofilms formed by cells of *L. discophora* SS-1. The findings in this study resulted in a set of eleven lectins useful for future biofilm and MIC studies to identify glycoconjugate residues. The results are backed by identification of carbohydrate monomers by gas chromatographic analysis. The EPS analysis showed that the EPS of *L. discophora* SS-1 possess all features to facilitate biofilm formation on SS and identified uronic acids as a possible key factor in retaining manganese ions for subsequent oxidation. This indicates the importance of EPS analysis for future biofilms studies.

OCP and E_{pit} measurements proved their status as a criterion in risk assessment of corrosion. They are regularly used in past and recent corrosion studies and identified in this study a potential risk of pitting corrosion due to an anodic shift of the OCP (ennoblement). This study also demonstrates that the combination of EFM and SKPFM could reliably visualize biofilms and single cells as well as identify manganese oxides as cathodic areas with a negative CPD and anodic areas with a positive CPD towards the steel surface. Therefore, the combination of EFM and SKPFM has the potential to elucidate electrochemical degradation processes associated with biofilm formation in general and concomitant with precipitation of manganese oxides directly at the interface of cells and SS.

7 References

Adams, L., and Ghiorse, W. C. (1987). "Characterization of extracellular Mn2+-oxidizing activity and isolation of an Mn2+-oxidizing protein from Leptothrix discophora SS-1." *Journal of bacteriology*, 169(3), 1279-1285.

Adams, L. F., and Ghiorse, W. C. (1985). "Influence of Manganese on Growth of a Sheathless Strain of Leptothrix discophora." *Appl Environ Microbiol*, 49(3), 556-62.

Adams, L. F., and Ghiorse, W. C. (1986). "Physiology and ultrastructure of Leptothrix discophora SS-1." *Archives of microbiology*, 145(2), 126-135.

Aguilera, A., Souza-Egipsy, V., San Martín-Úriz, P., and Amils, R. (2008). "Extraction of extracellular polymeric substances from extreme acidic microbial biofilms." *Applied microbiology and biotechnology*, 78(6), 1079-1088.

Ahmad, Z. (2006). "Basic concepts in Corrosion", in Z. Ahmad, (ed.), *Principles of corrosion engineering and corrosion control*. Oxford: Butterworth-Heinemann, pp. 9-56.

Ahn, S. J., Costa, J., and Rettig Emanuel, J. (1996). "PicoGreen quantitation of DNA: effective evaluation of samples pre-or psost-PCR." *Nucleic acids research*, 24(13), 2623-2625.

Akob, D. M., Bohu, T., Beyer, A., Schäffner, F., Händel, M., Johnson, C. A., Merten, D., Büchel, G., Totsche, K. U., and Küsel, K. (2014). "Identification of Mn (II)-oxidizing bacteria from a low-pH contaminated former uranium mine." *Applied and environmental microbiology*, 80(16), 5086-5097.

Al-Halbouni, D., Dott, W., and Hollender, J. (2009). "Occurrence and composition of extracellular lipids and polysaccharides in a full-scale membrane bioreactor." *Water Research*, 43(1), 97-106.

Ali, S. H., and Stokes, J. (1971). "Stimulation of heterotrophic and autotrophic growth ofSphaerotilus discophorus by manganous ions." *Antonie van Leeuwenhoek*, 37(1), 519-528.

Baier, R. E. (1975). "Applied chemistry at protein interfaces". ACS Publications, pp. 1 - 25.

Bargar, J. R., Fuller, C. C., Marcus, M. A., Brearley, A. J., De la Rosa, M. P., Webb, S. M., and Caldwell, W. A. (2009). "Structural characterization of terrestrial microbial Mn oxides from Pinal Creek, AZ." *Geochimica et Cosmochimica Acta*, 73(4), 889-910.

Beech, I. B. (1996). "The potential use of atomic force microscopy for studying corrosion of metals in the presence of bacterial biofilms—an overview." *International biodeterioration & biodegradation*, 37(3-4), 141-149.

Beech, I. B. (2002). "Biocorrosion: role of sulfate–reducing bacteria", in G. Bitton, (ed.), *Encyclopedia of Environmental Microbiology*. New York: Wiley, pp. 465-475.

Beech, I. B., and Gaylarde, C. C. (1999). "Recent advances in the study of biocorrosion: an overview." *Revista de microbiologia*, 30(3), 117-190.

Beech, I. B., and Sunner, J. (2007). "Sulphate-reducing bacteria and their role in corrosion of ferrous materials", *Sulphate-Reducing Bacteria*. Cambridge: Cambridge University Press, pp. 459-482.

Beech, I. B., and Tapper, R. C. (1999). "Exopolymers of sulphate-reducing bacteria", *Microbial Extracellular Polymeric Substances*. Springer, pp. 119-126.

Beijerinck, M. (1913). "Oxydation des mangancarbonates durch Bakterien und Schimmelpilze." *Folia Microbiol (Delft)*, 2, 123-134.

Bellenberg, S., Díaz, M., Noël, N., Sand, W., Poetsch, A., Guiliani, N., and Vera, M. (2014). "Biofilm formation, communication and interactions of leaching bacteria during colonization of pyrite and sulfur surfaces." *Research in microbiology*, 165(9), 773-781.

Bellenberg, S., Leon-Morales, C.-F., Sand, W., and Vera, M. (2012). "Visualization of capsular polysaccharide induction in Acidithiobacillus ferrooxidans." *Hydrometallurgy*, 129, 82-89.

Betts, M. J., and Russell, R. B. (2003). "Amino acid properties and consequences of substitutions", in M. Barnes and I. Gray, (eds.), *Bioinformatics for geneticists*. Chichester, UK: Wiley, pp. 289.

Binnig, G., Gerber, C., Stoll, E., Albrecht, T., and Quate, C. (1987). "Atomic resolution with atomic force microscope." *EPL (Europhysics Letters)*, 3(12), 1281.

Binnig, G., Quate, C. F., and Gerber, C. (1986). "Atomic force microscope." *Physical review letters*, 56(9), 930.

Birkenhauer, E., and Neethirajan, S. (2014). "Characterization of electrical surface properties of mono-and co-cultures of Pseudomonas aeruginosa and methicillin-resistant Staphylococcus aureus using Kelvin probe force microscopy." *RSC Advances*, 4(80), 42432-42440.

Blumenkrantz, N., and Asboe-Hansen, G. (1973). "New method for quantitative determination of uronic acids." *Analytical biochemistry*, 54(2), 484-489.

Bocioaga, D. (2013). *Understanding the molecular mechanism of manganese oxidation in Leptothrix discophora SS-1*: Cornell University.

Böckelmann, U., Manz, W., Neu, T. R., and Szewzyk, U. (2002). "Investigation of lotic microbial aggregates by a combined technique of fluorescent in situ hybridization and lectin-binding-analysis." *Journal of microbiological methods*, 49(1), 75-87.

Booth, G., Elford, L., and Wakerley, D. (1968). "Corrosion of mild steel by sulphate-reducing bacteria: an alternative mechanism." *British Corrosion Journal*, 3(5), 242-245.

Boulangé-Petermann, L., Doren, A., Baroux, B., and Bellon-Fontaine, M.-N. (1995). "Zeta potential measurements on passive metals." *Journal of colloid and interface science*, 171(1), 179-186.

Bradford, M. M. (1976). "A rapid and sensitive method for the quantitation of microgram quantities of protein utilizing the principle of protein-dye binding." *Analytical biochemistry*, 72(1-2), 248-254.

Bräuer, S., Adams, C., Kranzler, K., Murphy, D., Xu, M., Zuber, P., Simon, H., Baptista, A., and Tebo, B. (2011). "Culturable Rhodobacter and Shewanella species are abundant in estuarine turbidity maxima of the Columbia River." *Environmental microbiology*, 13(3), 589-603.

Brouwers, G., Vijgenboom, E., Corstjens, P., De Vrind, J., and De Vrind-De Jong, E. (2000). "Bacterial Mn2+ oxidizing systems and multicopper oxidases: an overview of mechanisms and functions." *Geomicrobiology Journal*, 17(1), 1-24.

Brown, M. J., and Lester, J. N. (1980). "Comparison of bacterial extracellular polymer extraction methods." *Applied and Environmental Microbiology*, 40(2), 179-185.

Brözel, V., and Cloete, T. (1989). "The role of sulphate-reducing bacteria in microbial induced corrosion. Paper SA."

Brunelle, J. (1978). "Preparation of catalysts by metallic complex adsorption on mineral oxides." *Pure and Applied Chemistry*, 50(9-10), 1211-1229.

Bryers, J. D., and Ratner, B. D. (2004). "Bioinspired implant materials befuddle bacteria." *ASM News-American Society for Microbiology*, 70(5), 232-232.

Butterfield, C. N., Soldatova, A. V., Lee, S.-W., Spiro, T. G., and Tebo, B. M. (2013). "Mn (II, III) oxidation and MnO2 mineralization by an expressed bacterial multicopper oxidase." *Proceedings of the National Academy of Sciences*, 110(29), 11731-11735.

Campbell, S., Geesey, G., Lewandowski, Z., and Jackson, G. (2004). "Influence of the distribution of the manganese-oxidizing bacterium, Leptothrix discophora, on ennoblement of Type 316L stainless steel." *Corrosion*, 60(7), 670-680.

Carpén, L., Raaska, L., Kujanpää, K., and Hakkarainen, T. (2003). "Effects of Leptothrix discophora on the potential behavior of stainless steel." *Materials and Corrosion*, 54(7), 515-519.

Characklis, W. G. (1990). "Microbial fouling", *Biofilms*. pp. 523-584.

Cheng, Y. S., Zheng, Y., and VanderGheynst, J. S. (2011). "Rapid quantitative analysis of lipids using a colorimetric method in a microplate format." *Lipids*, 46(1), 95-103.

Chukhrov, F., Gorshkov, A., Beresovskaya, V., and Sivtsov, A. (1979). "Contributions to the mineralogy of authigenic manganese phases from marine manganese deposits." *Mineralium Deposita*, 14(3), 249-261.

Cloete, T. E., Jacobs, L., and Brözel, V. S. (1998). "The chemical control of biofouling in industrial water systems." *Biodegradation*, 9(1), 23-37.

Coetser, S., and Cloete, T. E. (2005). "Biofouling and biocorrosion in industrial water systems." *Critical reviews in microbiology*, 31(4), 213-232.

Comte, S., Guibaud, G., and Baudu, M. (2006). "Relations between extraction protocols for activated sludge extracellular polymeric substances (EPS) and EPS complexation properties." *Enzyme and Microbial Technology*, 38(1-2), 237-245.

Conrad, A., Kontro, M., Keinänen, M. M., Cadoret, A., Faure, P., Mansuy-Huault, L., and Block, J.-C. (2003). "Fatty acids of lipid fractions in extracellular polymeric substances of activated sludge flocs." *Lipids*, 38(10), 1093-1105.

Control, C. f. D., and Prevention. (2001). "Issues in Healthcare Settings: CDC's Seven Healthcare Safety Challenges." *United States Department of Health and Human Services*.

Corstjens, P., De Vrind, J., Goosen, T., and Jong, E. d. V. d. (1997). "Identification and molecular analysis of the Leptothrix discophora SS-1 mofA gene, a gene putatively encoding a manganese-oxidizing protein with copper domains." *Geomicrobiology Journal*, 14(2), 91-108.

Costello, J. (1974). "Cathodic depolarization by sulfate-reducing bacteria." *South African Journal of Science*, 70(7), 202-204.

Costerton, J. W., Cheng, K., Geesey, G. G., Ladd, T. I., Nickel, J. C., Dasgupta, M., and Marrie, T. J. (1987). "Bacterial biofilms in nature and disease." *Annual Reviews in Microbiology*, 41(1), 435-464.

Czaczyk, K., and Myszka, K. (2007). "Biosynthesis of extracellular polymeric substances (EPS) and its role in microbial biofilm formation." *Polish Journal of Environmental Studies*, 16(6).

D'Abzac, P., Bordas, F., Van Hullebusch, E., Lens, P. N., and Guibaud, G. (2010). "Extraction of extracellular polymeric substances (EPS) from anaerobic granular sludges: comparison of chemical and physical extraction protocols." *Applied microbiology and biotechnology*, 85(5), 1589-1599.

Das, T., Sehar, S., and Manefield, M. (2013). "The roles of extracellular DNA in the structural integrity of extracellular polymeric substance and bacterial biofilm development." *Environmental microbiology reports*, 5(6), 778-786.

Davies, D. (2003). "Understanding biofilm resistance to antibacterial agents." *Nature reviews. Drug discovery*, 2(2), 114.

Davis, J. (1987). "Metals Handbook". Metals Park, Ohio: ASM International, pp. 235.

de Bruyn, J. C., Boogerd, F. C., Bos, P., and Kuenen, J. G. (1990). "Floating filters, a novel technique for isolation and enumeration of fastidious, acidophilic, iron-oxidizing, autotrophic bacteria." *Applied and environmental microbiology*, 56(9), 2891-2894.

Decho, A. W. (1990). "Microbial exopolymer secretions in ocean environments: their role (s) in food webs and marine processes", in H. Barnes and M. Barnes, (eds.), *Oceanogr. Mar. Biol. Annu. Rev*. Aberdeen: Aberdenn University Press, pp. 73-153.

Dickinson, W., Caccavo, F., and Lewandowski, Z. (1996). "The ennoblement of stainless steel by manganic oxide biofouling." *Corrosion Science*, 38(8), 1407-1422.

Dickinson, W., and Lewandowski, Z. (1996). "Manganese biofouling and the corrosion behavior of stainless steel." *Biofouling*, 10(1-3), 79-93.

Dickinson, W. H., Caccavo, F., Olesen, B., and Lewandowski, Z. (1997). "Ennoblement of Stainless Steel by the Manganese-Depositing Bacterium Leptothrix discophora." *Applied and environmental microbiology*, 63(7), 2502-2506.

Dignac, M.-F., Urbain, V., Rybacki, D., Bruchet, A., Snidaro, D., and Scribe, P. (1998). "Chemical description of extracellular polymers: implication on activated sludge floc structure." *Water Science and Technology*, 38(8-9), 45-53.

DIN_EN_ISO_8044. (2015). "Corrosion of metals and alloys-Basic terms and definitions."

Dinh, H. T., Kuever, J., Mußmann, M., Hassel, A. W., Stratmann, M., and Widdel, F. (2004). "Iron corrosion by novel anaerobic microorganisms." *Nature*, 427(6977), 829-832.

Donlan, R. M., and Costerton, J. W. (2002). "Biofilms: survival mechanisms of clinically relevant microorganisms." *Clinical microbiology reviews*, 15(2), 167-193.

DuBois, M., Gilles, K. A., Hamilton, J. K., Rebers, P. t., and Smith, F. (1956). "Colorimetric method for determination of sugars and related substances." *Analytical chemistry*, 28(3), 350-356.

Ehrlich, H. (2000). "Ocean manganese nodules: biogenesis and bioleaching possibilities." *Minerals and Metallurgical Processing(USA)*, 17(2), 121-128.

Ehrlich, H. L. (1972). "The role of microbes in manganese nodule genesis and degradation." *Ferromanganese deposits on the ocean floor*, 63-70.

Ehrlich, H. L. (1978). "Inorganic energy sources for chemolithotrophic and mixotrophic bacteria." *Geomicrobiology Journal*, 1(1), 65-83.

Ehrlich, H. L., and Newman, D. K. (2009). "Geomicrobiology of Manganese", in H. L. Ehrlich and D. K. Newman, (eds.), *Geomicrobiology*. New York: CRC press, pp. 347-406.

Ehrlich, H. L., Newman, D. K., and Kappler, A. (2015). "Geomicrobiology of Manganese", in H. L. Ehrlich, D. K. Newman, and A. Kappler, (eds.), *Ehrlich's geomicrobiology*. Boca Raton: CRC press, pp. 401 - 451.

Ehrlich, H. L., and Salerno, J. C. (1990). "Energy coupling in Mn 2+ oxidation by a marine bacterium." *Archives of Microbiology*, 154(1), 12-17.

El Gheriany, I. A., Bocioaga, D., Hay, A. G., Ghiorse, W. C., Shuler, M. L., and Lion, L. W. (2009). "Iron requirement for Mn (II) oxidation by Leptothrix discophora SS-1." *Applied and environmental microbiology*, 75(5), 1229-1235.

El Gheriany, I. A., Bocioaga, D., Hay, A. G., Ghiorse, W. C., Shuler, M. L., and Lion, L. W. (2011). "An uncertain role for Cu(II) in stimulating Mn(II) oxidation by Leptothrix discophora SS-1." *Arch Microbiol*, 193(2), 89-93.

Enning, D., Venzlaff, H., Garrelfs, J., Dinh, H. T., Meyer, V., Mayrhofer, K., Hassel, A. W., Stratmann, M., and Widdel, F. (2012). "Marine sulfate-reducing bacteria cause serious corrosion of iron under electroconductive biogenic mineral crust." *Environmental microbiology*, 14(7), 1772-1787.

Entner, N., and Doudoroff, M. (1952). "Glucose and gluconic acid oxidation of Pseudomonas saccharophila." *Journal of Biological Chemistry*, 196(2), 853-862.

Epstein, N. (1981). *Fouling of heat transfer equipment*: Hemisphere Pub.

Eul, U., von Rege, H., Heitz, E., and Sand, W. (1996). "Simulation and Control of MIC by the Miniplant Technique." *Microbially Influenced Corrosion of Materials*, 187-203.

Flemming, H.-C. (1996). "Biofouling and microbiologically influenced corrosion (MIC)-an economical and technical overview." *Microbial deterioration of materials*.

Flemming, H.-C. (2002). "Biofouling in water systems–cases, causes and countermeasures." *Applied microbiology and biotechnology*, 59(6), 629-640.

Flemming, H.-C. (2011a). "Microbial biofouling: unsolved problems, insufficient approaches, and possible solutions", *Biofilm highlights*. Springer, pp. 81-109.

Flemming, H.-C., Neu, T. R., and Wozniak, D. J. (2007). "The EPS matrix: the “house of biofilm cells”." *Journal of bacteriology*, 189(22), 7945-7947.

Flemming, H.-C., Schmitt, J., and Marshall, K. (1996). "Sorption properties of biofilms", *Sediments and toxic substances*. Springer, pp. 115-157.

Flemming, H. C. (2011b). "The perfect slime." *Colloids Surf B Biointerfaces*, 86(2), 251-9.

Flemming, H. C., and Wingender, J. (2010). "The biofilm matrix." *Nat Rev Microbiol*, 8(9), 623-33.

Ford, T., and Mitchell, R. (1990). "The ecology of microbial corrosion", *Advances in microbial ecology*. New York: Plenum Press, pp. 231-262.

Francis, C. A., and Tebo, B. M. (1999). "Marine Bacillus spores as catalysts for oxidative precipitation and sorption of metals." *Journal of molecular microbiology and biotechnology*, 1(1), 71-78.

Francis, C. A., and Tebo, B. M. (2001). "cumA Multicopper Oxidase Genes from Diverse Mn (II)-Oxidizing and Non-Mn (II)-OxidizingPseudomonas Strains." *Applied and environmental microbiology*, 67(9), 4272-4278.

Frølund, B., Palmgren, R., Keiding, K., and Nielsen, P. H. (1996). "Extraction of extracellular polymers from activated sludge using a cation exchange resin." *Water research*, 30(8), 1749-1758.

Fuqua, C., and Greenberg, E. P. (2002). "Listening in on bacteria: acyl-homoserine lactone signalling." *Nature reviews. Molecular cell biology*, 3(9), 685.

Gadd, G. M., and Griffiths, A. J. (1977). "Microorganisms and heavy metal toxicity." *Microbial ecology*, 4(4), 303-317.

Gehrke, T., Hallmann, R., Kinzler, K., and Sand, W. (2001). "The EPS of Acidithiobacillus ferrooxidans-a model for structure-function relationships of

attached bacteria and their physiology." *Water Science and Technology*, 43(6), 159-167.

Gehrke, T., Telegdi, J., Thierry, D., and Sand, W. (1998). "Importance of extracellular polymeric substances from Thiobacillus ferrooxidans for bioleaching." *Applied and Environmental Microbiology*, 64(7), 2743-2747.

Geiser, M., Lewandowski, Z., and Avci, R. "Pit initiation on 316L stainless steel in the presence of bacteria Leptothrix discophora." *Presented at CORROSION 2001*.

Geszvain, K., Butterfield, C., Davis, R. E., Madison, A. S., Lee, S.-W., Parker, D. L., Soldatova, A., Spiro, T. G., Luther, G. W., and Tebo, B. M. (2012). "The molecular biogeochemistry of manganese (II) oxidation". City: Portland Press Limited.

Ghiorse, W. (1984). "Biology of iron-and manganese-depositing bacteria." *Annual reviews in microbiology*, 38(1), 515-550.

Ghiorse, W., and Hirsch, P. (1979). "An ultrastructural study of iron and manganese deposition associated with extracellular polymers of Pedomicrobium-like budding bacteria." *Archives of Microbiology*, 123(3), 213-226.

Giessibl, F. J. (2005). "AFM's path to atomic resolution." *Materials Today*, 8(5), 32-41.

Gong, J., and Zangari, G. (2002). "Electrodeposition and characterization of manganese coatings." *Journal of The Electrochemical Society*, 149(4), C209-C217.

Goodman, M. F., Keener, S., Guidotti, S., and Branscomb, E. (1983). "On the enzymatic basis for mutagenesis by manganese." *Journal of Biological Chemistry*, 258(6), 3469-3475.

Graedel, T. (1978). "Chemical Compounds in the Atmosphere Academic." *New York*, 162.

Guillaumin, V., Schmutz, P., and Frankel, G. (2001). "Characterization of corrosion interfaces by the scanning Kelvin probe force microscopy technique." *Journal of the electrochemical society*, 148(5), B163-B173.

Hajj, H., and Makemson, J. (1976). "Determination of growth of Sphaerotilus discophorus in the presence of manganese." *Applied and environmental microbiology*, 32(5), 699-702.

Hamilton, W. A. (1985). "Sulphate-reducing bacteria and anaerobic corrosion." *Annual Reviews in Microbiology*, 39(1), 195-217.

Harneit, K., Göksel, A., Kock, D., Klock, J.-H., Gehrke, T., and Sand, W. (2006). "Adhesion to metal sulfide surfaces by cells of Acidithiobacillus ferrooxidans, Acidithiobacillus thiooxidans and Leptospirillum ferrooxidans." *Hydrometallurgy*, 83(1), 245-254.

Hays, G. F., and General, P. D. (2010). "World Corrosion Organization." *Corrodia. NACE International, Houston*.

Hedberg, Y., Karlsson, M.-E., Blomberg, E., Wallinder, I. O., and Hedberg, J. (2014). "Correlation between surface physicochemical properties and the release of iron from stainless steel AISI 304 in biological media." *Colloids and Surfaces B: Biointerfaces*, 122, 216-222.

Heitz, E., Henkhaus, R., and Rahmel, A. (1990). *Korrosionskunde im Experiment*, Weinheim: VCH Weinheim, New York, Basel, Cambridge.

Henning, A. K., Hochwitz, T., Slinkman, J., Never, J., Hoffmann, S., Kaszuba, P., and Daghlian, C. (1995). "Two-dimensional surface dopant profiling in silicon using scanning Kelvin probe microscopy." *Journal of applied physics*, 77(5), 1888-1896.

Heyer, A. (2013). "Microbiologically influenced corrosion in ship ballast tanks." *Delft University of Technology, Delft*, Dissertation.

Higgins, M. J., and Novak, J. T. (1997). "Characterization of exocellular protein and its role in bioflocculation." *Journal of environmental engineering*, 123(5), 479-485.

Hochella, M. F., Moore, J. N., Putnis, C. V., Putnis, A., Kasama, T., and Eberl, D. D. (2005). "Direct observation of heavy metal-mineral association from the Clark Fork River Superfund Complex: Implications for metal transport and bioavailability." *Geochimica et cosmochimica acta*, 69(7), 1651-1663.

Hochwitz, T., Henning, A. K., Levey, C., Daghlian, C., Slinkman, J., Never, J., Kaszuba, P., Gluck, R., Wells, R., and Pekarik, J. (1996). "Imaging integrated circuit dopant profiles with the force-based scanning Kelvin probe microscope." *Journal of Vacuum Science & Technology B: Microelectronics and Nanometer Structures Processing, Measurement, and Phenomena*, 14(1), 440-446.

Horn, D. R., Horn, B., and Delach, M. (1972). "Distribution of ferromanganese deposits in the world ocean", in D. R. Horn, (ed.), *Ferromanganese Deposits on the Ocean Floor*. Washington, DC: Natl. Sci. Found Washington, DC, pp. 9-17.

Iverson, W., and Olson, G. (1983). *Anaerobic corrosion by sulfate-reducing bacteria due to a highly-reactive volatile phosphorus compound. Final report*. National Bureau of Standards, Washington, DC (USA).

Iverson, W. P. (1987). "Microbial corrosion of metals." *Advances in applied microbiology*, 32, 1-36.

Jahn, A., and Nielsen, P. (1995). "Extraction of extracellular polymeric substances (EPS) from biofilms using a cation exchange resin." *Water Science and Technology*, 32(8), 157-164.

Jitrapakdee, S., Vidal-Puig, A., and Wallace, J. (2006). "Anaplerotic roles of pyruvate carboxylase in mammalian tissues." *Cellular and Molecular Life Sciences*, 63(7), 843-854.

Jorand, F., Boue-Bigne, F., Block, J., and Urbain, V. (1998). "Hydrophobic/hydrophilic properties of activated sludge exopolymeric substances." *Water Science and Technology*, 37(4-5), 307-315.

Julin, L., Sunila, P., and Enqvist, J. (1983). "New precision method for automatic quality control of raw materials in the soap industry." *Chromatographia*, 17(10), 549-552.

Karunakaran, E., Mukherjee, J., Ramalingam, B., and Biggs, C. A. (2011). ""“Biofilmology”: a multidisciplinary review of the study of microbial biofilms." *Applied microbiology and biotechnology*, 90(6), 1869-1881.

Kielemoes, J., Bultinck, I., Storms, H., Boon, N., and Verstraete, W. (2002). "Occurrence of manganese-oxidizing microorganisms and manganese deposition during biofilm formation on stainless steel in a brackish surface water." *FEMS microbiology ecology*, 39(1), 41-55.

King, R., Miller, J., and Wakerley, D. (1973). "Corrosion of mild steel in cultures of sulphate-reducing bacteria: effect of changing the soluble iron concentration during growth." *British Corrosion Journal*, 8(2), 89-93.

King, R., and Wakerley, D. (1973). "Corrosion of mild steel by ferrous sulphide." *British Corrosion Journal*, 8(1), 41-45.

Kratochvílová, I., Taylor, A., Fendrych, F., Kovalenko, A., and Nesládek, M. (2009). "Surface potential of functionalised nanodiamond layers." *MRS Online Proceedings Library Archive*, 1203.

Krumbein, W., and Altmann, H. (1973). "A new method for the detection and enumeration of manganese oxidizing and reducing microorganisms." *Helgoländer Wissenschaftliche Meeresuntersuchungen*, 25(2-3), 347-356.

Kuklinski, A. (2017). "Development of Extracellular Polymeric Substance-derived Protective Films Against Microbiologically Influenced Corrosion by Desulfovibrio Vulgaris." *Universität Duisburg-Essen, Essen*, Dissertation.

Kuklinski, A., and Sand, W. (2014). "Microbiologically Influenced Corrosion", in G. Kreysa, K. Ota, and R. Savinell, (eds.), *Encyclopedia of Applied Electrochemistry*. New York: Springer, pp. 1276-1290.

Lafferty, B. J., Ginder-Vogel, M., and Sparks, D. L. (2010). "Arsenite oxidation by a poorly crystalline manganese-oxide 1. Stirred-flow experiments." *Environmental science & technology*, 44(22), 8460-8466.

Laspidou, C. S., and Rittmann, B. E. (2002). "A unified theory for extracellular polymeric substances, soluble microbial products, and active and inert biomass." *Water research*, 36(11), 2711-2720.

Law, K.-Y. (2014). "Definitions for hydrophilicity, hydrophobicity, and superhydrophobicity: getting the basics right". City: ACS Publications.

Law, N. A., Caudle, M. T., and Pecoraro, V. L. (1998). "Manganese redox enzymes and model systems: properties, structures, and reactivity." *Advances in inorganic chemistry*, 46, 305-440.

Lawrence, J., Korber, D., and Neu, T. (2007). "Analytical imaging and microscopy techniques", *Manual of Environmental Microbiology, Third Edition*. American Society of Microbiology, pp. 40-68.

Learman, D., and Hansel, C. (2014). "Comparative proteomics of Mn (II)-oxidizing and non-oxidizing Roseobacter clade bacteria reveal an operative manganese transport system but minimal Mn (II)-induced expression of manganese oxidation and antioxidant enzymes." *Environmental microbiology reports*, 6(5), 501-509.

Learman, D., Voelker, B., Vazquez-Rodriguez, A., and Hansel, C. (2011). "Formation of manganese oxides by bacterially generated superoxide." *Nature Geoscience*, 4(2), 95.

Learman, D. R., Voelker, B. M., Madden, A. S., and Hansel, C. M. (2013). "Constraints on superoxide mediated formation of manganese oxides." *Frontiers in microbiology*, 4, 262.

Leckie, H., and Uhlig, H. (1966). "Environmental factors affecting the critical potential for pitting in 18–8 stainless steel." *Journal of the Electrochemical Society*, 113(12), 1262-1267.

Lee, W., Lewandowski, Z., Nielsen, P. H., and Hamilton, W. A. (1995). "Role of sulfate-reducing bacteria in corrosion of mild steel: A review." *Biofouling*, 8(3), 165-194.

Lefèvre, G., Čerović, L., Milonjić, S., Fédoroff, M., Finne, J., and Jaubertie, A. (2009). "Determination of isoelectric points of metals and metallic alloys by adhesion of latex particles." *Journal of colloid and interface science*, 337(2), 449-455.

Lewandowski, Z., Avci, R., Geiser, M., Shi, X., Braughton, K., and Yurt, N. (2002). "Biofouling and corrosion of stainless steels in natural waters." *Water Science and Technology: Water Supply*, 2(4), 65-72.

Lewandowski, Z., and Beyenal, H. (2013). *Fundamentals of biofilm research*: CRC press.

Lewus, M., Tupholme, K., Hobson, S., Lee, B., and Dulieu, D. (1997). *Stainless steels for water systems*. Office for official Publications of the European communities, Luxembourg.

Licina, G. J., and Cubicciotti, D. (1989). "Microbial-induced corrosion in nuclear power plant materials." *JOM Journal of the Minerals, Metals and Materials Society*, 41(12), 23-27.

Lieske, R. (1919). "Zur ernährungsphysiologie der Eisenbakterien." *Zentralbl Bakteriol Parasitenk Infektionskr Hyg Abt II*, 49, 413-425.

Linhardt, P. (1997). "Corrosion of metals in natural waters influenced by manganese oxidizing microorganisms." *Biodegradation*, 8(3), 201-210.

Linhardt, P. (2004). "Microbially influenced corrosion of stainless steel by manganese oxidizing microorganisms." *Materials and Corrosion*, 55(3), 158-163.

Linhardt, P. (2006). "MIC of stainless steel in freshwater and the cathodic behaviour of biomineralized Mn-oxides." *Electrochimica acta*, 51(27), 6081-6084.

Linhardt, P. (2010). "Twenty years of experience with corrosion failures caused by manganese oxidizing microorganisms." *Materials and Corrosion*, 61(12), 1034-1039.

Little, B., and Ray, R. (2002). "A perspective on corrosion inhibition by biofilms." *Corrosion*, 58(5), 424-428.

Little, B. J., Ray, R. I., and Lee, J. S. (2011). "Diagnosing, Measuring and Monitoring Microbiologically Influenced Corrosion (MIC)", in R. Revie, (ed.), *Uhlig's Corrosion Handbook, Third Edition*. New Jersey: John Wiley and Sons, pp. 1203 - 1216.

Lorenz, M. G., and Wackernagel, W. (1994). "Bacterial gene transfer by natural genetic transformation in the environment." *Microbiological reviews*, 58(3), 563-602.

Mack, D., Fischer, W., Krokotsch, A., Leopold, K., Hartmann, R., Egge, H., and Laufs, R. (1996). "The intercellular adhesin involved in biofilm accumulation of Staphylococcus epidermidis is a linear beta-1, 6-linked glucosaminoglycan: purification and structural analysis." *Journal of bacteriology*, 178(1), 175-183.

Mangold, S., Harneit, K., Rohwerder, T., Claus, G., and Sand, W. (2008). "Novel combination of atomic force microscopy and epifluorescence microscopy for visualization of leaching bacteria on pyrite." *Applied and environmental microbiology*, 74(2), 410-415.

Margolis, S. V., and Burns, R. G. (1976). "Pacific deep-sea manganese nodules: Their distribution, composition, and origin." *Annual Review of Earth and Planetary Sciences*, 4(1), 229-263.

McCord, J. M., and Fridovich, I. (1988). "Superoxide dismutase: the first twenty years (1968–1988)." *Free Radical Biology and Medicine*, 5(5-6), 363-369.

McLean, R. J., Whiteley, M., Stickler, D. J., and Fuqua, W. C. (1997). "Evidence of autoinducer activity in naturally occurring biofilms." *FEMS Microbiology Letters*, 154(2), 259-263.

McNaught, A. D., and Wilkinson, A. (1997). *Compendium of chemical terminology*: Blackwell Science Oxford.

Meroueh, S. O., Bencze, K. Z., Hesek, D., Lee, M., Fisher, J. F., Stemmler, T. L., and Mobashery, S. (2006). "Three-dimensional structure of the bacterial cell wall peptidoglycan." *Proceedings of the National Academy of Sciences of the United States of America*, 103(12), 4404-4409.

Meyer, G., and Amer, N. M. (1988). "Novel optical approach to atomic force microscopy." *Applied physics letters*, 53(12), 1045-1047.

Michalowski, W. D. (2012). "Composition, dynamics and function of extracellular polymeric substances in drinking-water biofilms." *Universität Duisburg-Essen*, Dissertation.

Moffett, J. W. (1997). "The importance of microbial Mn oxidation in the upper ocean: a comparison of the Sargasso Sea and equatorial Pacific." *Deep Sea Research Part I: Oceanographic Research Papers*, 44(8), 1277-1291.

Mortimer, C. E., and Müller, U. (2015). *Chemie: Das Basiswissen der Chemie*, Stuttgart: Georg Thieme Verlag.

Mulder, E. (1964). "Iron Bacteria, particularly those of the Sphaerotilus-Leptothrix Group, and Industrial Problems." *Journal of Applied Microbiology*, 27(1), 151-173.

Mulder, E., and Van Veen, W. (1963). "Investigations on theSphaerotilus-Leptothrix group." *Antonie van Leeuwenhoek*, 29(1), 121-153.

Mulder, E. G., and Deinema, M. H. (1981). "The sheathed bacteria", *The prokaryotes*. Springer, pp. 425-440.

Muto, Y., and Goto, S. (1986). "Transformation by extracellular DNA produced by Pseudomonas aeruginosa." *Microbiology and immunology*, 30(7), 621-628.

Nagarajan, N., Humadi, H., and Zhitomirsky, I. (2006). "Cathodic electrodeposition of MnOx films for electrochemical supercapacitors." *Electrochimica Acta*, 51(15), 3039-3045.

Najafpour, M. M., Rahimi, F., Aro, E.-M., Lee, C.-H., and Allakhverdiev, S. I. (2012). "Nano-sized manganese oxides as biomimetic catalysts for water oxidation in artificial photosynthesis: a review." *Journal of the Royal Society Interface*, 9(75), 2383-2395.

Nealson, K. H., Tebo, B. M., and Rosson, R. A. (1988). "Occurrence and mechanisms of microbial oxidation of manganese", *Advances in Applied Microbiology*. Elsevier, pp. 279-318.

Nelson, Y. M., Lion, L. W., Ghiorse, W. C., and Shuler, M. L. (1999). "Production of biogenic Mn oxides by Leptothrix discophora SS-1 in a chemically defined growth medium and evaluation of their Pb adsorption characteristics." *Applied and Environmental Microbiology*, 65(1), 175-180.

Neu, T., Dengler, T., Jann, B., and Poralla, K. (1992). "Structural studies of an emulsion-stabilizing exopolysaccharide produced by an adhesive, hydrophobic Rhodococcus strain." *Microbiology*, 138(12), 2531-2537.

Neu, T. R., and Lawrence, J. R. (1999). "In situ characterization of extracellular polymeric substances (EPS) in biofilm systems", in J. Wingender, T. R. Neu, and H. C. Flemming, (eds.), *Microbial Extracellular Polymeric Substances*. Berlin: Springer, pp. 21-47.

Neu, T. R., Manz, B., Volke, F., Dynes, J. J., Hitchcock, A. P., and Lawrence, J. R. (2010). "Advanced imaging techniques for assessment of structure, composition and function in biofilm systems." *FEMS microbiology ecology*, 72(1), 1-21.

Neu, T. R., Swerhone, G. D., and Lawrence, J. R. (2001). "Assessment of lectin-binding analysis for in situ detection of glycoconjugates in biofilm systems." *Microbiology*, 147(2), 299-313.

Ng, F.-W., and Dawes, E. (1973). "Chemostat studies on the regulation of glucose metabolism in Pseudomonas aeruginosa by citrate." *Biochem. J*, 132, 129-140.

Nichols, P. D., and Nichols, C. A. M. (2008). "Microbial signature lipid profiling and exopolysaccharides: experiences initiated with Professor David C White and transported to Tasmania, Australia." *Journal of microbiological methods*, 74(1), 33-46.

Nielsen, P. H., and Jahn, A. (1999). "Extraction of EPS." *Microbial extracellular polymeric substances*, 49-72.

Nishikawa, S., and Kuriyama, M. (1968). "Nucleic acid as a component of mucilage in activated sludge." *Water Research*, 2(11), 811-812.

Noël, N., Florian, B., and Sand, W. (2010). "AFM & EFM study on attachment of acidophilic leaching organisms." *Hydrometallurgy*, 104(3), 370-375.

Nonnenmacher, M., o'Boyle, M., and Wickramasinghe, H. K. (1991). "Kelvin probe force microscopy." *Applied physics letters*, 58(25), 2921-2923.

O'Toole, G., Kaplan, H. B., and Kolter, R. (2000). "Biofilm formation as microbial development." *Annual Reviews in Microbiology*, 54(1), 49-79.

Olesen, B., Yurt, N., and Lewandowski, Z. (2001). "Effect of biomineralized manganese on pitting corrosion of type 304L stainless steel." *Materials and Corrosion*, 52(11), 827-832.

Olesen, B. H., Nielsen, P. H., and Lewandowski, Z. (2000). "Effect of biomineralized manganese on the corrosion behavior of C1008 mild steel." *Corrosion*, 56(1), 80-89.

Pawley, J. B. (2006). "Fundamental limits in confocal microscopy", *Handbook of biological confocal microscopy*. Springer, pp. 20-42.

Petitprez, M., and Leclerc, H. "Bacteria of the Sphaerotilus-Leptothrix group." *Presented at Annales de l'Institut Pasteur de Lille*.

Platt, R., Geesey, G. G., Davis, J. D., and White, D. (1985). "Isolation and partial chemical analysis of firmly bound exopolysaccharide from adherent cells of a freshwater sediment bacterium." *Canadian journal of microbiology*, 31(8), 675-680.

Poncin-Epaillard, F., Vrlinic, T., Debarnot, D., Mozetic, M., Coudreuse, A., Legeay, G., El Moualij, B., and Zorzi, W. (2012). "Surface treatment of polymeric materials controlling the adhesion of biomolecules." *Journal of functional biomaterials*, 3(3), 528-543.

Post, J. E. (1999). "Manganese oxide minerals: Crystal structures and economic and environmental significance." *Proceedings of the National Academy of Sciences*, 96(7), 3447-3454.

Pringsheim, E. G. (1949). "The filamentous bacteria Sphaerotilus, Leptothrix, Cladothrix, and their relation to iron and manganese." *Philosophical Transactions of the Royal Society of London. Series B, Biological Sciences*, 453-482.

Ras, M., Girbal-Neuhauser, E., Paul, E., Spérandio, M., and Lefebvre, D. (2008). "Protein extraction from activated sludge: an analytical approach." *Water research*, 42(8-9), 1867-1878.

Raymond, J., and Blankenship, R. E. (2008). "The origin of the oxygen-evolving complex." *Coordination Chemistry Reviews*, 252(3), 377-383.

Reddy, B., Doherty, M., and Sykes, J. (2004). "Breakdown of organic coatings in corrosive environments examined by scanning kelvin probe and scanning acoustic microscopy." *Electrochimica acta*, 49(17), 2965-2972.

Ristl, R., Steiner, K., Zarschler, K., Zayni, S., Messner, P., and Schäffer, C. (2010). "The S-layer glycome—adding to the sugar coat of bacteria." *International journal of microbiology*, 2011.

Rogers, S. R., and Anderson, J. J. (1976). "Measurement of growth and iron deposition in Sphaerotilus discophorus." *Journal of bacteriology*, 126(1), 257-263.

Rohwerder, M., and Turcu, F. (2007). "High-resolution Kelvin probe microscopy in corrosion science: scanning Kelvin probe force microscopy (SKPFM) versus classical scanning Kelvin probe (SKP)." *Electrochimica Acta*, 53(2), 290-299.

Rosson, R. A., and Nealson, K. H. (1982). "Manganese binding and oxidation by spores of a marine bacillus." *Journal of Bacteriology*, 151(2), 1027-1034.

Roth, A. (1797). "Catalecta botanica quibus plantae novaeet minus cognitae describuntur atque illistrantur." *Lipsiae in Bibliopolio I.G. Mulleriano. fasc. 1.*

Rubio, C., Costa, D., Bellon-Fontaine, M., Relkin, P., Pradier, C., and Marcus, P. (2002). "Characterization of bovine serum albumin adsorption on chromium and AISI 304 stainless steel, consequences for the Pseudomonas fragi K1 adhesion." *Colloids and Surfaces B: Biointerfaces*, 24(3-4), 193-205.

Saenger, W. (2013). in C. R. Cantor, (ed.), *Principles of nucleic acid structure*. New York: Springer.

Sand, W. (1997). "Microbial mechanisms of deterioration of inorganic substrates—a general mechanistic overview." *International Biodeterioration & Biodegradation*, 40(2-4), 183-190.

Sand, W., and Gehrke, T. (2003). "Microbially influenced corrosion of steel in aqueous environments." *Reviews in Environmental Science and Biotechnology*, 2(2), 169-176.

Sand, W., and Gehrke, T. (2006). "Extracellular polymeric substances mediate bioleaching/biocorrosion via interfacial processes involving iron(III) ions and acidophilic bacteria." *Res Microbiol*, 157(1), 49-56.

Santelli, C. M., Pfister, D. H., Lazarus, D., Sun, L., Burgos, W. D., and Hansel, C. M. (2010). "Promotion of Mn (II) oxidation and remediation of coal mine drainage in passive treatment systems by diverse fungal and bacterial communities." *Applied and environmental microbiology*, 76(14), 4871-4875.

Savidge, T., and Pothulakis, C. (2004). *Microbial imaging*: Academic Press.

Schmitt, J., and Flemming, H.-C. (1998). "FTIR-spectroscopy in microbial and material analysis." *International Biodeterioration & Biodegradation*, 41(1), 1-11.

Schopf, J., Hayes, J., and Walter, M. (1983). "Evolution of earth's earliest ecosystems- Recent progress and unsolved problems." *Earth's earliest biosphere: Its origin and evolution(A 84-43051 21-51). Princeton, NJ, Princeton University Press, 1983*, 361-384.

Schwers, H. (1912). "Megalothrix discophora, eine neue Eisenbakterie." *Zentralblatt für Bakteriologie, Parasitenkunde und Infektionskrankheiten*, 33, 273-276.

Schwertmann, U. (1991). "Solubility and dissolution of iron oxides." *Plant and soil*, 130(1-2), 1-25.

Scotto, V., Di Cintio, R., and Marcenaro, G. (1985). "The influence of marine aerobic microbial film on stainless steel corrosion behaviour." *Corrosion Science*, 25(3), 185-194.

Scrutton, M. C., Griminger, P., and Wallace, J. C. (1972). "Pyruvate Carboxylase BOUND METAL CONTENT OF THE VERTEBRATE LIVER ENZYME AS A FUNCTION OF DIET AND SPECIES." *Journal of Biological Chemistry*, 247(10), 3305-3313.

Shi, X., Avci, R., and Lewandowski, Z. (2002a). "Electrochemistry of passive metals modified by manganese oxides deposited by Leptothrixdiscophora: two-step model verified by ToF-SIMS." *Corrosion science*, 44(5), 1027-1045.

Shi, X., Avci, R., and Lewandowski, Z. (2002b). "Microbially deposited manganese and iron oxides on passive metals-Their chemistry and consequences for material performance." *Corrosion*, 58(9), 728-738.

Shi, X., Avci, R., and Lewandowski, Z. (2002c). "Microbially deposited manganese and iron oxides on passive metals—their chemistry and consequences for material performance." *Corrosion*, 58(9), 728-738.

Shively, J., and Benson, A. (1967). "Phospholipids of Thiobacillus thiooxidans." *Journal of bacteriology*, 94(5), 1679-1683.

Silverman, D. (2011). "Practical corrosion prediction using electrochemical techniques", in R. Revie, (ed.), *Uhlig's Corrosion Handbook, Third Edition*. New Jersey: John Wiley and Sons, pp. 1129-1166.

Söhngen, N. (1914). "Umwandlungen von Manganverbindungen unter dem Einfluss mikrobiologischer Prozesse." *Zentr. Bakteriol. Parasitenk. II*, 40, 545-554.

Späth, R., Flemming, H.-C., and Wuertz, S. (1998). "Sorption properties of biofilms." *Water Science and Technology*, 37(4-5), 207-210.

Speller, F. N. (1926). *Corrosion Causes And Prevention: An Engineering Problem*: Mcgraw-Hill Book Company, Inc.; New York.

Spring, S. (2006). "The genera Leptothrix and Sphaerotilus", in M. Dworkin, S. Falkow, E. Rosenberg, K.-H. Schleifer, and E. Stackebrandt, (eds.), *The prokaryotes*. New York: Springer, pp. 758-777.

Spring, S., Kampfer, P., Ludwig, W., and Schleifer, K.-H. (1996). "Polyphasic Characterization of the Genus Leptothrix: New Descriptions of Leptothrix mobilis sp. nov. and Leptothrix discophora sp. nov. nom. rev. and Emended Description of Leptothrix cholodnii emend." *Systematic and applied microbiology*, 19(4), 634-643.

Stratmann, M., and Streckel, H. (1990). "On the atmospheric corrosion of metals which are covered with thin electrolyte layers—I. Verification of the experimental technique." *Corrosion Science*, 30(6-7), 681-696.

Stratmann, M., Streckel, H., and Feser, R. (1991). "A new technique able to measure directly the delamination of organic polymer films." *Corrosion science*, 32(4), 467-470.

Su, J., Bao, P., Bai, T., Deng, L., Wu, H., Liu, F., and He, J. (2013). "CotA, a multicopper oxidase from Bacillus pumilus WH4, exhibits manganese-oxidase activity." *PLoS One*, 8(4), e60573.

Sutherland, I. W. (1999). "Biofilm exopolysaccharides", in J. Wingender, T. R. Neu, and H. C. Flemming, (eds.), *Microbial extracellular polymeric substances*. Berlin: Springer, pp. 73-92.

Sutherland, I. W. (2001). "Biofilm exopolysaccharides: a strong and sticky framework." *Microbiology*, 147(1), 3-9.

Swift, S., Throup, J. P., Williams, P., Salmond, G. P., and Stewart, G. S. (1996). "Quorum sensing: a population-density component in the determination of bacterial phenotype." *Trends in biochemical sciences*, 21(6), 214-219.

Takahashi, E., Ledauphin, J., Goux, D., and Orvain, F. (2010). "Optimising extraction of extracellular polymeric substances (EPS) from benthic diatoms: comparison of the efficiency of six EPS extraction methods." *Marine and Freshwater Research*, 60(12), 1201-1210.

Tang, Y., Zeiner, C. A., Santelli, C. M., and Hansel, C. M. (2013). "Fungal oxidative dissolution of the Mn (II)-bearing mineral rhodochrosite and the role of metabolites in manganese oxide formation." *Environmental microbiology*, 15(4), 1063-1077.

Tebo, B. M. (1991). "Manganese (II) oxidation in the suboxic zone of the Black Sea." *Deep Sea Research Part A. Oceanographic Research Papers*, 38, S883-S905.

Tebo, B. M., Bargar, J. R., Clement, B. G., Dick, G. J., Murray, K. J., Parker, D., Verity, R., and Webb, S. M. (2004). "BIOGENIC MANGANESE OXIDES: Properties and Mechanisms of Formation." *Annual Review of Earth and Planetary Sciences*, 32(1), 287-328.

Tebo, B. M., Clement, B. G., and Dick, G. J. (2007). "Biotransformations of manganese", in C. Hurst, R. Crawford, J. Garland, D. Lipson, A. Mills, and L. Stetzenbach, (eds.), *Manual of Environmental Microbiology*. Washington, DC: ASM Press, pp. 1223-1238.

Tebo, B. M., Ghiorse, W. C., Van Waasbergen, L. G., Siering, P. L., and Caspi, R. (1997). "Bacterially mediated mineral formation; insights into manganese (II) oxidation from molecular genetic and biochemical studies." *Reviews in Mineralogy and Geochemistry*, 35(1), 225-266.

Tebo, B. M., Johnson, H. A., McCarthy, J. K., and Templeton, A. S. (2005). "Geomicrobiology of manganese (II) oxidation." *TRENDS in Microbiology*, 13(9), 421-428.

Telegdi, J., Keresztes, Z., Pálinkás, G., Kálmán, E., and Sand, W. (1998). "Microbially influenced corrosion visualized by atomic force microscopy." *Applied Physics A: Materials Science & Processing*, 66, S639-S642.

Templeton, A. S., Staudigel, H., and Tebo, B. M. (2005). "Diverse Mn (II)-oxidizing bacteria isolated from submarine basalts at Loihi Seamount." *Geomicrobiology Journal*, 22(3-4), 127-139.

Teubner, N. (2018). "Functional components in the EPS -extracellular polymeric substances- of the iron-oxidizing biofilm forming Acidithiobacillus species." *Universität Duisburg-Essen*, Universitätsbibliothek Duisburg-Essen(Dissertation).

Thierry, D., and Sand, W. (2011). "Microbiologically influenced corrosion.", *In: Corrosion Mechanisms in Theory and Practice.* Boca Raton: CRC Press, pp. 737-776.

Thyssen, C., Holuscha, D., Kuhn, J., Walter, F., Fürbeth, W., and Sand, W. (2015). "Biofilm Formation and Stainless Steel Corrosion Analysis of Leptothrix discophora." *Advanced Materials Research*, 1130, 79-82.

Tuthill, A. (1990). "Design, water factors affect service water piping materials." *Power Engineering;(USA)*, 94(7).

Tuthill, A. H., and Avery, R. E. (1994). "Survey of stainless steel performance in low chloride waters." *Public Works*, 125(12).

Ulrich, T., and Kretzschmar, R. (2007). "Biogenic manganese oxides: Formation mechanisms, mineralogy and environmental relevance." *Term paper: Biogeoch. Pol. Dynamics*.

Van Veen, W. (1973). "Biological oxidation of manganese in soils." *Antonie van Leeuwenhoek*, 39(1), 657-662.

Van Veen, W., Mulder, E., and Deinema, M. H. (1978). "The Sphaerotilus-Leptothrix group of bacteria." *Microbiological Reviews*, 42(2), 329.

Van Waasbergen, L. G., Hildebrand, M., and Tebo, B. M. (1996). "Identification and characterization of a gene cluster involved in manganese oxidation by spores of the marine Bacillus sp. strain SG-1." *Journal of bacteriology*, 178(12), 3517-3530.

Venzlaff, H., Enning, D., Srinivasan, J., Mayrhofer, K. J., Hassel, A. W., Widdel, F., and Stratmann, M. (2013). "Accelerated cathodic reaction in microbial

corrosion of iron due to direct electron uptake by sulfate-reducing bacteria." *Corrosion Science*, 66, 88-96.

Videla, H. A., and Characklis, W. G. (1992). "Biofouling and microbially influenced corrosion." *International Biodeterioration & Biodegradation*, 29(3-4), 195-212.

von Wolzogen-Kühr, C. (1961). "Unity of anaerobic and aerobic iron corrosion process in the soil." *Corrosion*, 17(6), 293t-299t.

Von Wolzogen-Kühr, C., and Van der Vlugt, L. (1934). "The graphitization of cast iron as an electrochemical process in anaerobic soils." *Water*, 18, 147-165.

Walter, F. (2015). *"Analysis of Extracellular Polymeric Substances Composition and Biofilm Formation of Leptothrix discophora SS-1 using Photometric Determination and Fluorescence Lectin-Binding Analysis"*. Master Thesis. Aquatic Biotechnology, Universität Duisburg-Essen, Essen.

Watson, J. D., and Crick, F. H. (1953). "Molecular structure of nucleic acids." *Nature*, 171(4356), 737-738.

Wehrli, B., Friedl, G., and Manceau, A. (1995). "Reaction rates and products of manganese oxidation at the sediment-water interface". ACS Publications.

Weisenhorn, A., Drake, B., Prater, C. B., Gould, S., Hansma, P., Ohnesorge, F., Egger, M., Heyn, S., and Gaub, H. (1990). "Immobilized proteins in buffer imaged at molecular resolution by atomic force microscopy." *Biophysical journal*, 58(5), 1251-1258.

Whitchurch, C. B., Tolker-Nielsen, T., Ragas, P. C., and Mattick, J. S. (2002). "Extracellular DNA required for bacterial biofilm formation." *Science*, 295(5559), 1487-1487.

Wiggers, F. (2015). *"Influence of different substrata and evaluation of sample treatment on the EPS composition of Leptothrix discophora"*. Scientific Internship. Aquatic Biotechnology, Universität Duisburg-Essen, Essen.

Wikiel, A. J. (2013). "Role of extracellular polymeric substances on biocorrosion initiation or inhibition." *Universität Duisburg-Essen, Essen*, Dissertation.

Wikiel, A. J., Datsenko, I., Vera, M., and Sand, W. (2014). "Impact of Desulfovibrio alaskensis biofilms on corrosion behaviour of carbon steel in marine environment." *Bioelectrochemistry*, 97, 52-60.

Wingender, J., Neu, T. R., and Flemming, H.-C. (1999). "What are bacterial extracellular polymeric substances?", in J. Wingender, T. R. Neu, and H. C. Flemming, (eds.), *Microbial extracellular polymeric substances*. Berlin: Springer, pp. 1-19.

Wingender, J., Strathmann, M., Rode, A., Leis, A., and Flemming, H.-C. (2001). "Isolation and biochemical characterization of extracellular polymeric substances from Pseudomonas aeruginosa." *Methods in enzymology*, 336, 302-314.

Wolfaardt, G. M., Lawrence, J. R., and Korber, D. R. (1999). "Function of EPS", *Microbial extracellular polymeric substances*. Springer, pp. 171-200.

Wu, J., and Xi, C. (2009). "Evaluation of different methods for extracting extracellular DNA from the biofilm matrix." *Applied and environmental microbiology*, 75(16), 5390-5395.

Wu, Y.-H., Liao, L., Wang, C.-S., Ma, W.-L., Meng, F.-X., Wu, M., and Xu, X.-W. (2013). "A comparison of microbial communities in deep-sea polymetallic nodules and the surrounding sediments in the Pacific Ocean." *Deep Sea Research Part I: Oceanographic Research Papers*, 79, 40-49.

Xu, L.-C., Chan, K.-Y., and Fang, H. H. (2002). "Application of atomic force microscopy in the study of microbiologically influenced corrosion." *Materials characterization*, 48(2), 195-203.

Yang, W., Zhang, Z., Zhang, Z., Chen, H., Liu, J., Ali, M., Liu, F., and Li, L. (2013). "Population structure of manganese-oxidizing bacteria in stratified soils and properties of manganese oxide aggregates under manganese–complex medium enrichment." *PLoS One*, 8(9), e73778.

Yli-Hemminki, P., Jørgensen, K. S., and Lehtoranta, J. (2014). "Iron–manganese concretions sustaining microbial life in the Baltic Sea: the structure of the bacterial community and enrichments in metal-oxidizing conditions." *Geomicrobiology Journal*, 31(4), 263-275.

Zerweck, U., Loppacher, C., Otto, T., Grafström, S., and Eng, L. M. (2005). "Accuracy and resolution limits of Kelvin probe force microscopy." *Physical Review B*, 71(12), 125424.

Zhang, J., Lion, L. W., Nelson, Y. M., Shuler, M. L., and Ghiorse, W. C. (2002). "Kinetics of Mn (II) oxidation by Leptothrix discophora SS1." *Geochimica et Cosmochimica Acta*, 66(5), 773-781.

Zhang, R., Neu, T., Bellenberg, S., Kuhlicke, U., Sand, W., and Vera, M. (2015). "Use of lectins to in situ visualize glycoconjugates of extracellular polymeric substances in acidophilic archaeal biofilms." *Microbial biotechnology*, 8(3), 448-461.

Zhu, M., Farrow, C. L., Post, J. E., Livi, K. J. T., Billinge, S. J. L., Ginder-Vogel, M., and Sparks, D. L. (2012). "Structural study of biotic and abiotic poorly-crystalline manganese oxides using atomic pair distribution function analysis." *Geochimica et Cosmochimica Acta*, 81, 39-55.

Zhu, M., Paul, K. W., Kubicki, J. D., and Sparks, D. L. (2009). "Quantum chemical study of arsenic (III, V) adsorption on Mn-oxides: Implications for arsenic (III) oxidation." *Environmental science & technology*, 43(17), 6655-6661.

8 Appendix

8.1 Results of total organic carbon (TOC) determination

TOC measurements were performed exemplarily for the tightly and loosely bound EPS fractions of the 4 different growth conditions and compared to the EPS dry weight. Table 16 shows the proportion of the EPS dry weight which could be recovered (measured) as TOC.

Table 16: Percentage of TOC recovered from the dry weight of EPS. Loosely bound EPS, n = 1; tightly bound EPS, n = 2.

Condition	**EPS fraction**	**Recovery (%) TOC from dry weight**
-SS -Mn	Tightly bound	21.1 ± 5.2
	Loosely bound	24.3
-SS +Mn	Tightly bound	1.5 ± 1.4
	Loosely bound	23.5
+SS -Mn	Tightly bound	18.2 ± 1.7
	Loosely bound	24.1
+SS +Mn	Tightly bound	5.3 ± 0.4
	Loosely bound	25.1

8.2 Publications

Referred Publications

Thyssen, C., Walter, F., Sand, W. (2018). Biofilm formation by the manganese oxidizing *Leptothrix discophora* is causing biocorrosion of stainless steel. *Submitted to Corrosion Science*.

Issotta, F., Covarrubias, P.C., Moya-Beltrán, A., Bellenberg, S., **Thyssen, C.**, Sand, W., Nuñez, H., Mena, C., Holmes, D.S., Quatrini, R., Vera, M. (2017). 16S rRNA and Multilocus Phylogenetic Analysis of the Iron Oxidizing Acidophiles of the *Acidiferrobacteraceae* Family. Solid State Phenomena, 262, 339-343.

Thyssen, C., Holuscha, D., Kuhn, J., Walter, F., Fürbeth, W., Sand, W. (2015). Biofilm Formation and Stainless Steel Corrosion Analysis of Leptothrix discophora. *Advanced Materials Research*, 1130, 79-82.

Florian, B., Noël, N., **Thyssen, C.**, Felschau, I., Sand W. (2011). Some quantitative data on bacterial attachment to pyrite. Minerals Engineering, 24 , 1132-1138.

Janosch, C., **Thyssen, C.**, Vera, M., Bonnefoy, V., Rohwerder, T., Sand, W. (2009). Sulfur oxygenase reductase in different *Acidithiobacillus caldus*-like strains. *Advanced Materials Research*, 71-73, 239-242.

Oral Presentations (selection)

Thyssen, C., Holuscha, D., Kuhn, J., Walter, F., Fürbeth, W., Sand, W. (2015). Biofilm Formation and Stainless Steel Corrosion Analysis of Leptothrix discophora. Abstract in: *Proceedings of the IBS* 2015, Sancur, Bali, Indonesia

Thyssen, C., Noël, N., Kuklinski, A., Sand, W. (2015). Combined Epifluorescence and Kelvin Probe Force Microscopy (EFM-KPFM) for the study of bacterial attachment to ferrous surfaces. Abstract in: *BIOspektrum Sonderausgabe,* 2015, VAAM-Jahrestagung 2015, Marburg/Lahm, Germany.

Thyssen, C., Sand, W., Holuscha, D., Fürbeth, W. (2014). Oberflächenschutz durch Beschichtung mit (bakteriellen) EPS-Analoga. Abstract in: *Chemie Ingenieur Technik*, 86, 9, *ProcessNet* 2014, Aachen, Germany.

Thyssen, C., Kuklinski, A., Holuscha, D., Fürbeth, W., Sand, W. (2013). Influence of steel on the EPS composition and complementary corrosion analysis of *Leptothrix discophora.* Abstract in: *Proceedings of the Eurocorr* 2013, Estoril, Portugal.

Thyssen, C., Kuklinski, A., Holuscha, D., Fürbeth, W., Sand, W. (2012). Manganese-oxidizing bacteria: attachment pattern, EPS composition and influence on steel corrosion. Abstract in: *Proceedings of the Eurocorr* 2012, Istanbul, Turkey.

8.3 Curriculum Vitae

Der Lebenslauf ist in der Online-Version aus Gründen des Datenschutzes nicht enthalten.

8.4 Statement of original authorship

Hiermit versichere ich, dass ich die vorliegende Arbeit mit dem Titel

„Biofilm formation by the manganese-oxidizing bacterium *Leptothrix discophora* strain SS-1 and corrosion of stainless steel“

selbst verfasst und keine außer den angegebenen Hilfsmitteln und Quellen benutzt habe, und dass die Arbeit in dieser oder ähnlicher Form noch bei keiner anderen Universität eingereicht wurde.

Essen, im Mai 2018

(Christian Thyssen)